Fundamental Study of Heat Transport by Phonons and Electrons in Semiconductors at Micro and Nanoscale

Victor Bong Nee Shin

A thesis submitted in fulfilment of the requirements
for the degree of Doctor of Philosophy

Swinburne University of Technology
Melbourne, Australia

2017

To my beloved wife and children –
Ker Sing, Vincent, Vera and the little V

Abstract

The advancement of nanotechnology enabled the miniaturization of the electronic devices in the modern day. The down-scaling trend has led to many issues associated with high power density and heat dissipation issues, particularly in nano-devices. Comprehensive understanding of the heat distribution within nano-devices is therefore necessary to rectify such problems. To date, most available literatures tend to focus on phonon transport in regards to heat transport issues in nano-devices. Although phonons are known to be the pre-dominant heat carriers in semiconductors due to the scarcity of electrons, the inevitable phonon-electron interaction within the semiconductor medium means the inclusion of the electron transport will potentially provide a more holistic approach to the heat transport issues. This thesis involves a fundamental study on the phonon and electron transport in semiconductor materials commonly used in electronic devices at the micro and nanoscale. As such length scales, it is well-known that classical physics represented by the Fourier Law no longer applies. The carrier transport can be described by semi-classically by the Boltzmann Transport Equation. Solution to this equation can be tedious and cumbersome depending on the complexity of the transport model designed. To minimize assumptions and better capture the physics of the transport mechanisms, a stochastic approach known as the Monte Carlo method was adopted. This thesis therefore proposes Monte Carlo phonon and electron transport simulation models. Initially, Monte Carlo simulation codes are developed for phonon and electron transport independently, taking into account the correct bulk dispersion relations / band structures and the relevant scattering rates. Generally acceptable simplifications such as the use of parabolic bands and combined scattering rates were applied for a more efficient simulation process without compromising the underlying physics. Both frequency-dependent / energy-dependent transport models share a similar

algorithm, but a self-consistent Poisson‟s equation solver is incorporated in the electron transport to account for the effect of the electric field. The proposed coupled electron-phonon transport simulation involves energy generation by electron transport simulation and lattice temperature computation by phonon transport simulation. Results obtained from all three simulations are discussed, while preliminary results obtained from the coupled electron-phonon transport suggested no net energy is transferred from electrons to phonons under near thermal equilibrium condition. The current fundamental study remains a work in progress. Possible improvements are recommended at the end of the thesis.

Acknowledgements

It was almost unimaginable that I would even reach this stage at one point in time. A journey that was long and often uncertain, plagued by insomniac nights and continual self-doubts, finally hit this milestone. The feeling right now is unreal, truly unbelievable. And it will only be fitting to start with a popular cliché – which this thesis would not have been possible without the helpful guidance and kindest support of some of the most amazing individuals I have known in life.

My utmost gratitude has to first go to my principal supervisor, Associate Professor Dr. Basil Wong Tung Liong, for his passionate and masterful guidance throughout the course of my research study. He is, and will always be, a great role model for young and raw researchers. He has always been quick to respond to any doubts, and was particularly helpful in helping me easing into life in academics. His mentorship greatly aided my development into an independent researcher and a teacher of engineering. Not to forget his sincere effort to ensure that I am financially sound throughout the course of this study. I will always be indebted to him for the valuable experiences and knowledge which I have gained throughout the years working under his wing.

Equally important to the realization of this thesis are the funders and supporters of this research project – Ministry of Higher Education (MOHE), Malaysia via the Fundamental Research Grant Scheme (FRGS), and Ministry of Science, Technology and Innovation, Malaysia (MOSTI). A special mention must also go to my co-supervisor Associate Professor Dr. Wallace Wong Shung Shui and the members of the Research and Consultancy Office (RCO) who have been helpful throughout the course of my candidature. Not to forget Professor Anatoli Vakhguelt and Luk Tien Boh, both

of whom probably saved some of the best advices for me when I was still contemplating joining the research and academic world.

Next up I would also like to thank my two colleagues, Lai Jia Jiun and Japheth Lau Zi Jun, for the collaborations that we have enjoyed in the past. I wish both of you the best, and will always look forward to future collaborations. And to my childhood friend Dr. Chong Nguan Soon, my colleague Dr. Choo Chung Siung, my mentor and referee Don Gray, my regular partner in crime Rafal Lulko, and my fellow friends (you know who you are!) – Thank you for your inspirational presence throughout!

As to my parents and all my in-laws who have always been very supportive of me, I would like to also express my utmost heartfelt gratitude. The trust and consent I received especially from my parents have been extraordinary and I sincerely thank them for having the belief in me. In any case however, the time spent on this thesis was some of those taken away from our family time and I vow to make up for it in days to come. And to my sister Jessie Bong who is also actively pursuing her doctorate degree, good luck and all the best!

Finally, my deepest appreciation must go to my beloved wife. Maintaining a persistent presence in my life and an unwavering dedication to the upbringing of our children while remaining strongly committed to her career was never going to be a smooth sail. Yet, she juggled them well, in addition to having the patience to bear with me and put up with my utter nonsense at times throughout this journey. *A true wonder woman.*

Thank you.

Declaration

I declare that this thesis contains no material which has been accepted for the award to the candidate of any other degree or diploma, except where due reference is made in the text of the examinable outcome, and to the best of my knowledge contains no material previously published or written by another person except where due reference is made in the text of the examinable outcome.

Victor Bong Nee Shin

Table of Contents

List of Tables

List of Figures

Nomenclature

B	scattering parameter
D	density of states [/m^3-s]
d	diameter [m]
E	energy [J]
f	particle distribution function [-]
g	particle distribution function [-]
$\dot{g}'''$	power density / volumetric heat generation [W/m^3]
h	Planck constant
K	thermal conductivity [W/m-K]
$\vec{k}$	wavenumber [m^{-1}]
$\hat{k}$	unit vector [-]
N	number of ensembles [-]
N_b	number of discretization [-]
n	arbitrary number [-]
P	Probability [-]
p	phonon polarization branch [-]
q	heat flux per unit area [W/m^{-2}]

$\dot{q}$ heat flux per unit length [W/m]

R random number [-]

S distance of travel [m]

T temperature [K]

t time [s]

U potential [V]

$\bar{v}$ velocity [m/s]

X width of the geometry [m]

x location in the X-direction [m]

Y length of the geometry [m]

y location in the Y-direction [m]

Z depth or thickness of the geometry [m]

z location in the Z-direction [m]

Symbols

ε permittivity[F/m]

θ polar angle [rad]

μ direction cosine [-]

ρ charge density [number/m^3]

ξ ratio [-]

Γ scattering rate [1/s]

τ relaxation time [s]

φ azimuthal angle [rad]

ω angular frequency [rad/s]

Subscripts

0	initial condition
Abs	absorption
bound	Boundary
coll	collision
cond	conduction
DOS	density of states
elec	electron
emi	emission
en	ensemble
final	final
g	group
gap	gap
gen	heat generation
i	state
ini	initial
l	longitudinal
latt	lattice
L	left
LA	longitudinal acoustic
m	medium
mfp	mean free path
min	minimum
N	discretization
ph	phonon

r	relative
R	right
ref	reference
scatt	scattering
t	transverse
TA	transverse acoustic

Constants

e	electron charge, $e = 1.602 \times 10^{-19}$ [C]
h	Planck constant, $h = 4.136 \times 10^{-15}$ [eV-s]
m_0	electron mass, $m_0 = 9.109 \times 10^{-31}$ [kg]
ε_0	vacuum permittivity, $\varepsilon_0 = 8.854 \times 10^{-12}$ [C/V-m]
k_B	Boltzmann constant, $k_B = 8.617 \times 10^{-5}$ [eV/K]

CHAPTER 1

Introduction

1.1 Background of the Research

Nanoscience and nanotechnology involve studies and applications related to the manipulation of matter conducted at the atomic or molecular level, i.e. in the order of 100 nm or smaller. They form the fundamental physics of our macroscale applications, ranging from golf balls to smart phones. Ever since the first inception of the idea in 1959 by Richard Feynman (Feynman 1960), various efforts have been invested into advancing the art of manipulating atoms and molecules to improve our macroscale products and applications across various fields, such as semiconductor physics, organic chemistry, biotechnology, microfabrication etc. As one of the main area that receives heavy research funding and investment, it is unsurprising that semiconductor electronics continues to witness significant breakthroughs over the years.

The computer chips in present days easily contain millions of transistors. The realization of such miniaturization is only possible through the advancement in various fields, ranging from materials science to fabrication technologies. The shrinkage of electronic components calls for in-depth understanding of semiconductor material properties at the atomic level, which is different from the bulk material properties as commonly known in classical Newtonian physics. In the sub-100 nm regime, quantum mechanics, as represented by the Schrodinger's equation, is relied upon to quantitatively describe the physical behaviour of materials (Wolf 2008). At such length scales, the

carrier-carrier interaction and carrier-environment interaction will potentially affect material properties. Information on the carrier properties and behaviour is therefore essential to come up with materials with favourable properties (Chen 2000). Unconventional materials with desirable properties can be created via doping of conventional materials such as silicon (Si) and germanium (Ge), while sophisticated nanostructures such as nanowire (NW), nanotube (NT), nanofilm (NF), nanoribbon and nanosphere can also be engineered, giving rise to endless possibilities in applications within the nanometer regime (Hernández-Vélez 2006; Iijima 1991; Shi et al. 2001; Wang, Cai & Zhang 2008).

Concurrent with the miniaturization trend, the manufacturing technology is also evolving over the years. Greater precision, accuracy and capacity are required, which usually involves very high capital costs. Nano-manufacturing has become essential and manufacturers are known to invest on upgrading their manufacturing equipment and fabrication technologies in order to produce state of the art nanostructures (Wong & Mengüç 2008). For example, by gaining control over several parameters such as the growth directions, defects and structural transformation, the „growth" of NW with desirable properties is made possible. Another instance involves nano-machining using electron beam in which the understanding of energy exchanges between electrons and the work piece is able to prevent unintended detrimental effect from the resulting temperature rise during the process.

With the aforementioned innovations and the continual development in complementary metal-oxide semiconductor (CMOS) technologies, scalability has been greatly improved and new components are created (Fischetti et al. 2007). Components such as metal oxide semiconductor field effect transistor (MOSFET) and silicon-on-insulator (SOI) have been engineered and widely used various electronic devices. These progresses have enabled the production of very powerful devices without compromising on the size and weight of the devices. At present, the size of a computer system has shrunk down to the size of a chip with the development of system-on-chip (SoC), something which is probably unthinkable in the past. Without doubt, these sophisticated technologies will continue to evolve as researchers continue to explore the quantum space in search of further improvement.

Nevertheless, such progresses are not without their pitfall. Most researches and studies in the early days emphasized on the electrical aspect to enhance device performance. Relatively little concerns have been placed over the thermal aspect, at least not until power density became a cause of concern as the size of electronic devices continued to shrink. In realizing that the aforementioned breakthroughs have directly led to heating issues, thermal management gained increased traction amongst researchers. As device size is shrunk to several microns or recently several nanometres, thermal management can no longer be investigated from the classical physics point of view alone.

In general, most of the modern day applications and implementations of semiconductor technologies still fall between the micro and nanoscale level, which ultimately lies in between the diffusive and ballistic limits. At the bulk level, thermal management is relatively straightforward as heat is transported in a diffusive manner easily explained by the Fourier Law. At the length scale of several nanometres however, thermal transport becomes fully ballistic and can only be explained with an in-depth understanding of quantum-mechanical science. Current modelling capabilities on heat transport at micro and nanoscale rely heavily on either the ballistic or diffusive approaches. Semi-classical theories in solid state physics involving the Boltzmann Transport Equation (BTE) are required to describe this semi-ballistic thermal transport behaviour (Ashcroft & Mermin 1976; Ziman 1960; Ziman 1964). These theories generally involved both classical and quantum-mechanical treatment. They zoom in to the subatomic level but treat the major heat carriers – phonons and electrons – as classical particles. While electrons are physical subatomic particle, phonons are basically just a term given to lattice vibrations. Although phonons are the major heat carriers in semiconductors, a complete analysis of the heat transport in semiconductors should consist of the interaction between phonons and electrons, which is a relatively unexplored research frontier (Phillpot & McGaughey 2005). Moreover, the available semi-classical theories are still relatively insufficient to completely predict the semi-ballistic heat transport behaviour at the micro and nanoscale and are unable to completely bridge the gap between ballistic and diffusive transports.

1.2 Research Motivation and Objectives

Increased power density, sophisticated boundaries, unconventional device structures and nano-engineered device materials are changing the usual pattern of heat transport, a phenomenon especially pronounced at the micro and nanoscale. An understanding of the heat transport at the micro and nanoscale is of significant importance to the design and development of the semiconductor devices at such length scales, and to prolong the life span of these devices. This fundamental study aims to explore the heat transport by both phonons and electrons at the micro and nanoscale. A valid theoretical model incorporating all the correct physics is developed to simulate the heat transport process. A breakdown of the scope and objectives is provided as follows:

1. To propose a methodology to simulate and investigate the ballistic / semi-ballistic phonon transport in semiconductors
2. To propose a methodology to simulate and investigate the ballistic / semi-ballistic electron transport in semiconductors
3. To propose a methodology to simulate and investigate coupled ballistic / semi-ballistic phonon and electron transport in semiconductors

The coupling requires careful consideration of the interactions between phonons and electrons. Once established, there will be endless possibilities with such fundamental simulations. One major application of these combined simulations would be the study of the electron-phonon transport inside nano-sized thin-film solar cells and photovoltaic cells. Without doubt, this can also be extended to other semiconductor devices at the micro and nanoscale.

1.3 Thesis Outline

This thesis consists of seven major chapters. Chapter 1 highlights the background and motivation of this research. Chapter 2 provides an overview to the theoretical background of thermal transport at the micro and nanoscale. This includes an introduction to the Boltzmann Transport Equation (BTE), which is the governing equation for semi-classical micro and nanoscale heat transport, and a brief discussion on

the solution via a stochastic approach known as the Monte Carlo (MC) method. The general algorithm for MC simulations is also provided. Chapter 3 highlights the solution to the BTE for phonon transport, which includes a speed-up strategy to reduce simulation times and required computational resources. Chapter 4 highlights the solution to the BTE for electron transport which includes a built-in Poisson‟s equation solver to account for the effect of electric field. The methodology for the coupling of the phonon transport and electron transport is discussed in Chapter 5. Chapter 6 provides the simulation results for phonon transport, electron transport and coupled phonon-electron transport, and also a parametric study of the MC simulation by using the phonon transport simulation. Chapter 7 concludes this thesis, while also proposing the possible future directions for this fundamental study.

CHAPTER 2

Theoretical Background

2.1 Thermal Transport at the Micro and Nanoscale

Modern day advancement of nanoscience and nanotechnology has resulted in the production of extremely small electronic components in the order of sub-100 nm. The ever growing obsession for small, compact yet powerful devices means increasing number of electronic components has to be assembled on a very small chip area to maintain a compact yet capable device. Intel co-founder George Moore has boldly predicted that the number of transistors on a chip will double approximately every two years (Moore 1998). However, the cramming of so many components onto a small chip invariably increases the power density and thus, heat generation inside the chip. The wide use of sophisticated semiconductor materials and nanostructures with relatively low thermal conductivity only add to the heat dissipation issue. This includes the use of derivative of semiconductor material with lower thermal conductivity than its original bulk form and also the use of complicated, irregularly shaped nanostructure which disrupts the normal motion of the heat carriers. In all these instances, poor thermal management will easily lead to device failure (Cahill, Goodson & Majumdar 2002; Pop 2010; Pop & Goodson 2006). As such, the demand for effective and efficient thermal management has never been more crucial. The issue on heat dissipation at such length scales calls for intense scrutiny by designers and scientists alike. It is of the utmost importance for them to comprehend the heat transport and dissipation patterns within

the designed components to prevent component failure, optimize component performance, and prolong component life (Phillpot & McGaughey 2005). To achieve this, the underlying law of physics at the micro and nanoscale has to be investigated. In classical physics, heat conduction in bulk materials is governed by the well-established Fourier Law, as represented by Eq. (2-1) below.

$$q = -k\nabla T \tag{2-1}$$

Fourier Law states that the rate of heat conduction through an area is directly proportional to the material‟s thermal conductivity and the temperature gradient across the material. However, at such length scales, it can no longer predict the transport behaviour accurately as it fails to capture the essence of the semi-ballistic and ballistic transport effect. The diminishing temperature gradient along with the reduction of medium thickness at the microscale and nanoscale renders thermal conductivity inaccurate (Ashcroft & Mermin 1976; Chen 2005; Wong & Mengüç 2008). To verify the type of transport phenomena, two parameters must be taken in account, namely the characteristic length of the medium of interest, l and wavelength of the energy propagation, λ (Wong & Mengüç 2008). The ratio of l *to* λ, ξ is given by Eq. (2-2) (Bong & Wong 2014; Péraud, Landon & Hadjiconstantinou 2014).

$$\xi = \frac{l}{\lambda} \tag{2-2}$$

When ξ is greater than unity ($\xi >> 1$), heat transport will be ballistic whereby the heat carriers are expected to travel without resistance from one end to the other (Zhang 2007). On the other hand, when ξ is reduced to below unity ($\xi << 1$), the heat transport is generally diffusive or semi-ballistic in which heat carriers undergo various scattering before travelling l. Within the later transport regime, the particle transport theories can be applied to describe the carrier transport process; otherwise the wave aspects such as tunnelling and interference must be accounted for (Chen 2005; Wong & Mengüç 2008; Zhang 2007). Within the scope of this thesis in which the micro and nano length scales will be both accounted for, a semi-ballistic transport behaviour will be placed under the spotlight.

The understanding of semi-ballistic transport requires thorough knowledge on carrier properties. This includes material properties such as phonon dispersion relations and electronic bands, as well as various scattering rates including carrier-carrier, carrier-impurity and carrier-boundary. Any transport model should incorporate the aforementioned information in certain. Most studies however, consider the physical electron transport and phonon transport separately. The accounting of both physical simulations in a combined electron-phonon simulation while maintaining all the important material properties and scattering effects remains relatively rare. To conduct a study on thermal transport in semiconductor materials, both of them should be accounted for and it would be most beneficial to understand their interactions. The importance of such an effect is significant such that it will provide insight to heat transport at nanoscale and will definitely aid in the effort of predicting the heat distribution in various nanostructures, which is generally an active on-going effort. Strategies for effective thermal management can then be carefully devised based on in-depth knowledge on the aforementioned matters.

To understand the thermal transport behavior, the mechanics of the carrier transport have to be understood. Snowden (Snowden 1998) provided a detailed explanation over the different approaches used in carrier transport. Classical carrier transport involves the treatment of carrier as particle. It is characterized by description of carrier transport based on the use of a single carrier distribution function. This only applies in diffusive transport at the macroscale but becomes questionable when the dimension considered approaches the nanoscale. In view of this, new semiconductor modelling techniques have been developed and refined over the years. Quantum mechanics form the basis of the carrier transport theories and include the wave nature of carriers involved, but are very complex both mathematically and theoretically. At the atomic level where carrier transport is ballistic, it is without doubt the best way to approach any transport problems. However, in the semi-ballistic regime, a combination of classical theory and quantum theory can be applied describe carrier transport. This combination is termed semi-classical, in which the motion of the carriers is described by classical mechanics while the collisions are treated by quantum approach. Vasileska et al. (Vasileska et al. 2008) provided a brief account on the evolution of the different transport models for semiconductor device modelling. Back in the early days of semiconductor boom,

classical and semi-classical approaches in the form of Drift-Diffusion (DD) models were widely applied. Since then, continual improvement and refinement were carried out to accurately capture the transport phenomena in the ever-shrinking devices. Hydrodynamic equation (HDE) and the Boltzmann transport equation (BTE) gain a commonplace in semiconductor device simulations, before the quantum approaches begin to gain traction for ultra-small scale devices. The latter involves adding quantum correction to the semi-classical approaches in more simplistic models, while the most exact ones involve Green‟s functions and Schrodinger equations. These highly complicated approaches are able to consider simultaneously correlations in space and time, which are essential in considering carrier transport at nanoscale. The amount of computational power required is often high, while the theoretical models and mathematical representations are often difficult to comprehend. Depending on the applications involved, certain modelling and simulation can do without going through those kinds of rigorous analytical analysis.

For the length scale being considered in this thesis, which range from several tens nanometers to several microns, a semi-classical approach is often sufficient and practical to predict the transport behavior. This involves the adoption of the particle transport theory based on the BTE whilst considering the various scattering mechanisms derived from quantum approaches. Such an approach is widely applied in simulations of electron transport and phonon transport in low-dimensional structures as well as coupled electron-phonon transport which has gained a lot of traction in the modern day.

2.2 The Boltzmann Transport Equation

The governing equation for particle transport in the semi-classical approach is the BTE. Anything that goes beyond the quantum limit will call for quantum approaches governed by Green‟s functions and Schrödinger equations, which is not within the scope of this thesis. The BTE was first derived in 1872 by Ludwig Boltzmann, initially as a means of describing dilute gases at the kinetic level and placed more interest in the velocity distribution function (Boltzmann 1964; Péraud, Landon & Hadjiconstantinou 2014). Since then, it appears extensively in various fields ranging from gaseous transport to solid state physics. In the simulation of carrier transport, the particle motion

is described classically based on the Liouville equation while the particle interactions are treated quantum-mechanically based on the perturbation theory. Its flexibility allows for combined electro-thermal simulations with self-consist computations related to electric field and the inclusion of various effects such as the dispersion relations. Within the scope of this thesis, it is applicable for both the phonon and electron transport provided the characteristic length of the medium is larger than the wavelength of the energy carriers.

In general, the BTE describes the statistical behaviour of a non-equilibrium thermodynamic system, for instance fluid with temperature gradients within a defined space. It is based on the concept that the particles can be characterized by their occupation of a position in space ($\vec{r}$) with momentum ($\vec{k}$) at a point in time (t) using a carrier probability distribution function $f(\vec{k},\vec{r},t)$ (Ashcroft & Mermin 1976; Wong & Mengüç 2008; Ziman 1960; Ziman 1964). The BTE describes the evolution of the distribution function as the particles experience scatterings and external forces along their trajectories and is given in its general form in Eq. (2-3) below.

$$\frac{\partial f}{\partial t} + \vec{v}_{\vec{k}} \cdot \nabla_{\vec{r}} f + \dot{\vec{k}} \cdot \nabla_{\vec{k}} f = \left(\frac{\partial f}{\partial t} \right)_{coll} \tag{2-3}$$

The terms of the left-hand side include the change of f with respect to t, $\vec{r}$ and $\vec{k}$, which are balanced out by the collision term on the right-hand side. Note that the third term on the left-hand side $\dot{\vec{k}} \cdot \nabla_{\vec{k}} f$ corresponds to external forces and is commonly associated with particles being accelerated through electric and / or magnetic fields. In cases when only phonons are considered as the heat carriers, this term will be neglected. For electron transport however, this term is significant as electrons are bound to accelerate through an applied field. The collision term meanwhile, is evaluated using the scattering probabilities of the heat carriers. Physically, the collision term can be pictured as the transitions or scatterings of the heat carriers which would alter their wave vector from the original state $\vec{k}$ to $\vec{k}'$ or vice versa and thus change their momentum. Mathematically, the collision term can be represented as follows.

$$\left(\frac{\partial f}{\partial t}\right)_{coll} = \sum_{\vec{k}'} \bar{W}\left(\vec{k}' \to \vec{k}\right) f' - \sum_{\vec{k}'} \bar{W}\left(\vec{k} \to \vec{k}'\right) f \tag{2-4}$$

It is vital to note that Eq. (2-4) applies well for phonons only. For it to be viable for electrons, it has to incorporate the Pauli exclusion principle as electrons are fermions and no two fermions can occupy the same quantum states simultaneously (Ashcroft & Mermin 1976; Ziman 1960; Ziman 1964). In contrast, phonons are bosons and are not subjected to the Pauli exclusion principle. Therefore, the collision term for electrons has to be modified as in Eq. (2-5).

$$\left(\frac{\partial f}{\partial t}\right)_{coll} = \sum_{\vec{k}'} \bar{W}\left(\vec{k}' \to \vec{k}\right) f'\left(1-f\right) - \sum_{\vec{k}'} \bar{W}\left(\vec{k} \to \vec{k}'\right) f\left(1-f'\right) \tag{2-5}$$

To date, the BTE models remain one of the main tools in analysis of various transport phenomena in semiconductor devices, ranging from radiation to phonon transport and electron transport. While recent studies have proven that the exact solutions to the BTE are always mathematically well-behaved because a perturbed system following the BTE in non-equilibrium will always return to its equilibrium state instead of diverging to infinity (Gressman & Strain 2010), the solution to the BTE is complicated and never straightforward. The three main approaches to solve the BTE are analytical, numerical and statistical approaches (Jacoboni & Reggiani 1983). The different approaches are normally applied under different circumstances depending on the type of outcome aspired. The deterministic approaches, such as analytical and numerical approaches, can be extremely complex due to the integro-differential nature of the BTE, in addition to the seven independent variables involved, including two directional angles (i.e., zenith and azimuthal angles), three space coordinates, time and the wavelength or frequency of the particles. Incorporation of realistic energy dispersion relations or band structures and scattering models can be a huge challenge. Assumptions are often made to simplify the solution process. This is sometimes undesirable as the solution might not reflect the true process occurring within the medium of interest. The MC method, a stochastic approach, provides an alternative to avoid the aforementioned issues. Widely regarded as one of the most accurate approaches to solve the BTE, the method relies on repeated random samplings in treating the transport process. The heat carriers, hereby referring to

electrons and phonons, are allowed to propagate and scatter around within the medium, thus mimicking the actual physics in reality. Complex geometries, phonon dispersion relations and the polarization branches or electron band structures, and relevant individual scattering processes can be incorporated for realistic analysis, thus minimalizing artificial assumptions. The method has its own major drawbacks in the past, mainly owing to the immense computational power required to generate the results. To obtain acceptable statistical convergence and thus reasonable results, the sample size involved has to be sufficiently large, which will inevitably increase the computational time. Nonetheless, such an issue is not a major constraint in the present day with the availability of advanced computational resources and various parallelization strategies (Cumber & Beeri 1998; Ni & Murthy 2009; Srinivasan, Miller & Marotta 2004; Wong & Mengüç 2008).

2.3 The Monte Carlo Method

The MC method in general, refers to computational algorithms that rely on repeated random sampling to obtain numerical results. This approach is stochastic and non-deterministic in nature. It uses probabilities to solve problems that might be deterministic in principle, and is commonly deployed when other solution approaches are deemed too complicated or close to impossible. Throughout the years, the method has been an important tool for solving complex estimation and optimization problems in engineering, finance, statistics, mathematics, computer science, and the physical and life sciences (Kroese et al. 2014). Its popularity stems from its versatility and flexibility in treating complex scenarios, especially in solving problems with a probabilistic interpretation. In this work, it is applied to the BTE, which is essentially an integro-differential equation – involving differentials on the left hand side and integrals on the right hand side (see. Eqs. (2-3) to (2-5)). In simple terms, the working principle of the MC method can be explained using the scenario as shown in Figure 2.1. By assuming a single valued function f shown in the figure, the goal is to determine the integral of the function f, which is basically the area under the curve. To implement the MC method, two parameters are needed – f_{max} and x_{max}, which denote the maximum of f and x respectively. Two independent random numbers between 0 and 1 are drawn, each multiplied with f_{max} and x_{max} respectively to obtain one set of coordinate, or in this case,

also referred to as a sample. This sample will then be checked if it is above or below the curve. In general sense, any samples that lies below the curve will be "accepted", while anything above the curve will be "rejected". The maximum area under the graph – assuming a rectangle which encompasses f_{max} and x_{max} (as represented by the dotted lines in Figure 2.1) is determined by the product of f_{max} and x_{max}. The exact area under the curve can thus be determined by taking the fraction of the total number of samples "accepted" against the total number of samples obtained, and multiply with the maximum area under the graph. Statistically speaking, the accuracy of the outcome is also heavily dependent on the number of samples used. If insufficient samples are drawn, the outcome may be skewed. The "randomness" of the samples is another key as it has to ensure that the entire spectrum of the possible outcomes can be covered. The outcome should be repeatable using different set of random numbers and samples in order to justify its validity. Most MC methods tend to follow a distinct pattern such that a domain of possible inputs will be pre-defined at the beginning, followed by the generation of random input from the probability distribution over the domain which is then used in the computation on the inputs. The deterministic results will be aggregated, following a converging pattern, and will be accepted once an acceptable convergence is achieved.

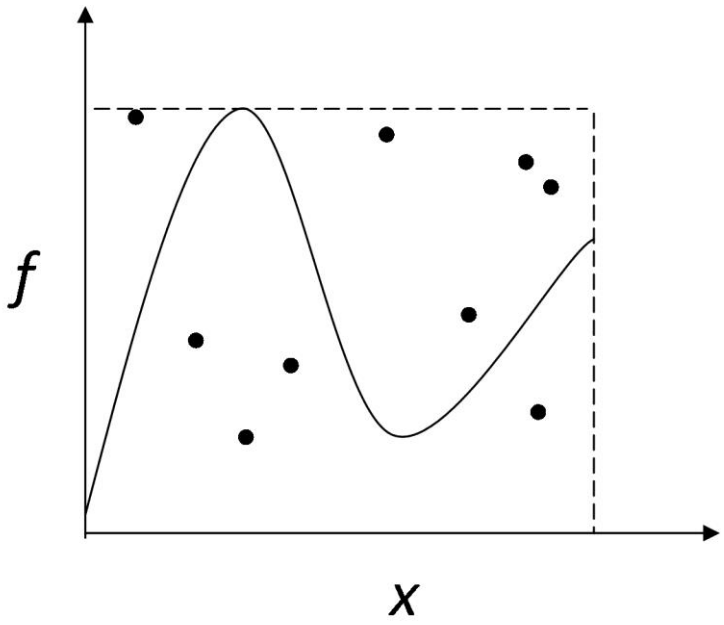

Figure 2.1 An example of how the MC method can be used to solve an integral equation.

Since the first application of the MC method in this research field in 1966 (Snowden 1988), it has been used extensively to simulate various carrier transport phenomena in semiconductors. Some of the major advantages of this method include transparent microscopic interpretation of transport phenomena, relatively easier extension to time- and space-dependent transport phenomena, and relatively easier inclusion of realistic energy dispersion relation / band structure and scattering mechanisms (Jacoboni & Reggiani 1983). The MC approach is termed semi-classical because scattering mechanisms can be treated quantum-mechanically, often using the Fermi‟s Golden Rule, while the carrier propagation is often treated based on the classical particle theory. The models work on the tracking of particle trajectories and choosing the distinct scattering mechanisms encountered stochastically, while minimizing the assumptions on the form of carrier distribution in any of the *k*-space involved. To put it simply, for all carrier motion consisting of free flights interrupted by various scattering mechanisms, the computer will simulate the trajectories of all the energy carrying particles (assumed to be in random motion unless acted upon by an external force such as electric field) as they move across space in between defined boundaries. All scattering events, free flight durations and trajectories of these simulated particles are determined through the use of large amounts of random numbers. In most cases, a pseudo-random number generator is used, in which the numbers generated may not be completely random as they are determined by a set of initial values commonly known as random seed. However, this has been proven to be a reliable and cost-effective way as compared to hardware generated random number, and are widely used in MC simulations. The degree of randomness is significant and cannot be underestimated, as it will ultimately have an effect on the results generated. However, this represents a separate topic and will not be discussed in detail in this thesis.

In the past, the MC method has been widely deployed to study electron transport in the fields of microelectronics where electronic characteristics receive most attention, having been spurred by the advancement in the semiconductor industry (Snowden 1988). It has been used to theoretically study electron transport in some of the most common semiconductors, such as Si, Ge and gallium arsenide (GaAs). The MC method allows the incorporation of complicated band structures and the relevant scattering properties to ensure accurate theoretical studies which compare well to the experimental results in

the literatures. To date, there are various simulators for electron transport which can be found commercially and within the literatures, each of them build upon different simulation models with different assumptions and simplifications. While most electron transport has sights set on studying the electronic characteristics, the phonon transport area has centred mostly on heat conduction and dissipation characteristics. Again, various MC simulation models have been built to incorporate information the dispersion relations as well as relevant scattering rates, with different level of depth depending on the expected outcome. It has to be noted that however, phonon transport only gained traction amongst researchers in more recent years due to the increased concern over heating issues in very small semiconductor devices. It represents a relatively „new" research frontier as compared to electron transport, and available MC simulation models for phonon transport remains relatively fewer as compared to the MC simulation models for electron transport. All these independent transport models have been well documented in various literatures over the years and will not be discussed in detail in this chapter (Bong & Wong 2014, 2015a, b, 2016; Brunetti et al. 1981; Canali et al. 1975; Chen et al. 2005; Fischetti & Laux 1996a; Fischetti & Laux 1988; Hao, Chen & Jeng 2009; Jacoboni & Reggiani 1983; Jeng et al. 2008; Kukita, Adisusilo & Kamakura 2013; Lacroix, Joulain & Lemonnier 2005; Lacroix et al. 2006; Maltby & Kornblum 1990; Mazumder & Kersch 2000; Mazumder & Majumdar 2001; Mittal & Mazumder 2010; Péraud 2011; Péraud, Landon & Hadjiconstantinou 2014; Pop, Dutton & Goodson 2004; Randrianalisoa & Baillis 2008; Sangiorgi, Ricco & Venturi 1988; Sidorov, V'yurkov & Orlikovsky 2004; Snowden 1988; Wang, Quan & Ruan 2011; Wong 2001; Wong et al. 2013; Wong, Francoeur & Pinar Mengüç 2011; Wong & Mengüç 2002; Wong & Mengüç 2004; Wong & Mengüç 2010). In the following section, the general algorithm of the MC method for any carrier transport phenomena will be discussed.

2.4 General Monte Carlo Algorithm for Carrier Transport

The MC method is one of the most versatile methods in solving the BTE for carrier transport problems. The simulation procedure is generic for all carrier transports (Wong & Mengüç 2010) in which they are all treated as randomly propagating „particles". Each of these „particles" is defined by its position within the medium, direction of

propagation and energy level. These „particles" are launched from within the medium and pre-defined source locations such as temperature boundaries. They are then allowed to randomly propagate, and their direction and energy level will be modified according to the corresponding scattering rates. To put it simply, the „particles" represent parcels of energy being passed through a medium. By tallying the „particles" at any point in time, a snapshot of the total energy level within the medium at that particular point can be obtained. A look into a history of this number tally will provide a snapshot of how energy is transferred in the medium, thus allowing the understanding of how energy is transported across the medium.

In most simulations, the number of „particles" that exists at any point in time could be huge, and thus rendering the tracking tedious. In any simulations, efficiency in terms of simulation time and computational resource, while ensuring acceptable results, is pivotal. Therefore, these energy carriers are often clustered together in a statistical "ensemble". Each ensemble represents a certain number of energy carriers with similar characteristics, which is represented by a scaling factor, $W_{scaling}$. $W_{scaling}$ is determined by dividing the initial number of energy carriers with the number of ensembles desired, as shown in Eq. (2-6). This approach is widely known as the ensemble MC method, which allows for more efficient solution process However, $W_{scaling}$ must be carefully defined so as to ensure there are statistically sufficient samples to minimize the statistical noise in the outcome of the simulation. This will be further discussed in the parametric study in Chapter 6.4.

$$W_{scaling} = \frac{N_{carrier,ini}}{N_{en,m}} \tag{2-6}$$

In general, MC simulations will start with the setting up of a grid system for storing carrier histories. A prescribed number of statistical ensembles will be launched with initial launching locations and angles. These ensembles will be allowed to move along a straight path following randomly drawn distance of interaction (distance travelled without encountering any absorption or scattering event) and direction of propagation. They will be allowed to propagate and scatter for as long as they remain within the medium. In the event that they hit the wall, they will be reflected back into the medium.

Once they exit the medium, they will no longer be a subject of interest and will be deleted from the history.

2.4.1 Sampling Initial Positions, Launching Angles and Scattering Angles

The exact positions of the simulated ensembles are commonly defined using the Cartesian coordinate system. The launching angles and scattering angles, as well as the direction cosines however, are defined using spherical coordinate system. The definition of the spherical coordinate system used in this thesis is shown in Figure 2.2, followed by the common geometries considered in MC simulations for carrier transport in Figure 2.3. The geometry of the medium of interest is commonly assumed as a cuboid. Very few available studies have accounted for the exact cylindrical boundary treatment of the boundary condition. For any of these boundaries, the principle for the sampling of initial positions, launching angles and scattering angles is similar. Ensembles are launched from within the medium and from the temperature boundary. For a cuboid geometry considered, initial positions of the ensembles are determined by multiplying a random number between 0 and 1 to the maximum dimensions in the *X*-, *Y*- and *Z*-directions (hereby refer to as *X*, *Y* and *Z* respectively) as shown in Eqs. (2-7) to (2-9) below.

$$x = R \times X \tag{2-7}$$

$$y = R \times Y \tag{2-8}$$

$$z = R \times Z \tag{2-9}$$

It is vital to note that the random number for sampling of location in the in the *X*-, *Y*- and *Z*-directions must be different. These random numbers will be sampled every time during the determination of a location in the in the *X*-, *Y*- and *Z*-directions respectively, so as to ensure a higher degree of randomness, and a more realistic representation of the random locations of the energy carriers.

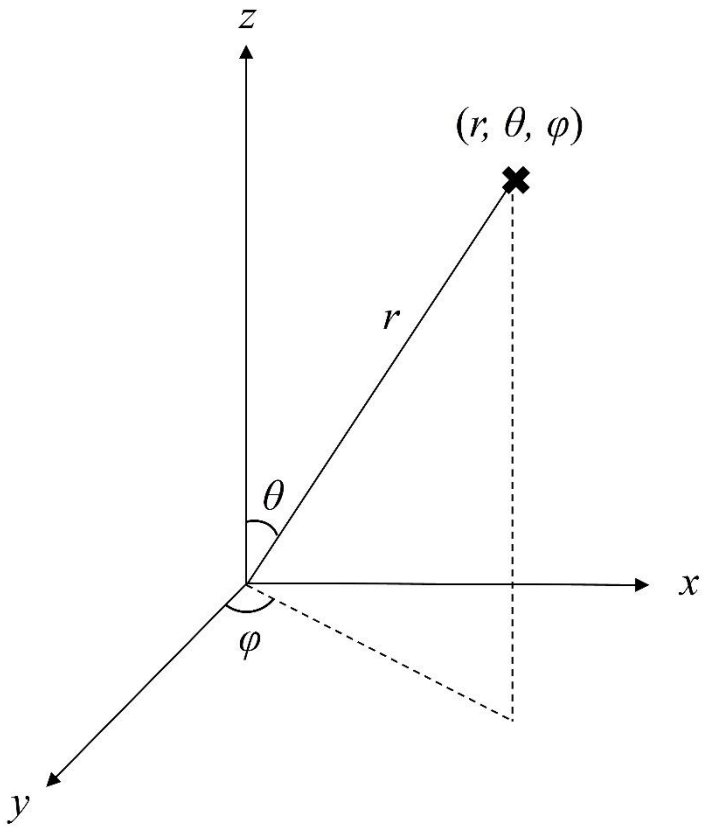

Figure 2.2 The spherical coordinate system used in this thesis, including the definition of the polar and azimuthal angles.

If any of the ensembles are launched from any of the boundaries however, *R* can only be taken as 0 or 1. On some rarer occasions where cylinder is considered, the sampling of initial positions in the *X*- and *Y*-directions has to be done using the maximum radius and the maximum azimuthal angle. Eqs. (2-10) and (2-11) below are referred.

$$x = R \times \frac{d}{2} \times \cos(\varphi) \tag{2-10}$$

$$y = R \times \frac{d}{2} \times \sin(\varphi) \tag{2-11}$$

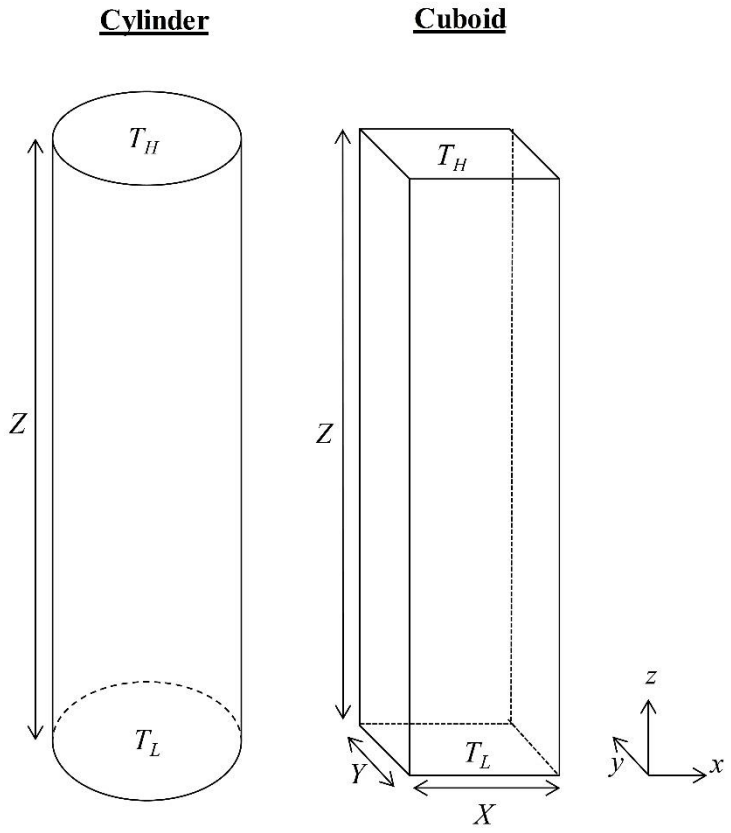

Figure 2.3 The geometry of the medium of interest is commonly assumed as a cuboid. Very few available studies have accounted for the exact cylindrical boundary treatment of the boundary condition (Bong & Wong 2015a).

For position in the *Z*- direction, Eq. (2-9) still applies. The initial azimuthal angle can be determined by Eq. (2-12)

$$\varphi = R \times 2\pi \tag{2-12}$$

Once the initial positions are established, the launching angles need to be sampled. For ensembles to be launched from within the medium with isotropic nature, the launching and scattering angles will be uniform in all directions. This will be also the scenario when the ensembles encounter isotropic scattering within the medium. Sampling of the angles within the medium and from the isothermal boundary is slightly different mainly in terms of the sampling of the ensemble"s polar angle of emission θ. Within the

medium, θ is sampled from a solid angle following Eq. (2-13) by assuming that the ensembles have a uniform chance to propagate in all spherical directions.

$$\int_0^{2\pi}\int_0^{\pi}\sin\theta d\theta d\varphi = 4\pi \tag{2-13}$$

The CPDF for sampling θ is thus derived as

$$R(\theta) = \frac{1}{2}\int_0^{\theta}\sin\theta d\theta = \frac{1}{2}(1-\cos\theta) \tag{2-14}$$

Replacing $R(\theta)$ with a random number, Ran_θ, θ can be found by the following

$$\theta = \cos^{-1}(1-2Ran_\theta) \tag{2-15}$$

The azimuthal angle, ϕ on the other hand, can be sampled via

$$\varphi = 2\pi Ran_\phi \tag{2-16}$$

In contrast, the ensembles launched from the isothermal boundary are assumed to diffuse into the medium hemispherically as shown in Figure 2.4, following Eq. (2-17).

$$\int_0^{2\pi}\int_0^{\pi/2}\cos\theta\sin\theta d\theta d\varphi = \pi \tag{2-17}$$

This scenario also applies to the ensembles being reflected back into the medium from any of the diffusive and adiabatic boundary, as compared to a specular and adiabatic boundary in which the law of reflection is abided. The CPDF for sampling θ is thus derived as

$$R(\theta) = 2\int_0^{\theta}\cos\theta'\sin\theta' d\theta' = \sin^2\theta \tag{2-18}$$

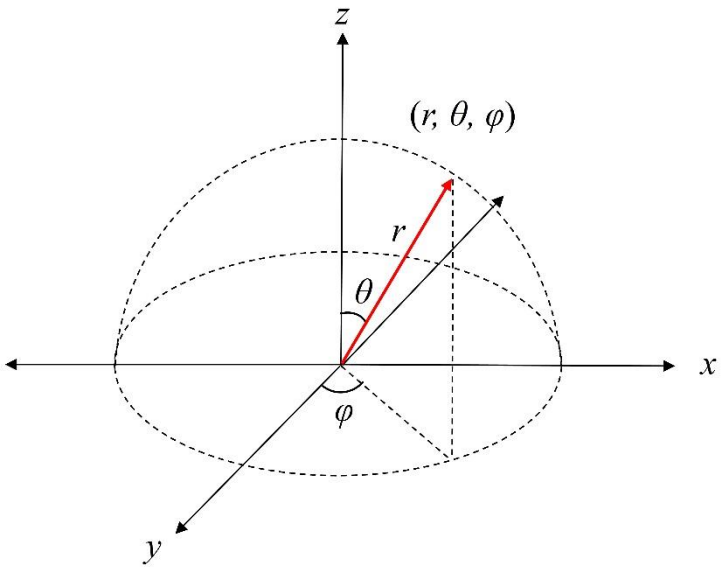

Figure 2.4 Sampling of launching angles from the boundary. Ensembles are launched hemispherically from the boundary.

Replacing $R(\theta)$ with a random number Ran_θ, θ can be found by the following

$$\theta = \sin^{-1}\sqrt{Ran_\theta} \tag{2-19}$$

The azimuthal angle, on the other hand, remains the same as Eq. (2-16).

2.4.2 The Three-Dimensional Ray Tracing Algorithm

The three-dimensional ray tracing method is used to trace each ensemble within the medium of interest. Assuming that the initial position and direction of the ensemble are known priori, this step aims to establish a fixed coordinate frame in which all ensemble coordinates, before and after scattering, are expressed. A moving coordinate frame is however, required during scattering events since the polar angle is sampled with respect to the direction of propagation. Therefore, it is vital to map the moving coordinate frame of the scattered direction cosines onto the fixed coordinate frame after the scattering events, to ensure all ensemble coordinates can be calculated and recorded accordingly in the simulation. An example of the trajectory is shown in Figure 2.5.

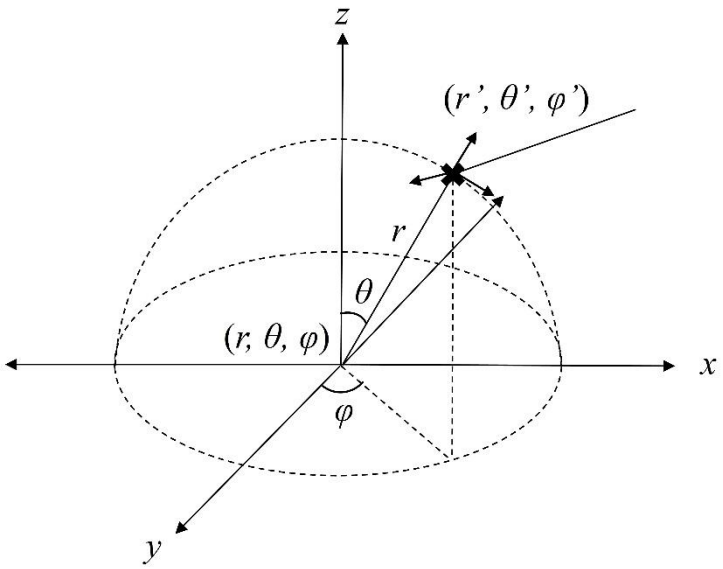

Figure 2.5 Example of trajectory from initial position (r, θ, φ) to scattered position (r', θ', φ'). The scattered direction cosines must realign itself according to the newly determined direction.

As previously discussed, each ensemble carries a discrete amount of energy as it propagates through the medium. Only when it encounters a scattering event, this energy is altered. The velocity of the ensemble can be determined from the phonon dispersion relation or electron band structure by simply determining the gradient of the phonon dispersion relations (see Chapter 3.3) and the electronic band structures (see Chapter 4.3). With the known velocity and the specified time interval, the distance travelled by the ensemble is determined by

$$S = v\Delta t \tag{2-20}$$

Using S, as well as the previous location (x_{old}, y_{old}, z_{old}) and direction cosines (μ_x, μ_y, μ_z), the new location can be determined via the following equations.

$$x_{new} = x_{old} + \mu_x S \tag{2-21}$$

$$y_{new} = y_{old} + \mu_y S \tag{2-22}$$

$$z_{new} = z_{old} + \mu_z S \tag{2-23}$$

In the case of isotropic scattering in which it is assumed that scattering is equal in all directions, obtaining the new direction cosines is a straightforward matter as the moving coordinate frame is not required. The direction cosines of the ensembles can thus be obtained by:

$$\mu_x = \cos\varphi \sin\theta \tag{2-24}$$

$$\mu_y = \sin\varphi \sin\theta \tag{2-25}$$

$$\mu_z = \cos\theta \tag{2-26}$$

However, when scattering is anisotropic, the direction cosines of the ensembles need to be modified accordingly. The moving coordinate frame is required because the polar and azimuthal angles after scattering are measured with the respect to the propagating direction. The scattered direction cosines (μ'_x, μ'_y, μ'_z) are computed based on its incident direction cosines (μ_x, μ_y, μ_z) and the polar and azimuthal scattering angles (θ, φ). They are given as (Ding & Shimizu 1996; Joy 1995; Wang & Jacques 1992; Wong 2001; Wong & Mengüç 2008; Wong & Mengüç 2010):

$$\mu'_x = \frac{\sin\theta}{\sqrt{1-\mu_z^2}}\left(\mu_x\mu_z\cos\varphi - \mu_y\sin\varphi\right) + \mu_x\cos\theta \tag{2-27}$$

$$\mu'_y = \frac{\sin\theta}{\sqrt{1-\mu_z^2}}\left(\mu_y\mu_z\cos\varphi + \mu_x\sin\varphi\right) + \mu_y\cos\theta \tag{2-28}$$

$$\mu'_z = -\sin\theta\cos\varphi\sqrt{1-\mu_z^2} + \mu_z\cos\theta \tag{2-29}$$

This set of equations is commonly used in solving the Radiative Transfer Equation (RTE) where scattering by particles is often anisotropic. For the condition where $\mu_z \sim 1$, Eqs. (2-27) to (2-29) becomes undefined. Therefore, Eqs. (2-24) to (2-26) are to be used instead. Notice that in the scattering event, the scattered polar angle (i.e. θ) is always defined with respect to the μ_z-direction cosine.

2.4.3 Accounting for Isothermal and Adiabatic Boundary

Two major types of boundaries are defined in the simulation: the adiabatic boundary, and the isothermal boundary. When an ensemble encounters the adiabatic boundary, it is reflected back into the medium following an angle of reflection. In cases where specular reflection is defined, the reflected angle is the same as the incident angle, adhering to the law of reflection. This is useful for simulation of thin films, in which the dimensions in the *X*- and *Y*-directions can be reduced. Under such circumstance, it can be assumed that these two dimensions are of infinite length, and the simulation thus becomes essentially one directional (i.e. in the *Z*-direction) (Bong & Wong 2014; Wong, Francoeur & Pinar Mengüç 2011). On the other hand, a literal surface can be taken into account by considering a diffusive reflection. This scenario is analogical to launching an ensemble from the boundary assuming isotropy. The azimuthal and polar angles can be determined following Eqs. (2-16) to (2-19) respectively. The diffusive boundary scattering mechanism in the *XY*-plane for both geometries, namely cylinder and cuboid, is depicted in Figure 2.6. In the event where the boundary is encountered, the exact point at which an ensemble hits the boundary can be determined easily by solving the simultaneous equation involving its trajectory and the boundary plane. For the cuboids, the solution is straightforward. For example, knowing that the phonon ensemble exits on the *X*-plane, the corresponding *Y*- and *Z*-coordinates can be computed using that *X*-coordinate (i.e. the plane) can be found using the following set of equations.

$$m_x = \frac{x_{bound} - x_{ini}}{x_{final} - x_{ini}} \tag{2-30}$$

$$y_{bound} = m_x \times \left(y_{final} - y_{ini} \right) + y_{ini} \tag{2-31}$$

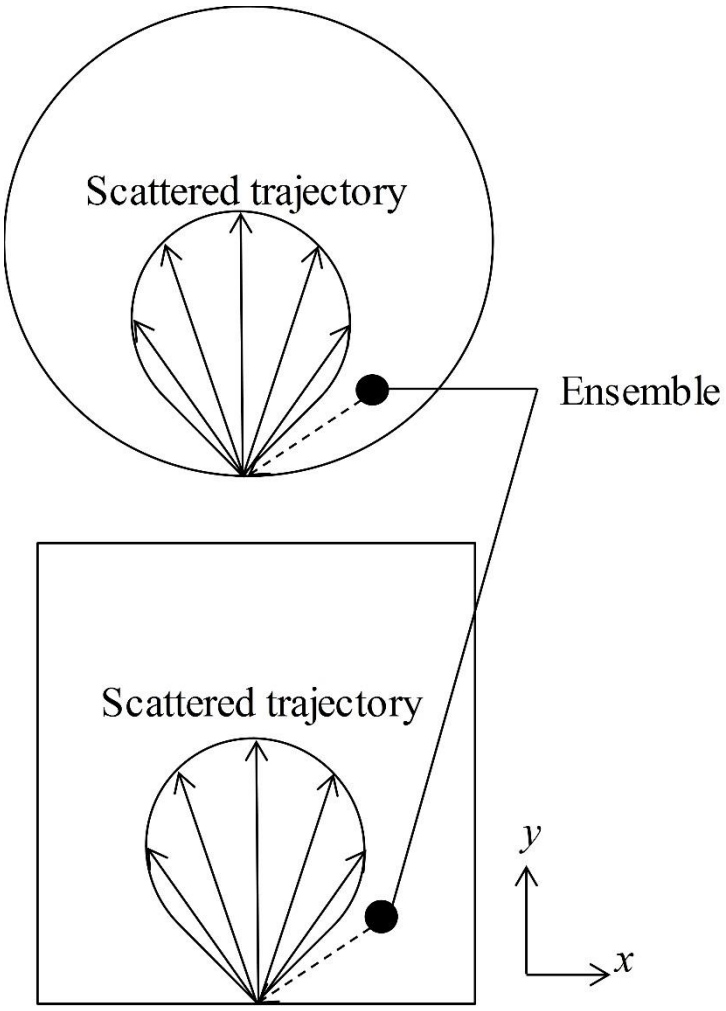

Figure 2.6 The diffusive boundary scattering mechanism in the XY-plane, in which the particle is assumed to be relaunched back into the medium at the boundary surface, and have equal chances of being launched in any angles (Bong & Wong 2015a).

$$z_{bound} = m_x \times \left(z_{final} - z_{ini} \right) + z_{ini} \tag{2-32}$$

Note that the subscripts *ini* and *final* denote the initial and final location of the ensemble during that particular trajectory. For the intersection point on the curved surface of the cylinder, the following equations need to be solved to obtain the *X*- and *Y*-coordinates, while the *Z*-coordinate can be found using Eq. (2-32).

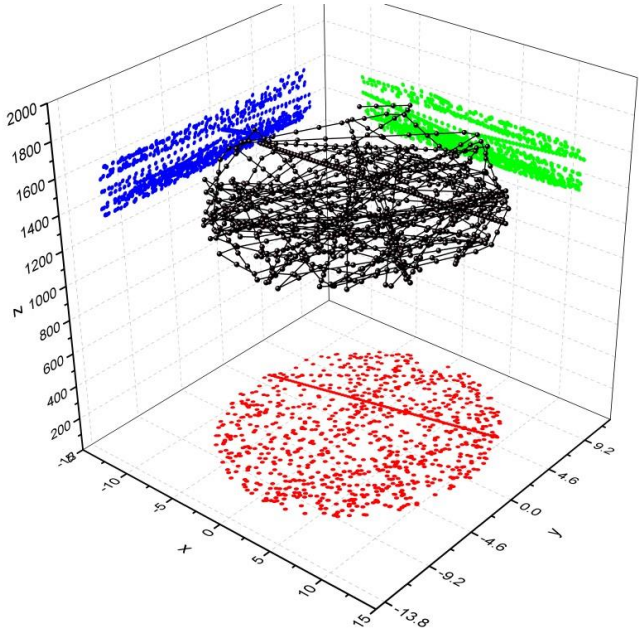

Figure 2.7 A plot of the trajectory of a random ensemble within a cylindrical medium with a diameter of 20nm (d = 20nm) and a length of 2000nm (L = 2000nm). This is analogous to the carrier transport within a nanowire (Bong & Wong 2015a).

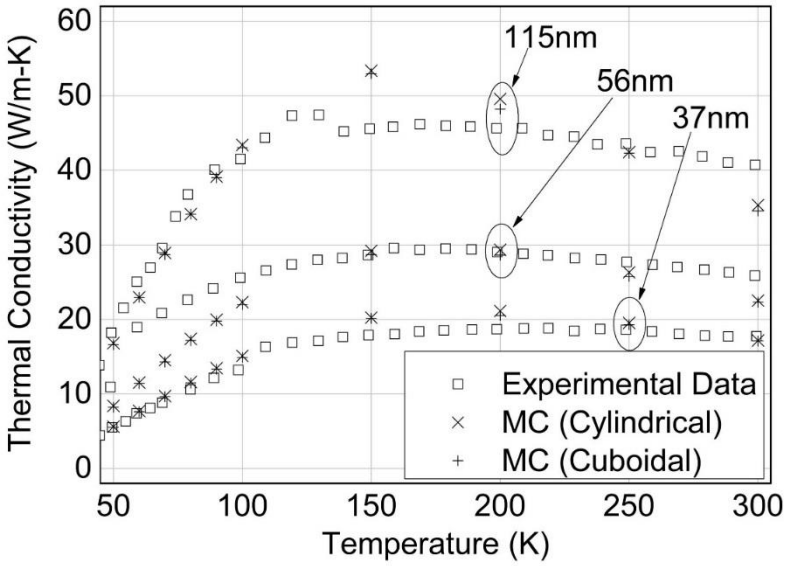

Figure 2.8 A plot of the comparison between experimental data (Li et al. 2003) and results obtained from the MC phonon simulations for Si nanowires of diameter 115nm, 56nm and 37nm at temperature range of 50K – 300K in the current work (Bong & Wong 2015a).

$$m = \frac{y_{final} - y_{ini}}{x_{final} - x_{ini}} \tag{2-33}$$

$$\left(m^2 + 1\right) x_{bound}{}^2 + 2mkx_{bound} + \left(k^2 - \frac{d^2}{4}\right) = 0,\ k = y_{ini} - mx_{ini} \tag{2-34}$$

$$y_{bound} = mx_{bound} + k,\ k = y_{ini} - mx_{ini} \tag{2-35}$$

Part of the trajectory of a simulated ensemble within a cylindrical medium is plotted, as shown in Figure 2.7. The cylindrical medium is assumed to have a diameter of 20nm (d = 20nm) and a length of 2000nm (L = 2000nm). This is analogous to the carrier transport within a nanowire (Bong & Wong 2015a). The XY-projection verifies that the ensemble is indeed confined within a circular boundary. In any case that it hits the circular boundary, it will be scattered back into the medium diffusively. However, within this thesis, the sole focus would be placed on the use of cuboid medium for simulations of the phonon and electron transport, as with most scenarios found in the literatures. A plot of the comparison between experimental data (Li et al. 2003) and results obtained from our MC phonon simulations for Si nanowires of diameter 115nm, 56nm and 37nm at temperature range of 50K – 300K is provided in Figure 2.8. In general, the results are observed to be consistent with the experimental data, with minimal differences observed for the use of cylindrical and cuboidal medium, although the thermal conductivities predicted by cylindrical boundary model tend to be slightly higher than that predicted by the cuboidal boundary model. A point to note is that in both models, the total computational volume of the medium is maintained constant by equating both cross sectional areas for a more relevant comparison between the two. Although the difference in the simulation results is insignificant, it remains interesting to investigate the extent of the effect of a curved boundary as compared to squared ones, as well as different heating phenomena such as heating up of the curved boundary instead of the planar boundary at both ends of the cylinder. Recent studies from Kukita et al. (Kukita, Adisusilo & Kamakura 2014) has also included the treatment of cylindrical boundary in their model, while also taking into consideration a realistic phonon dispersion relation. This would be particularly useful in helping to understand

heat dissipation issues for cylindrical nanowires in the future. However, this is not within the scope of this thesis and will not be scrutinized here.

The second boundary condition – the isothermal boundary, or temperature boundary – is the boundary at which temperature is applied. At these boundaries, ensembles are launched into the boundary, with the azimuthal and polar angles again determined by Eqs. (2-16) and (2-19) respectively. When the ensembles encounter these boundaries and are found to exit them, they are „deleted" from the history and will no longer be simulated in the next iteration. In other words, the simulation will take it as energy being transferred into the medium when ensembles are launched into the medium, and vice versa. The net number of ensembles entering or leaving these boundaries would represent the net amount of energy transferred.

2.4.4 Accounting for Scattering Events

MC models can be designed and built to simulate both the steady state and transient state. In most carrier transport involving phonons and electrons, it is common to have transient models. Under such circumstance, the important parameter is the relaxation time of the ensemble, and the probability of an ensemble being scattered in a given time step, Δt can be related to its relaxation time, τ by the following equation. (Wong & Mengüç 2008):

$$P(\Delta t) = 1 - \exp\left(-\frac{\Delta t}{\tau}\right) \tag{2-36}$$

Clearly, as the Δt increases, so is the probability of scattering. Within the defined Δt, the ensembles are allowed to travel ballistically (i.e. without encountering scattering event or absorption scenario) from one point to the next within the medium. This can also be termed as a free flight, and a random number will be drawn at the end of it to compare with $P(\Delta t)$ computed in Eq. (2-36). A scattering event occurs when the random number is smaller than $P(\Delta t)$. To speed up the MC simulations, it is common to construct a cumulative probability density function (CPDF) for ensemble scattering between a particular time, t and the following one, $t + \Delta t$ at the beginning of simulations. Results

can be tabulated and retrieved during simulation later. If several scatterings are included in τ, another random number has to be drawn to decide which scattering occurs, following the aforementioned comparison method. Common types of scattering incorporated include elastic scattering and inelastic scattering. The common strategy to treat these scattering events is to change only the direction of propagation in elastic scattering events, while in inelastic scattering events, both the energy and direction of the ensemble are altered (Wong & Mengüç 2010). Such transient models are especially handy to scrutinize the time evolution of phonons and electrons, which ultimately shows the evolution of the temperature distribution within the medium.

2.4.5 Storage and Normalization of Carrier Histories

The information of all the ensembles within the medium has to be collected and stored for later computations and analysis. To achieve this, computational grids are needed to tally the contribution of each of the ensembles at any location points within the defined space. These computation grids are set up to represent infinitesimal control volume which contains discrete number of ensembles. For the sake of simplicity and normalization, each of these control volumes is represented by the center grid point. In the case of one direction simulations, the medium of interest can be defined as shown in Figure 2.9. It is also vital to note that one of the advantages of the MC method is that grid discretization is unlikely to cause errors in the generated results, unlike most other numerical methods. However, the computational grid size must be chosen such that it is more than the mean free path of the energy carrier. A scenario of energy carrier travelling ballistically past any computational grid would adversely affect the results of the simulation. Secondly, it should not contain too few energy carriers to be representative of any realistic scenario. This would lead to statistical noise in the final results obtained, and affect the convergence of the simulated results. In summary, the general algorithm for the MC method in solving the BTE for phonon and electron transport can be described as in Figure 2.10. More detailed accounts for each of the transport models will be discussed in the Chapter 3 for phonon transport and Chapter 4 for electron transport.

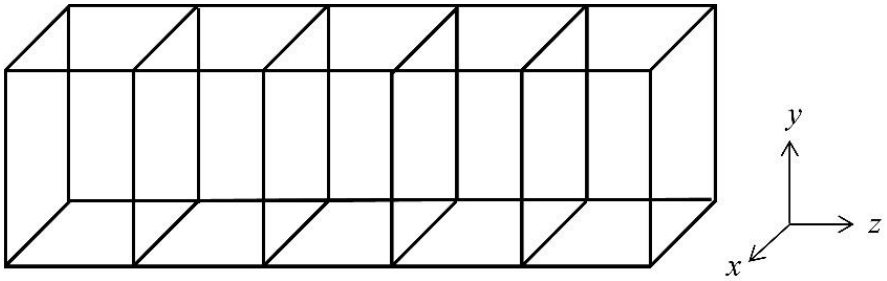

Figure 2.9 A sample of the computational grid for storage and normalization of carrier histories.

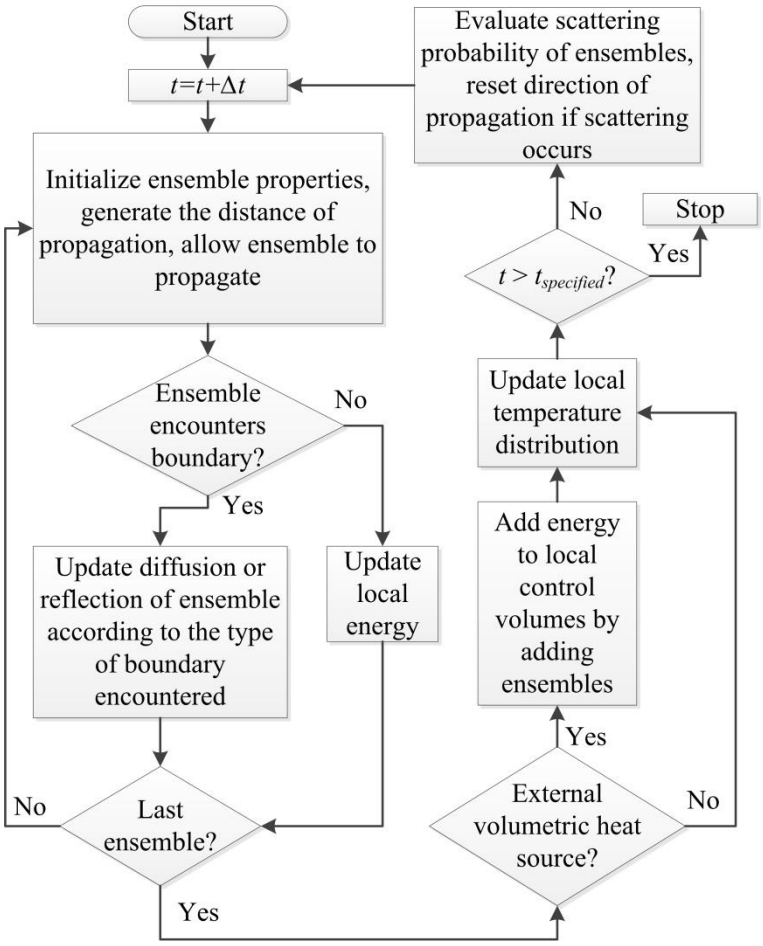

Figure 2.10 A general flow chart for transient MC simulations of independent phonon and electron transport.

CHAPTER 3

Monte Carlo Simulation for Phonon Transport

3.1 Overview of the MC Phonon Transport Simulation

Phonon is a term given to quanta of energy due to lattice vibrations in a material. It is the main heat carrier in semiconductors and insulators where a scarcity in free electrons clearly implies that only a small fraction of the energy would be carried by the charged particles (Cahill et al. 2003; Cahill, Goodson & Majumdar 2002). As aforementioned, with the increased use of semiconductors such as Si, Ge and GaAs, and insulators in electronic components, coupled with the rigorous miniaturization process over the years which have seen increasing number of electronic components packed into an ever-shrinking integrated circuit, it is becoming increasingly important to gain insights to the phonon behaviour and its impact on the heat transport in solids at the nanoscale to resolve issues pertaining heat dissipation (Pop & Goodson 2006). This is not only important to enhance heat dissipation, but also to prevent device overheating and prolong component life.

While early studies have been mostly related to electron transport due to the necessity to enhance electrical properties, increased emphasis has been placed on phonon transport, which is directly responsible for heat transport particularly in semiconductors. The main

concern in such studies often involves thermal conductivity. Indeed, when approaching the nanoscale, the diminishing thermal gradient means heat is transferred from one end to another much faster than anticipated. Without any good dissipation measures, it will accumulate and escalate the temperature within the medium, thus leading to device failure. With this basic understanding, various studies on phonon transport have been conducted. Meanwhile, a more recent notable study has proven that there is a difference in the in-plane and cross-plane thermal conductivities (Terris et al. 2009). This may lead to further studies on the effect of crystallographic directions and anisotropic scatterings, and may be utilized in favour of better heat dissipation mechanisms, or better thermoelectric properties. Speaking of thermoelectric, it would be tough to leave out recent studies on phonon transport involving utilization of the low thermal conductivity for better thermal management and possibly, power scavenging by making use of the thermoelectric properties and thermos-photovoltaic energy conversions (Chen 2006; Chen, Narayanaswamy & Dames 2004; Chen et al. 2000). The growing interest in these fields calls for better understanding of the phonon transport in addition to the electrical properties and has led to phonon engineering in nanostructures and the relevant materials. The BTE of phonon transport can also be expressed in terms of phonon intensity when the distribution function is not of interest. Often, the transformed equation is referred to as the Phonon Radiative Transfer Equation (PRTE) (Chen 2005; Wong & Mengüç 2008). Cahill et al. (2003) has reviewed the nanoscale thermal transport in terms of phonon transport and also briefly discussed the MC approach for use in such studies. In developing the phonon transport simulation, the correct dispersion relations and interactions between the longitudinal and transverse branches during the propagation process must be included. The importance of incorporating the former information has been justified by the results from Ju and Goodson (1999): if phonon dispersion in Si is neglected, the average mean free path of phonons is only about 43 nm, as opposed to 300 nm when dispersion is accounted for. The information on polarizations on the other hand, has been absent in most prior studies. The three-phonon scattering algorithm was used to account for transition of phonons between the polarization branches, and frequency dependent phonon lifetimes. By using that model, it was found out that transverse acoustic phonons are dominant in heat transport in Si at temperatures above 100K (Mazumder & Majumdar, 2001). Lacroix et al. (2005) studied the transient phonon transport in Si and Ge using a model which takes into account

media frequency properties through the dispersion curves for longitudinal and transverse acoustic branches like previous studies by Mazumder and Majumdar (2001). The approach has also been referred to by Wong & Mengüç (2011).

In this thesis, the BTE of phonon transport is solved using a speed-up version of transient MC method previously published in Numerical Heat Transfer, Part B: Fundamentals (Bong & Wong 2014). A transient MC model, which uses a reference temperature for truncating unnecessary phonon propagation, is presented with the inclusion of the phonon polarizations, dispersion relations and the relevant scattering rates. A flow chart of the phonon transport procedures is provided in Figure 3.1, while a schematic view of the medium geometry considered in this work is provided in Figure 3.2.

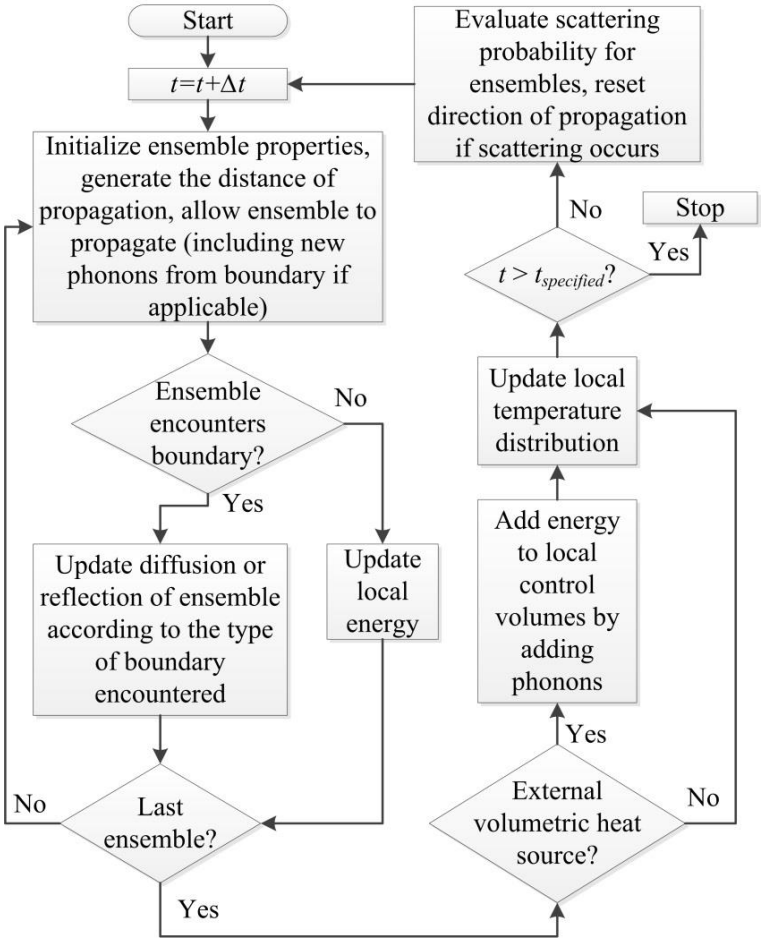

Figure 3.1 Flowchart of the MC phonon simulation algorithm applied in this thesis (Bong & Wong 2014).

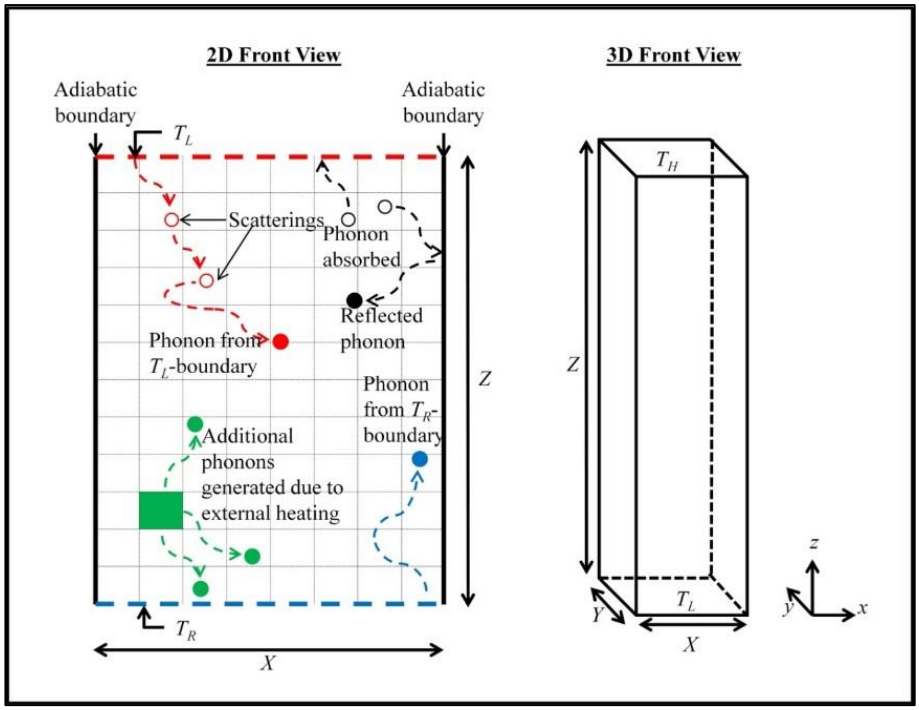

Figure 3.2 2D and 3D schematic view of the medium geometry considered in phonon transport. The isothermal boundaries are labelled with T_H of higher temperature and T_L of lower temperature respectively.

3.2 Initialization of Phonon Ensembles

The first step in all ensemble MC simulations involves the setting up of the scaling factor, $W_{scaling}$, which is determined via Eq. (3-1) as follows.

$$W_{scaling} = \frac{N_{ph,ini}}{N_{en,m}} \tag{3-1}$$

The initial number of phonons, $N_{ph,ini}$ available in the medium can be calculated from the following equation.

$$N_{ph,ini} = XYZ \sum_{p} \sum_{i} \left[f_0\left(\omega_i, T_{ini}, p\right) - f_0\left(\omega_i, T_{ref}, p\right) \right] D\left(p, \omega_i\right) \Delta\omega_i \tag{3-2}$$

Note that a term T_{ref} is introduced in Eq. (3-2). In this case, instead of simulating all available phonons with energy levels up to the current temperature, only those within the range of the current temperature and T_{ref} will be accounted for, while anything below T_{ref} will be neglected. The lower the value of the chosen T_{ref}, the higher is the number of phonons to be simulated. As phonons are bosons, the equilibrium distribution function, f_0 corresponds to the Bose-Einstein distribution shown as follows.

$$f_0\left(\omega,T\right)=\frac{1}{e^{\hbar\omega/k_BT}-1} \tag{3-3}$$

Once the number of phonon ensembles has been determined, a CPDF of the number of phonons to be launched from T_H- and T_L-boundary over frequency spectrum can be constructed as

$$R_i=\frac{\sum_{j=1}^{i}N_j}{\sum_{j=1}^{N_b}N_j} \tag{3-4}$$

Note that the frequency spectrum in this case is divided into N_b intervals. This discretization, though arbitrary, has to be chosen carefully so that it can sufficiently represent the whole range of selections available while avoiding excessive computational time. On the other hand, the term N_j is given by

$$N_j=\Delta\omega_j\left\{\left[f_0\left(\omega_j,T\right)-f_0\left(\omega_j,T_{ref}\right)\right]D\left(\omega_j,LA\right)+2D\left(\omega_j,TA\right)\right\} \tag{3-5}$$

Note that the T can be replaced with T_H and T_L to determine the corresponding CPDF. To determine the polarization of the ensemble, a random number, Ran_ω is first drawn where

$$R_{i-1}<Ran_\omega<R_i \tag{3-6}$$

The actual frequency, ω of the statistical ensemble is thus calculated as

$$\omega = \omega_i + \left(2Ran_\omega - 1\right)\frac{\Delta\omega_i}{2} \tag{3-7}$$

Following that, the polarization can be computed by taking the ratio of the *LA*-phonons to the total number of phonons in all polarization branches in the ω-interval, as in Eq. (3-8). A new random number, Ran_p may now be drawn and compared to the ratio $P_{LA,i}$ whereby anything less than $P_{LA,i}$ would imply *LA*-branch, while anything above that would mean *TA*-branch.

$$P_{LA,i} = \frac{\left[f_0\left(\omega_i, T_R\right) - f_0\left(\omega_i, T_{ref}\right)D\left(\omega_i, LA\right)\right]}{\left[f_0\left(\omega_i, T_R\right) - f_0\left(\omega_i, T_{ref}\right)\right]\left[D\left(\omega_i, LA\right) + 2D\left(\omega_i, TA\right)\right]} \tag{3-8}$$

3.3 Phonon Polarizations and Dispersion Relations

The phonon dispersion relation, which is dependent on the crystallographic direction, shows the correlation between the angular frequency of a phonon and its wave vector. As phonons travel through different directions, their energy levels differ. A preference in such directions will actually lead to a different thermal conductivity. The few dispersion models which have been developed over the years include the Debye model, the Holland model, the sine-function model, the Tiwari model, and the Brillouin zone boundary condition (BZBC) model (Chung, McGaughey & Kaviany 2004). Each material has a unique phonon dispersion relation which is often directional and complex, although several researches in recent years have managed to incorporate them in phonon transport related studies (Kukita, Adisusilo & Kamakura 2014; Kukita & Kamakura 2013; Mingo 2003; Mingo et al. 2003; Wu, Hu & Luo 2016). Nonetheless, for the sake of simplicity, it is common to assume isotropic dispersion in a single direction to maintain an efficient computation process (Lacroix, Joulain & Lemonnier 2005; Mazumder & Majumdar 2001; Wong, Francoeur & Pinar Mengüç 2011).

It is also important to note that contribution of each phonon polarization branch to heat transport is different and should be treated separately. Technically, solids exhibit two types of phonons, namely acoustic phonons and optical phonons (Ashcroft & Mermin

1976; Chen 2005; Zhang 2007; Ziman 1960). These phonons can be further categorized, depending on the polarization, into longitudinal or transverse branches, thus yielding four major phonon types, namely acoustic (LA) phonons, transverse acoustic (TA) phonons, longitudinal optical (LO) and transverse optical (TO) phonons. Previous studies have concluded that the faster moving acoustic phonons are the primary heat carriers in semiconductors like Si, Ge and GaAs, and that the slower optical phonons have relatively small influence on the overall transport process (Ju & Goodson 1999; Pop, Sinha & Goodson 2006). This consideration can be limited by the assumed medium size and medium temperature. Mittal and Mazumder"s work (Mittal & Mazumder 2010) showed that optical phonons can have significant contribution to the heat transport where up to 25% of the total heat are carried by optical phonons in a 420nm thick medium at 300K. This contribution nonetheless, decreases with the increase in thickness of the medium. In the current work, the thicknesses of up to a few micrometres are considered and thus the contribution by optical phonons can be safely neglected.

The phonon dispersion relations for Si, Ge and GaAs can be obtained from the literatures (Brockhouse 1959; Nilsson & Nelin 1971; Waugh & Dolling 1963). The respective data are fitted to quadratic expressions following that of Eqs. (3-9) to (3-14), as shown below

$$\omega_{LA,Si} = 9280 \times \vec{k} - 2.234 \times 10^{-7} \vec{k}^2 \tag{3-9}$$

$$\omega_{TA,Si} = 5240 \times \vec{k} - 2.278 \times 10^{-7} \vec{k}^2 \tag{3-10}$$

$$\omega_{LA,Ge} = 7280 \times \vec{k} - 2.9 \times 10^{-7} \vec{k}^2 \tag{3-11}$$

$$\omega_{TA,Ge} = 3150 \times \vec{k} - 1.4 \times 10^{-7} \vec{k}^2 \tag{3-12}$$

$$\omega_{LA,GaAs} = 5200 \times \vec{k} - 1.18 \times 10^{-7} \vec{k}^2 \tag{3-13}$$

$$\omega_{TA,GaAs} = 3050 \times \vec{k} - 1.38 \times 10^{-7} \vec{k}^2 \tag{3-14}$$

The quadratic fits will be used to approximate the angular frequency given a wave vector and vice versa in the simulation (Lacroix, Joulain & Lemonnier 2005; Wong, Francoeur & Pinar Mengüç 2011). The raw data and quadratic fits are all shown from Figure 3.3 for Si, Figure 3.4 for Ge, and Figure 3.5 for GaAs. Different fits, however, can also be used to approximate the dispersion relations to a different degree of accuracy, and a study on the impacts of different fits may be considered in the future works. Differentiating each of the above equations with respect to the wave vector yields the phonon group velocity for the particular polarization branch, p, which is conveniently represented by Eq. (3-15).

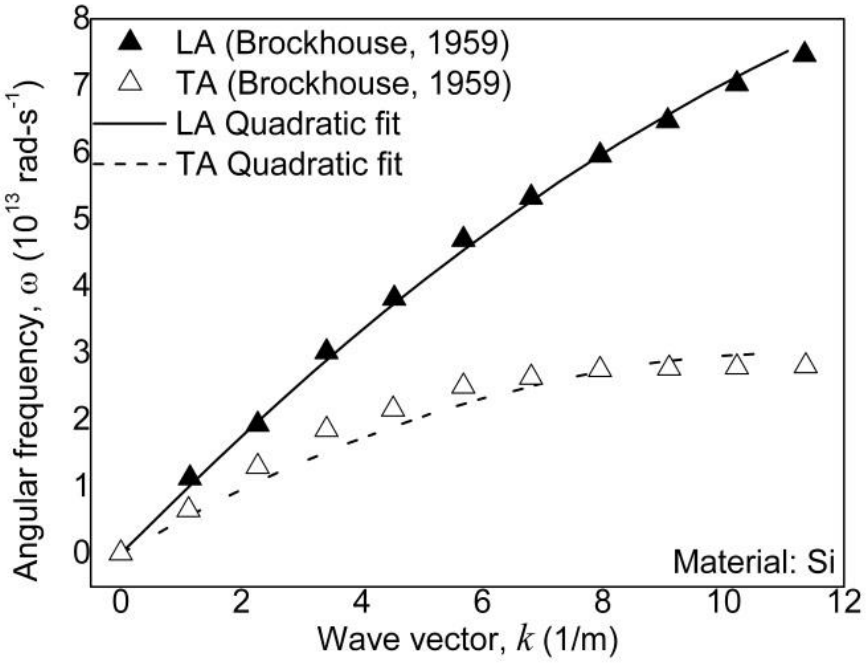

Figure 3.3 Data points of dispersion relation of Si obtained from the literatures (Brockhouse 1959) and the quadratic fit used in this study.

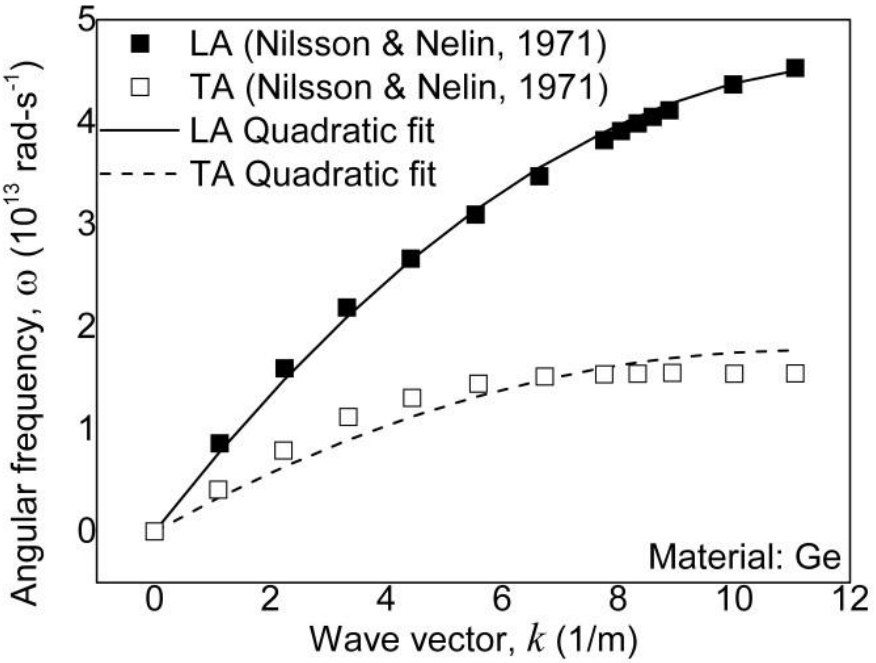

Figure 3.4 Data points of dispersion relation of Si obtained from the literatures (Nilsson & Nelin 1971) and the quadratic fit used in this study.

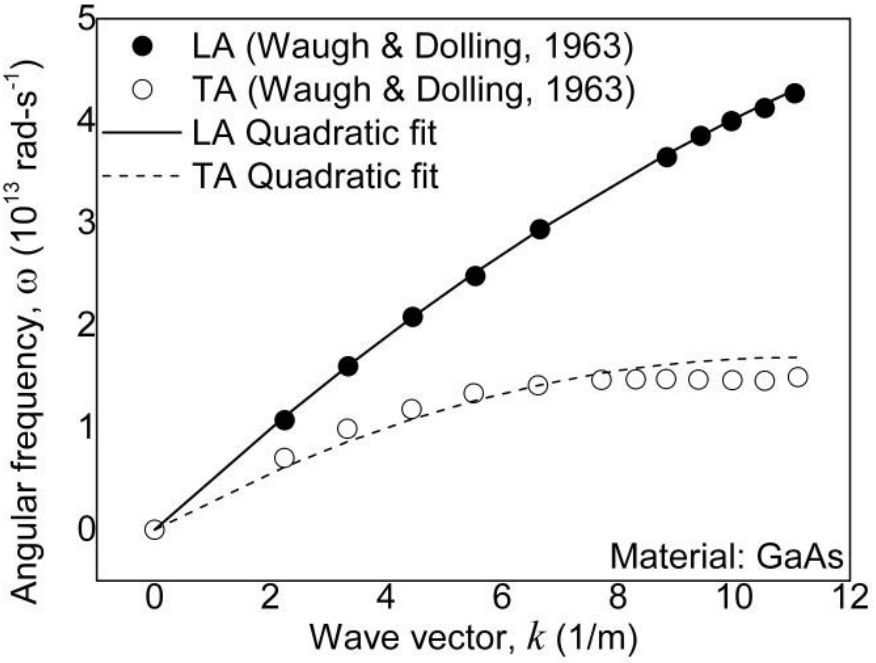

Figure 3.5 Data points of dispersion relation GaAs obtained from the literatures (Waugh & Dolling 1963) and the respective quadratic fit used in this study.

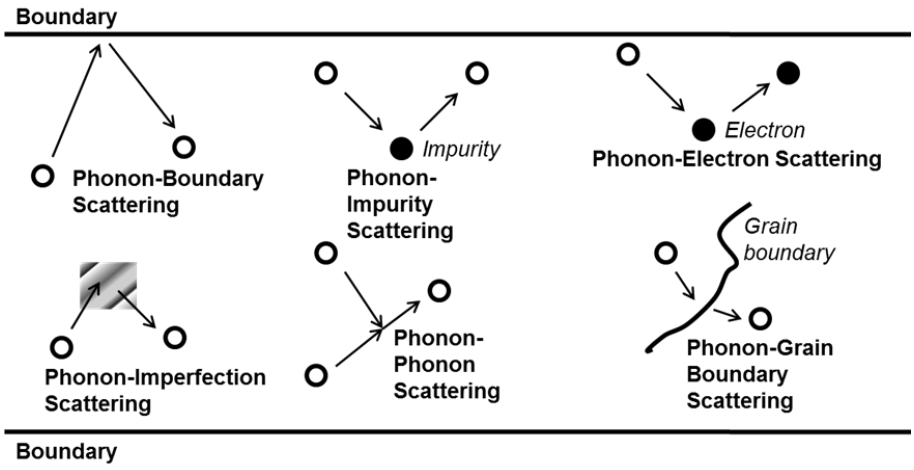

Figure 3.6 The various phonon scattering mechanisms, though the role of each in thermal conduction differ depending on the temperatures considered (Asheghi et al. 1997).

$$\vec{v}_g(\omega, p) = \frac{\partial \omega}{\partial \vec{k}} \tag{3-15}$$

With the phonon group velocity, the phonon density of states can therefore be determined via

$$D(\omega, p) = \frac{\vec{k}^2}{2\pi^2 \vec{v}_g(\omega, p)} \tag{3-16}$$

3.4 Scattering Treatment

There are various types of phonon scatterings which are likely going to occur in the medium, including phonon-boundary scattering, phonon imperfection scattering, phonon-impurity scattering, phonon-electron scattering and phonon-grain boundary scattering, as shown in Figure 3.6 (Asheghi et al. 1997).

Phonons may collide with other phonons, electrons, impurities, boundaries etc., depending on the size and temperature ranges of the medium. Hence, depending on the material and temperature involved in the simulation, certain scattering mechanisms have

negligible impact and can be left out to maintain efficiency of the simulation without compromising on the transport physics. The collisions scatter the phonons in different directions and it takes multiple scatterings for the phonons to finally "relax" or achieve steady state. Depending on the nature of the collision – elastic or inelastic – energy might be gained or lost during the process.

In general, at temperatures close to the ambient temperature, the main contribution to relaxation time originates from the anharmonic phonon interaction, including the Normal (*N*-) processes and the Umklapp (*U*-) processes. While both processes are needed to restore equilibrium, it is vital to remember that only the *U*-processes contribute directly to thermal resistivity (Lacroix, Joulain & Lemonnier 2005; Mazumder & Majumdar 2001; Wong, Francoeur & Pinar Mengüç 2011). In the event of phonon scatterings at high temperature, it is probable for three or more phonons to collide and scatter but this work accounts for the three-phonon cases only, which has to satisfy the energy conservation in Eq. (3-17) as well as the momentum conservation in Eqs. (3-18) and (3-19) respectively (Lacroix, Joulain & Lemonnier 2005; Mazumder & Majumdar 2001; Wong, Francoeur & Pinar Mengüç 2011).

For both *N*- and *U*-processes: $\hbar\omega_1 + \hbar\omega_2 \rightarrow \hbar\omega_3$ (3-17)

For *N*-processes: $\vec{k}_1 + \vec{k}_2 \leftrightarrow \vec{k}_3$ (3-18)

For *U*-processes: $\vec{k}_1 + \vec{k}_2 \leftrightarrow \vec{k}_3 + \vec{G}$ (3-19)

Both energy and momentum conservations are reversible processes. When considering the *U*-processes, a non-zero reciprocal lattice vector, $\vec{G}$ is introduced. The related fundamental physics can be found in other literatures and will not be covered in length here (Ashcroft & Mermin 1976; Ziman 1960; Ziman 1964). While it is possible to examine individual phonon scattering event in the MC simulation and enforce these conservation laws locally, such a treatment of each scattering event is utterly cumbersome and computationally expensive, as suitable phonon candidates with the appropriate wave vectors and frequencies for facilitating a particular scattering process

need to be located nearby the region. To this end, a typical MC simulation of phonon transport uses a total relaxation time to account for scattering which is derived from energy and momentum conservations. Based on the Mathiessen rule, the total relaxation time includes the individual relaxation times of all scatterings considered (Ashcroft & Mermin 1976; Ziman 1960). Hence, the total relaxation time becomes

$$\frac{1}{\tau_{NU}} = \frac{1}{\tau_N} + \frac{1}{\tau_U} \tag{3-20}$$

Table 3-1 Comparison of parameters used to evaluate phonon scattering rates for Si, Ge and GaAs (Bong & Wong 2014).

Source	Parameter		
	B_L [s-K^{-3}]	B_T [K^{-3}]	B_{TU} [s]
Si			
Holland, 1963 (Holland 1963)	2.0×10^{-24}	9.3×10^{-13}	5.5×10^{-18}
Chen et al., 2005(Chen et al. 2005)	1.0×10^{-30}	9.3×10^{-13}	5.5×10^{-18}
Randrianalisoa and Baillis, 2008 (Randrianalisoa & Baillis 2008)	2.0×10^{-24} if $\omega < \omega_{1/2}$; 8.03×10^{-25} else $\omega \geq \omega_{1/2}$	9.3×10^{-13}	7.4×10^{-19}
Baillis and Randrianalisoa, 2009 (Baillis & Randrianalisoa 2009)	2.0×10^{-24} if $\omega < \omega_{1/2}$; 9.4×10^{-25} else $\omega \geq \omega_{1/2}$	9.3×10^{-13}	1.1×10^{-18}
Wong et al., 2011 (Wong, Francoeur & Pinar Mengüç 2011)	2.0×10^{-24}	9.3×10^{-13}	1.7×10^{-18}
Present Study	2.0×10^{-24}	9.3×10^{-13}	2.9×10^{-18}
Ge			
Holland, 1963 (Holland 1963)	6.9×10^{-24}	1.0×10^{-11}	5.0×10^{-18}
Asen-Palmer, 1997 (Asen-Palmer et al. 1997)	9.0×10^{-30}	1.5×10^{-11}	4.5×10^{-18}
Present Study	6.9×10^{-24}	1.0×10^{-11}	1.4×10^{-18}
GaAs			
Bhandari and Verma, 1965 (Bhandari & Verma 1965)	1.75×10^{-23}	4.162×10^{-22}	6.01×10^{-18}
Tiwari et al., 1971 (Tiwari, Talwar & K Agrawal 1971)	3.4×10^{-24}	2.69×10^{-12}	
Present Study	3.4×10^{-24}	2.69×10^{-12}	7.5×10^{-18}

A cumulative probability density function (CPDF) for phonon scattering between a particular time, t and the following one, $t+\Delta t$ can be constructed based on the following equation.

$$R_{scatt} = 1 - \mathrm{e}^{-\Delta t/\tau_{NU}} \tag{3-21}$$

As relaxation times are temperature- and frequency-dependent, it is necessary to re-evaluate them at every time step with respect to the corresponding properties. The relaxation time expressions based on Holland's (Holland 1963) proposed model are shown as follows.

$$\tau_{LA,NU}^{-1} = B_L \omega^2 T^3 \tag{3-22}$$

$$\tau_{TA,N}^{-1} = \begin{cases} B_T \omega T^4 & \forall \quad \omega < \omega_{1/2} \\ 0 & \forall \quad \omega \geq \omega_{1/2} \end{cases} \tag{3-23}$$

$$\tau_{TA,U}^{-1} = \begin{cases} 0 & \forall \quad \omega < \omega_{1/2} \\ \dfrac{B_{TU}\omega^2}{\sinh\left(\hbar\omega/k_B T\right)} & \forall \quad \omega \geq \omega_{1/2} \end{cases} \tag{3-24}$$

B_L, B_T and B_{TU} are scattering parameters – constants which are determined from bulk thermal conductivity data, while $\omega_{1/2}$ is the frequency corresponding to $\vec{k}/\vec{k}_{\max} = 0.5$ which is based on the *TA*-phonon dispersion relation. The values of these constants as determined by our model are listed in Table 3-1. In addition, some of the constants used in other studies found in the literatures are also listed here for reference. Although they are all determined from the bulk thermal conductivity data, they are calibrated to fit each individual model, hence resulting in slight differences in each of the studies.

To determine whether or not a phonon ensemble has scattered after a time interval Δt, a random number R_{scatt} is drawn and compared to R_{scatt} in Eq. (3-21). Any number below that, the phonon ensemble will be scattered, and its frequency, polarization and directions are to be reset. Following the scattering event, additional energy may be

added or removed. The resetting of phonon frequency can be tricky due energy and momentum conservations, of which the effects will be discussed in Chapter 6.1.5 later. In reference to works by Lacroix et al. (Lacroix, Joulain & Lemonnier 2005) and Wong et al. (Wong, Francoeur & Pinar Mengüç 2011), this work adopted a similar approach by modifying the CPDF in Eq. (3-4) but with the introduction of T_{ref}, which eliminates the requirement of a creation / destruction scheme as proposed in (Mazumder & Majumdar 2001). The modified CPDF is given by

$$R_i = \frac{\sum_{j=1}^{i} N_j R_{scatt.,j}}{\sum_{j=1}^{N_b} N_j R_{scatt.,j}} \tag{3-25}$$

3.4.1 Isotropic Scattering

Isotropic scattering is commonly considered in most MC simulations for the sake of simplicity. By altering the scattering parameters in Table 3-1, acceptable simulation results can still be obtained. In considering such scenarios, previously derived Eqs. (2-13) to (2-19) can be applied to sample the polar and azimuthal angles following a scattering event.

3.4.2 Anisotropic Scattering Treatment

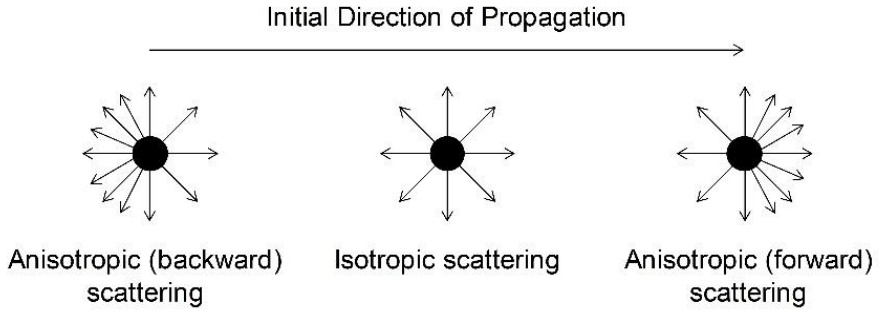

Figure 3.7 Isotropic and anisotropic scattering mechanisms are considered in the current MC simulation model. The anisotropic scattering involves a preference in forward or backward scattering by a phonon ensemble.

In consideration of the anisotropic scenario, it is presumed that there will be a directional preference following a scattering event. Normally, this is based on the belief that the dispersion relation corresponding to the different crystallographic directions will be affecting the scattering. Incorporating such mechanism required extensive work and understanding on the full phonon dispersion relation, which is both tedious and complicated. Therefore, the current work is based on the assumption that phonons will have a directional preference as in forward and backward scattering regardless of the dispersion relation. This represents a largely untapped research area to date.

A simple anisotropic scattering treatment can be done in which the *N*- and *U*-processes is differentiated when sampling the scattering angles of the scattered phonons can easily be implemented (Bong & Wong 2014; Wong, Francoeur & Pinar Mengüç 2011). This is based on the assumption that *N*-processes do not contribute directly to thermal resistance thus leading to phonons undergoing the *N*-processes being scattered in the forward direction. On the other hand, phonons undergoing the *U*–processes are scattered backwards against the temperature gradient. Therefore, they will be carrying heat backwards, thus contributing to thermal resistivity. While it is possible to consider each of the *N*- and *U*- processes independently, in-depth understanding and derivation of the complete anisotropic phonon dispersion relation with its corresponding anisotropic scattering rates are necessary in order to accurately describe the directional preference. Anisotropic dispersion relations are made available in some studies, but its various corresponding anisotropic scattering rates are not available, especially in the temperature range of interest. In addition, energy and momentum conservation laws have to be examined locally instead of stochastically, which calls for the location of suitable phonons with appropriate wave vectors and frequencies for facilitating the aforementioned anisotropic scattering process. Implementing such an approach in the phonon MC simulation will be able to capture the essence of the *N*- and *U*-processes in terms of thermal resistivity. It is also deemed most accurate but then again at the same time will be very complicated and computationally expensive.

Henceforth, simpler alternatives are incorporated to investigate anisotropy due to directional preference as shown in Figure 3.8. The first alternative can be easily achieved by resetting the polar angle in the forward or backward direction, following Eq.

(2-19) in the event of a *N*- and *U*-process respectively This however, does not allow any control over the degree of anisotropy or directional preference. To allow control over the degree of anisotropy, a simple scattering phase function used extensively in radiative transfer based on the Lorenz-Mie theory is adopted. This phase function varies the probability of scattering at a given polar angle using a prescribed constant. Commonly, the scattering phase function involves the Legendre polynomials (Mengüç & Viskanta 1983) which can be handful to solve in MC simulations. In this case, a Henyey and Greenstein (HG) probability density function (Henyey & Greenstein 1941) is used to represent a simple anisotropic phonon scattering phase function, as had been previously discussed in the literatures (Modest 1993; Wong 2001). The HG probability density function in terms of the polar angle, θ is given by

$$P(\theta) = \frac{1-g^2}{4\pi\left(1+g^2-2g\cos\theta\right)^{3/2}}$$

$$\text{such that } \int_0^{\pi} P(\theta)\, 2\pi \sin\theta d\theta = 1$$

$$\int_0^{\pi} P(\theta)\cos\theta 2\pi \sin\theta d\theta = g \tag{3-26}$$

It is a common practice to express the HG probability density function in terms of the direction cosine, $cos\theta$ as follows.

$$P(\cos\theta) = \frac{1-g^2}{2\left(1+g^2-2g\cos\theta\right)^{3/2}}$$

$$\text{such that } \int_{-1}^{1} P(\cos\theta)\, d(\cos\theta) = 1$$

$$\int_{-1}^{1} P(\cos\theta)\cos\theta d(\cos\theta) = g \tag{3-27}$$

Therefore, the probability of scattering into the $cos\theta$ direction can be obtained by performing the following integration

$$P(\cos\theta) = \int_{-1}^{\cos\theta} P(\cos\theta)\, d(\cos\theta) \tag{3-28}$$

Note that g is the anisotropy factor, which is the parameter to be used to determine the extent of the anisotropic scattering, as shown in Table 3-2. The plots of the HG probability density function in terms of θ and $cos\theta$ are shown in Figure 3.8 and Figure 3.9 respectively.

Table 3-2 Range of anisotropy factor and the corresponding type of scattering

Range of *g*	**Type of scattering**
$-1 \le g < 0$	Backward scattering
$0 < g \le +1$	Forward scattering
$g = 0$	Isotropic scattering

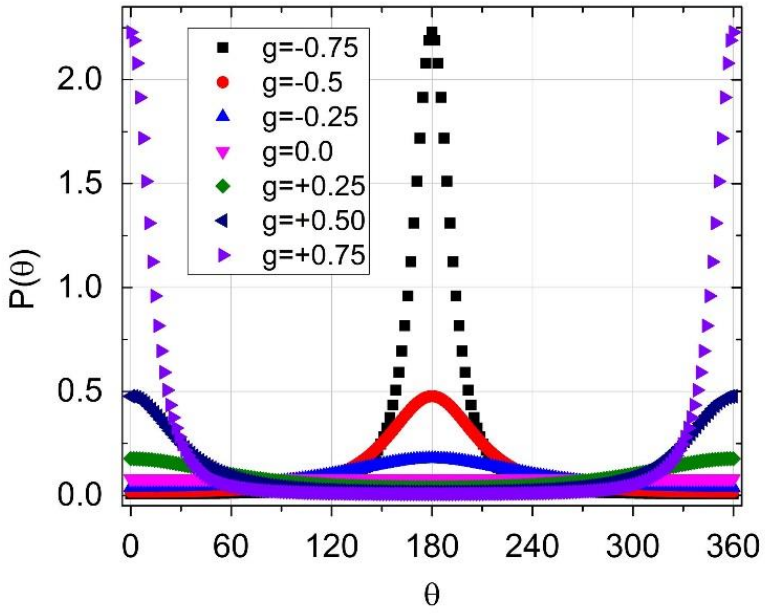

Figure 3.8 Plot of the HG probability density function in terms of θ.

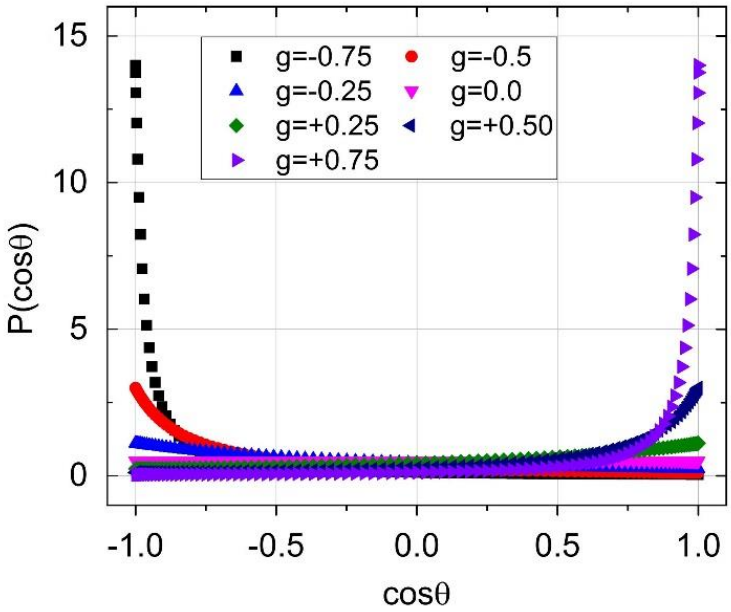

Figure 3.9 Plot of the HG probability density function in terms of *cosθ*.

Note that from Figure 3.9, $cos\theta = 1$ (or $\theta = 0^0$ or 360^0) denotes a forward direction along the phonon"s original trajectory, while $cos\theta = -1$ (or $\theta = 180^0$) denotes a backward direction. As g increases, the probability of scattering in the $cos\theta$ direction increases significantly while scattering in all other directions decreases. The same can be seen as g decreases, where backward scattering increases dramatically. At $g = 0$ however, a straight line is obtained, which denotes fully isotropic scattering such that there will be an equal probability of scattering in every single direction.

In the current work, the value of g is specified to modify the three phonon-phonon scattering to either forward or backward preference. The polar angle, θ after scattering can be obtained by inverting Eq. (3-27) and incorporating a random number, R, using the following equation (Bong & Wong 2014; Wong, Francoeur & Pinar Mengüç 2011).

$$\theta = \cos^{-1}\left\{\frac{1}{2g}\left[1+g^2-\left(\frac{1-g^2}{1-g+2gR}\right)^2\right]\right\} \tag{3-29}$$

Note that when $g = 0$, the above equation shall be undefined. Under such circumstance, θ shall be sampled randomly using the following equation.

$$\theta = \cos^{-1}\left(1-2R\right) \tag{3-30}$$

Following the anisotropic scattering event, the direction cosines after scattering need to be modified accordingly, strictly following Eqs. (2-27) to (2-29) derived in the previous chapter. However, this set of equations fail under two circumstances, namely when μ_z approaches unity and when g = 0. Under these conditions, the equations for isotropic scattering, i.e. Eqs. (2-24) to (2-26) should be applied instead.

3.5 Calculation of Temperature Distribution

As phonon ensembles are propagating within the medium, they will move between the different computational volumes and thereby disrupt local thermodynamic equilibrium. The concept of „pseudo-temperature", T_{pseudo} is employed here (Wong, Francoeur & Pinar Mengüç 2011). It is not literally the „real" temperature but rather the temperature obtained based on the assumption that the total energy carried by the ensembles of phonons in a local computational element is equal to the total phonon energy computed using the Bose-Einstein distribution for the same volume. T_{pseudo} is mainly used to determine scattering properties. Nonetheless, the local distribution functions remain non-equilibrium. The following equation is to be solved for T_{pseudo} at each time step.

$$\sum_{p}\sum_{i=0}^{N_b}\hbar\omega_i\left[f_0\left(\omega_i,T_{pseudo}\right)-f_0\left(\omega_i,T_{ref}\right)\right]D_i\left(\omega_i,p\right)\Delta\omega_i=\frac{E\left(x,y,z\right)}{\Delta x\Delta y\Delta z} \tag{3-31}$$

Note that $E\left(x,y,z\right)$ is the total energy carried by the ensembles within a computational volume of $\Delta x\Delta y\Delta z$. In order to avoid having to repeatedly solve the equation during the simulation each time T_{pseudo} is required, it can be first solved numerically before the start of the simulation where all the computed energies and the corresponding T_{pseudo} can be stored in a table to be accessed later when needed.

3.6 Calculation of Thermal Conductivity

The solution of the BTE allows for the calculation of thermal conductivity. Several models have been proposed over the years to describe the thermal conductivity characteristics, including the Klemens model (Klemens 1951), the Callaway‟s model (Callaway 1959), and the Holland‟s model (Holland 1963). As previously mentioned, our work so far has been based on the Holland‟s model but without considering the impurity and boundary scatterings since the target temperature range here is above the room temperature where these scattering events are not important. The calculation of the thermal conductivity in a scattering medium can be achieved via the following equation.

$$K = \frac{\dot{q}}{\Delta T} \tag{3-32}$$

The term ΔT refers to the temperature gradient in the medium at a particular point in time, while $\dot{q}$ is the corresponding net heat flux experienced by the medium. At any point in time, the net heat flux can be determined by summing up the energy carried by all the phonons in the medium across a particular cross section in the *z*-direction. Mathematically, it can be represented by the following equation (Lacroix, Joulain & Lemonnier 2005).

$$\dot{q} = \sum_{i=1}^{N_{en}} \frac{W_{scaling} \hbar \omega_i \vec{v}_{g,i} \cdot \hat{k}}{X_{cr} \times Y_{cr}} \tag{3-33}$$

3.7 Incorporation of Heat Generation

Although the goal of this work is to focus on the statistical behaviours of the speed-up version of the MC method, the method can be easily modified to include heat generation by implementing a phonon creation scheme (Wong et al. 2013; Wong, Francoeur & Pinar Mengüç 2011). The type of heat generation is unimportant at this point, as long as the rate of phonon production is known. The distribution of the volumetric power generated within the material, $\dot{g}'''$ is to be pre-determined prior to the simulation, which

can then be applied to determine the heat generated in a particular computational element at a particular point in time, following the Eq. (3-34).

$$E_{gen}\left(x,y,z\right)=\dot{g}'''\Delta x\Delta y\Delta z\Delta t \tag{3-34}$$

The additional energy will be added to the total energy carried by phonons at the same location and time to obtain the actual total energy and the corresponding $T_{pseudo.}$ Additional phonon ensembles, $N_{en,gen}$ will be generated continuously within the computational element until the total energy added tallies that in Eq. (3-35).

$$\sum_{i=1}^{N_{en,gen}}\hbar\omega_i W_{scaling}\approx E_{gen}\left(x,y,z\right) \tag{3-35}$$

CHAPTER 4

Monte Carlo Simulation for Electron Transport

4.1 Overview of the MC Electron Transport Simulation

Electron transport is a significant area of research for physicists and engineers alike due to their role in both data transfer and heat transfer. Data is transferred through electron flow in mediums, such as electrical wires or electronic components in circuits. Energy in the form of heat is also transferred via electron flow, although this phenomenon is only significant in metallic mediums such as copper wires. In semiconductors however, phonon transport is the dominant heat transport mechanism. Electron transport is often scrutinized for its role in data transport. In the early days of semiconductor technologies, the speed of which data can be transported was always a major concern. A thorough understanding in electron transport and the relevant material properties allowed an improvement in semiconductor devices‟ performance, thus providing faster data transport and computations.

A quick look at some of the studies done in the history of electron transport in semiconductor devices proves that significant improvements have been achieved in computational simulations. Canali et al. (1975) gave a general view of the electron transport properties in Si via experimental results and theoretical modelling. The MC

method enabled accurate incorporation of the intervalley scattering without assumption of strong or weak coupling between parallel and perpendicular valleys. Their theoretical model incorporates the many valley structure of the Si conduction band, acoustic intravalley scattering (including the correct momentum, energy relaxation and equilibrium phonon population), several valley scatterings and ionized impurity scattering. Brunetti et al. (1981) later explored the diffusion coefficient of electrons in Si due to velocity fluctuation as a function of electric field, crystallographic direction and temperature (77 – 300K), and then presented an improved electronic transport model based on their new findings. They had also included the six-valley phonon scatterings in their model. Jacoboni and Reggiani‟s works in 1983 provided a review of the MC method which remained largely relevant to this day, and a detailed methodology to simulate the electron transport at nanoscale. It is noteworthy that their works had also paid particular attention to the internal scatterings for a more accurate insight. Later work by Fischetti and Laux (1988) investigated the electron transport by including the band structure which was obtained from empirical-pseudopotential calculations, and space charge effects which was incorporated by coupling with a self-consistent two-dimensional Poisson‟s equation. They also included the electron-phonon, electron-impurity and electron-electron scatterings in their simulation. Extensive studies on band structure, deformation potentials, and carrier mobility in strained Si, Ge, and SiGe alloys was also conducted later (Fischetti & Laux 1996b).

In some instances of more specific MC studies related to applications and devices, investigation had been carried out to scrutinize the transport properties of Si/SiO_2 superlattice with a multiband one-particle MC simulator (Rosini, Jacoboni & Ossicini 2002). The simulation accounted for band structure and scattering mechanisms, and also included an in-plane electric field and the effects of the field were discussed. Studies have also been carried out on carrier transport in silicon-on-insulator (SOI) devices, where the role of volume inversion was one of the area of interest (Gamiz & Fischetti 2001). The main scattering mechanisms considered in the aforementioned work included are phonon scattering, surface roughness scattering and Coulomb scattering. Electron-phonon, electron-electron and electron-impurity scatterings are to be considered in the semi-ballistic transport (Fischetti & Laux 1988; Vasileska et al. 2008). Long range carrier-carrier interaction and space charge are other factors which may

affect the transport process and could hinder ballistic transport at 10-nm scale (Fischetti et al. 2007; Sidorov, V'yurkov & Orlikovsky 2004). The factors affecting the various scattering mechanisms have also been investigated in many literatures, to name a few, Coulomb interaction in nanoscale Si devices (Sano 2011) and impact ionization in Si (Sano, Tomizawa & Yoshii 1991; Tang & Hess 1983). The inclusion of such electron-electron interactions is especially necessary when a large range of electron energy and electric field is involved. To account for this, often the solution of the Poisson‟s equation was included in the simulation model. Some notable efforts were made to couple the Poisson‟s-Schrödinger equations and its accuracy was improved by quantum corrections (Ramayya & Knezevic 2010; Sampedro et al. 2007). Other scatterings accounted for in other studies included scatterings by ionized impurities and surface roughness (Borzdov & Petrovich 1997), and backscattering which is a common concern in the design of industrial electron beam evaporators (Maltby & Kornblum 1990). The MC method is also useful in computing scattering rates in dense medium (Liu et al. 2005), thermoelectric properties in Si nanowire (Ramayya et al. 2012), electrical conductivity (Fobelets et al. 2012). In addition, it is also useful in simulation of the electron mobility in various nano-electronic devices such as SOI transistors and multi-gate metal–oxide–semiconductor field-effect transistors (MOSFET) (Gamiz et al. 2009; Gámiz et al. 2008). Another common and practical use of the MC simulation involved the modelling of thermal conduction induced by electron beam. MC method incorporating the continuous slow down approach was deployed and a two-temperature approach model was used to overcome the limitation of Fourier Law which does not account for of electron temperature in the medium (Wong, Mengüç & Vallance 2007). The analysis of charge, momentum and energy transfer by an electron beam on a conductor was later conducted (Wong 2012).

Thus in the research history of semiconductor technology, electron transport has been a rather well established research area (Snowden 1988; Wong & Mengüç 2003). Not only have researchers managed to find ways to expedite data transfer, they have also managed to look into the various aspects and applications of the electron transport right up to micro and nano-machining processes. While it is indeed a well-known fact by now that electron transport is relatively insignificant in heat transport in semiconductor materials, its contribution to the heat transport is still relevant due to the interaction

between electrons and phonons. Both „particles" are found to inter-wine within a semiconductor medium and will interact with one another via collisions. In the event of collisions, energy is exchanged, while a phonon might be absorbed or emitted depending on the collision terms. In view of that, there is an urgency to study electron transport in semiconductor materials in order to correctly portray the heat transport in semiconductor mediums. In fact, many articles in more recent years have highlighted the need for such studies, thus involved the inclusion of heating effects by electrons in semiconductor devices (Pop 2008; Pop, Dutton & Goodson 2005; Raleva et al. 2008; Rowlette et al. 2005; Vasileska, Raleva & Goodnick 2008; Vasileska, Raleva & Goodnick 2010).

The general electron transport algorithm has been discussed extensively in the various literatures highlighted above. As with the phonon transport, the governing equation for semi-classical electron transport is also the BTE. In this thesis, the BTE of electron transport is also solved using the transient MC method. However, there lies one major difference between electron transport and phonon transport. In electron transport, the electric field (both local and applied) is an additional driving force in addition to the temperature gradient (Chen 2006; Li, Au Yeung & Chan 2012). In order to include this effect, a Poisson"s equation solver has to be coupled into the electron transport to evaluate the electric field. Another point to note is that the current model discounts hole transport in general, with the initial number of holes assumed to be the baseline for the entire simulation. A flow chart of the electron transport procedures is provided in Figure 4.1, while a schematic view of the medium is provided in Figure 4.2.

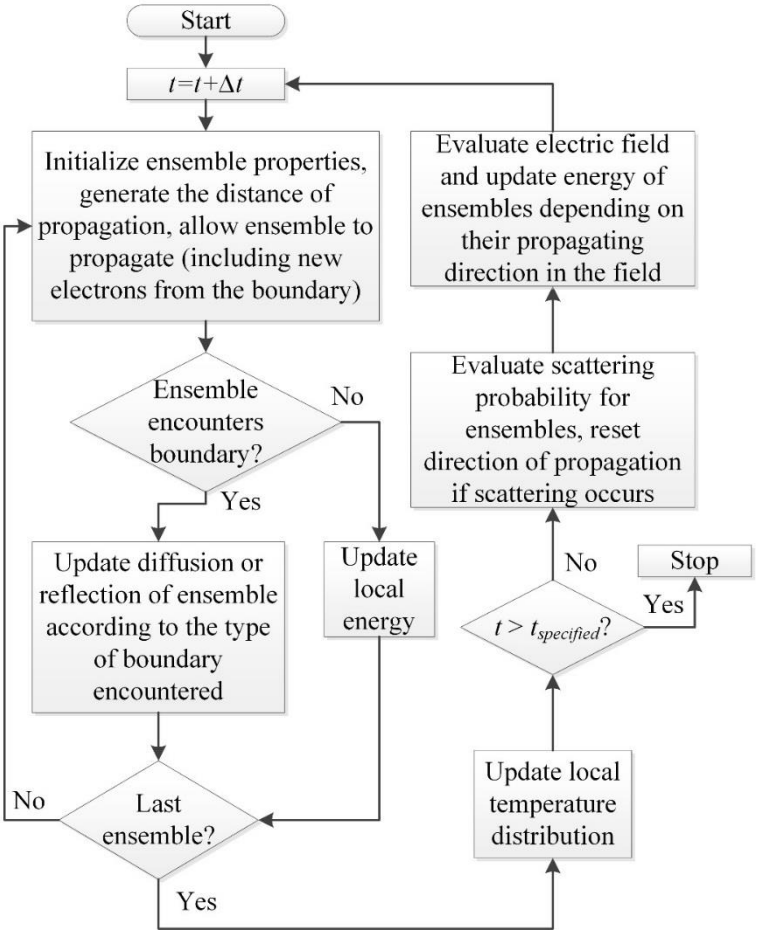

Figure 4.1 Flowchart of the MC electron simulation algorithm applied in this thesis.

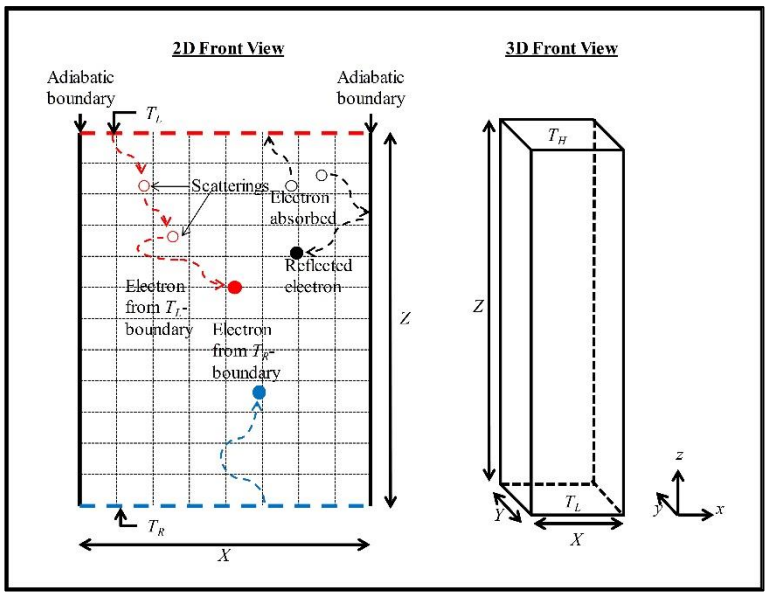

Figure 4.2 2D and 3D schematic view of the medium geometry considered in this electron transport. The isothermal boundaries are labelled with T_H of higher temperature and T_L of lower temperature respectively.

4.2 Initialization of Electron Ensembles

As with the MC phonon simulations the scaling factor, $W_{scaling}$ can be determined via Eq. (4-1) as follows.

$$W_{scaling} = \frac{N_{elec,ini}}{N_{en,m}} \tag{4-1}$$

The initial number of electrons, $N_{elec,ini}$ available in the medium can be calculated from the following equation.

$$N_{elec,ini} = XYZ \sum_i \left[f_0 \left(E_i, T_{ini} \right) \right] D\left(E_i \right) \Delta E \tag{4-2}$$

Note that the term T_{ref} first introduced in the previous chapter has not been included in Eq. (4-2). This is due to the scarcity of electrons in intrinsic semiconductors considered within the scope of this thesis, which means it is still possible to simulate electrons across the entire absolute temperature range. T_{ref} is expected to become handy in simulations involving doped semiconductors. Meanwhile, the infinitesimal electron energy considered, ΔE over a finite number of discretization, N_b considered can be approximated by

$$\Delta E = \frac{E_{\max} - E_{cond,\min}}{N_b} \tag{4-3}$$

The maximum electron energy taken into account corresponds to the wave vector π/a, where a is the lattice constant of the semiconductor material considered (see Table 4-1 for the values obtained from the literatures). Note that only conducting electrons are simulation, i.e. electrons with energy level higher than the conduction band minimum. The parabolic density of states for electrons can be computed by the following equation (Van Zeghbroeck 2011).

$$D\left(E_i \right) = \frac{8\pi\sqrt{2}}{h^3} \left(m_{DOS}{}^* \right)^{3/2} \sqrt{E_i - E_{cond,\min}} \tag{4-4}$$

As electrons are fermions, the equilibrium distribution function, f_0 corresponds to the Fermi-Dirac distribution shown as follows.

$$f_0\left(E_i,T\right)=\frac{1}{e^{\left(E_i-E_F\right)/k_BT}+1} \tag{4-5}$$

E_i is the energy of the electron state i in consideration, while E_F is the Fermi level of the semiconductor material considered, which is in the middle of the band gap for intrinsic semiconductor. Once the number of electron ensembles has been determined, a CPDF of the number of electrons to be launched from T_H- and T_L-boundary over frequency spectrum can be constructed as

$$R_i=\frac{\sum_{j=1}^{i}N_j}{\sum_{j=1}^{N_b}N_j} \tag{4-6}$$

The term N_j meanwhile, is given by

$$N_j=\Delta E\left\{\left[f_0\left(E_j,T\right)\right]D\left(E_j,T\right)\right\} \tag{4-7}$$

Note that the T can be replaced with T_H and T_L to determine the corresponding CPDF. Thus. the actual energy, E of the statistical ensemble is calculated as

$$E_i=E_{cond,\min}+\left(2i+1\right)\frac{\Delta E}{2},i=0,1,...N_b-1 \tag{4-8}$$

4.3 Electronic Band Structure and Effective Mass

To solve the BTE, one needs strong knowledge of the electronic band structure *E(k)*, normally depicted in an *E-k* diagram. Analogous to the phonon dispersion relation, the electronic band structure is a particular form of energy-wave vector relationship of velectrons. It describes the ranges of energy that an electron in a solid may have or may

not have, and determines the dynamic properties of an electron under the influence of an external force (electric field and / or magnetic field) (Ashcroft & Mermin 1976). It is noteworthy that while it is possible to obtain the energy bands via empirical-pseudopotential calculations (Fischetti & Laux 1988), the physics and mathematics involved can be overwhelming. In semiconductors, one significant characteristic is the existence of a band gap, which refers to the energy gap between the minimum of the conduction band and the maximum of the valence band. No free electrons can exist within this gap. In any case, electrons can exist in energy state higher than the conduction band minima, which can be of different value depending on the crystallographic directions in the crystal structure.

In general, three main types of band structure can be considered, namely the parabolic band structure, the non-parabolic band structure and the full band structure. Each of these approaches can be used under different assumptions for different scenarios. For example, in high energy transport, the full band simulation will be particularly useful. In low energy transport with supply voltages reduced below a material‟s band gap (where impact ionization becomes negligible), it is sufficient to use analytic (parabolic and non-parabolic) models (Pop, Dutton & Goodson 2004). Depending on the choice of energy band, the corresponding density of states will need to be correctly computed. The simplest form, which is also the adopted form in this thesis, is the parabolic band structure. In low field applications, electrons generally reside close to the minimum of the conduction band and remains close to equilibrium. As such the parabolic band can be represented by Eq. (4-9).

$$E\left(\vec{k}\right) = E_{cond,\min} + \frac{\hbar^2 \vec{k}^2}{2m^*} \tag{4-9}$$

The term m^* refers to effective mass of density of states, which can be found by multiplying the coefficient of effective mass of density of states, $m_{DOS}{}^*$ with the mass of an electron, as shown in Eq. (4-10).

$$m^* = m_{DOS}{}^* \times m_{elec} \tag{4-10}$$

Table 4-1 Properties of common semiconductor materials Si, Ge and GaAs used within the scope of this thesis (Snowden 1988; Van Zeghbroeck 2011)

Property	Si	Ge	GaAs
Lattice constant, a [Å]	5.431	5.657	5.653
Conduction band minima, $E_{cond,\min}$ [eV]	1.12	0.66	1.734
Longitudinal effective mass, m_l^*/m_0, [-]	0.98	1.64	1.98
Transverse effective mass, m_t^*/m_0, [-]	0.19	0.082	0.37
Effective mass for density of states, m_{DOS}^*/m_0, [-]	1.08	0.56	0.067
Effective mass for conductivity, m_{cond}^*/m_0, [-]	0.26	0.12	0.067

m_{DOS}^* can be determined by computing the geometric mean for one longitudinal mass and two transverse masses describing the single conduction band minimum, the following equation.

$$m_{DOS}^* = n_{cond}^{3/2} \sqrt[3]{m_l^* m_t^* m_t^*} \tag{4-11}$$

As parabolic band comes with the assumption of isotropy, it is assumed that the effective mass will be constant. This variable however, is not to be confused with the effective mass for conductivity, which is used only in conduction related calculations such as mobility (Van Zeghbroeck 2011). The effective mass for conductivity can be computed via the equation below when necessary.

$$m_{cond}^* = \frac{3}{\frac{1}{m_l} + \frac{1}{m_t} + \frac{1}{m_t}} \tag{4-12}$$

The non-parabolic band on the other hand, is important for consideration of high applied fields, but currently not within the scope of this thesis. However, under such circumstance, electrons are bound to gain higher energy level, and will reside high above the minimum of the conduction band. As such, it no longer satisfies the parabolic band. The non-parabolic band is represented by Eq. (4-13).

$$E\left(1+\alpha E\right)=\frac{\hbar^2\vec{k}^2}{2m_{DOS}{}^*} \tag{4-13}$$

Note that α is the coefficient of non-parabolicity, which is given by the following equation.

$$\alpha=\frac{\left(1-m^*/m_0\right)^2}{E_g} \tag{4-14}$$

The most complete approach is inevitably the full band structure, which used to be computationally expensive until the introduction of powerful computers in the modern days. This approach is mainly based on the empirical pseudopotential approach, which can be found in the available literature (Cohen & Bergstresser 1966). With the recent advancement in computational power however, it is viable as a more general approach, although most simulations would consider a simplified band approach and use the abundant of computational power to include other information such as realistic phonon dispersion relation (Rowlette & Goodson 2008). In most cases however, the non-parabolicity is sufficient for accurate modelling. But for the sake of simplicity and suitability of the current work, the parabolic band is opted instead. This can of course, be improved and replaced with the more complicated band structures in the future. The properties for common semiconductor materials Si, Ge and GaAs used within the scope of this thesis is provided in Table 4-1 Properties of common semiconductor materials Si, Ge and GaAs used within the scope of this thesis (Snowden 1988; Van Zeghbroeck 2011).

4.4 Scattering Treatment

As with the scattering treatment for phonon transport, the scattering rates for electron in semiconductor can be obtained via the Mathissen‟s rule. This normally involves the inclusion of several scattering mechanism including the electron-electron scattering, electron-phonon scattering and electron-impurity scattering (Ziman 1960; Ziman 1964), as shown in the following equation.

$$\frac{1}{\tau_{total}} = \frac{1}{\tau_{elec-ph}} + \frac{1}{\tau_{elec-elec}} + \frac{1}{\tau_{elec-imp}} \tag{4-15}$$

Since only intrinsic semiconductors are being considered in this work, the electron-impurity scattering component is being neglected. That leaves us with the electron-electron scattering and electron-phonon scattering. Electron-phonon scattering refers to scatterings of electrons by lattice vibrations and remains one of the most important scattering process in semiconductor transport. The effect on such scattering on the electron transport have been scrutinized in some recent studies (Akkerman & Murat 2015; Rideau et al. 2011). The electron-phonon scattering rate can be computed from the Fermi golden-rule expression. In some works, more general expressions have even been developed to treat intervalley and intravalley scatterings separately to account for the effect of phonon polarizations (Fischetti & Laux 1988; Pop 2014), while other works have developed more specific mathematical expressions for the scattering rates in specific materials and structures (Ramayya et al. 2007; Zou & Balandin 2001). These are equations however, are unsuitable to be incorporated in this work due to the omission of optical phonons in the current model and unavailability of certain information, unless they are included based on assumptions. Meanwhile, electron-electron interactions involve several variables such as short-range interactions and screening effects, and are often found to be difficult to treat in most simulations. Several literatures have been dedicated to introduce mathematical expression and MC algorithm for electron-electron scattering rate (Lugli & Ferry 1983; Matulionis, Požela & Reklaitis 1975; Montefusco & Jacoboni 1972). More recent studies have developed the scattering rate expression in relation to temperature and energy (Ashraf & Sharma 2006; Leyland et al. 2008). However, as some of these mathematical expressions involve several parameters which are not included in the current work, a different strategy to account for scattering events has to be proposed.

It has to be noted again that the current thesis is a fundamental study involving the building of a new simulation model to include the coupling of phonon and electron transport. Each and every element built in this simulation model has to cater for the coupling process later. Therefore, to simplify matters at this point, a simple energy relaxation model is deployed. The empirical model for the electron energy relaxation

time was introduced by Gonzalez et al. (1990) based on MC simulation results and is applicable to all relevant diamond and zinc-blende structure semiconductors. The electron relaxation time is defined as a function of the electron and lattice temperatures, which can be given as follows.

$$\tau = \tau_0 + \tau_1 \times \exp\left[C_1 \left(\frac{T_{elec}}{300K} + C_0 \right)^2 + C_2 \left(\frac{T_{elec}}{300K} + C_0 \right) + C_3 \left(\frac{T_{latt}}{300K} \right) \right] \tag{4-16}$$

The parameters τ_0, τ_1, C_0, C_1, C_2 and C_3 are provided in Table 4-2. However, it is important to note that energy relaxation time is for Ge is largely independent of lattice temperature and thus the term C_3 for Ge is ignored. The same goes to GaAs at high electron temperatures at which the relaxation time will be become independent of the lattice temperature. The electron temperature, T_{elec} can be computed by Eq. (4-17) (Gonzalez et al. 1999).

$$E = \frac{3}{2} k_B T_{elec} \tag{4-17}$$

Note that E refers to the electron energy. The lattice temperature, T_{latt} can be assumed to be a constant temperature of interest in the independent electron transport simulation. However, when coupled with phonon transport, the exact local lattice temperature profile as computed by the MC phonon simulation can be incorporated for a more accurate overall picture.

Table 4-2 Parameters to evaluate the scattering rates of Si, Ge and GaAs in electron transport (Gonzalez et al. 1999).

Parameter	Si	Ge	GaAs
τ_0 [ps]	1.0	0.26	0.48
τ_1 [ps]	-0.538	1.49	0.025
C_0	0	0	0
C_1	0.0015	-0.434	-0.053
C_2	-0.09	1.322	0.853
C_3	0.17	0	0.5

In the event of scattering, the direction cosines and energy of the electron ensemble is reset. It is assumed that all collisions are inelastic within these simulations. Meanwhile, isotropic scattering is assumed since the parabolic band is considered. Therefore, previously derived Eqs. (2-13) to (2-19) can be applied to sample the polar and azimuthal angles following a scattering event.

4.5 Calculation of Temperature Distribution

The temperature distribution can be determined in the same way as in phonon transport. T_{pseudo} is obtained based on the assumption that the total energy carried by the electron ensembles in a local computational element is equal to the total energy computed using the Fermi-Dirac distribution for the same volume, but under a non-equilibrium condition. The following equation is to be solved for T_{pseudo} at each time step.

$$\sum_{i=0}^{N_b} E_i \left[f_0 \left(E_i, T_{pseudo} \right) \right] D_i \left(E_i \right) \Delta E = \frac{E\left(x, y, z\right)}{\Delta x \Delta y \Delta z} \tag{4-18}$$

4.6 Calculation of Electric Field

The local electric field due to the disruption of the equilibrium of electron distribution can be computed by solving the Poisson‟s equation. Poisson‟s equation is commonly used to describe electrostatic phenomena quantitatively. It is useful to understand the diffusion and propagation of electrons in carrier transport and can be written as in Eq. (4-19).

$$\nabla^2 U = -\frac{\rho}{\varepsilon} \tag{4-19}$$

The permittivity, ε can be obtained by the multiplying the vacuum permittivity and the relative permittivity for specific materials as shown in Table 4-1. The charge density, ρ can be expanded to include the electrons, holes, acceptors and donors, following the equation below, where q is the point charge.

$$\frac{d^2U}{dz^2} = -\frac{q}{\varepsilon_r \varepsilon_0}\left[-n + p - N_A^- + N_D^-\right] \tag{4-20}$$

The current works do not account for hole transport. Holes are assumed to be static and its population is assumed to be the initial number of electrons for the duration of the simulation. Since no doped material is considered, both the acceptor and donor terms can be neglected. In order to self-consistently update the electric field as the electrons propagate during the simulation, The Poisson‟s equation must be solved at every time step. Considering a 1D Poisson‟s equation, several solution options are possible (Burkardt 2011; Gueye, Talla & Mbow 2014). Most of the solutions to Poisson‟s equation involve the use of matrix inversion and the finite difference method. In this work, two boundary conditions are considered, namely Dirichlet-Neumann (DN) boundary conditions and Dirichlet-Dirichlet (DD) boundary conditions. The DN boundary conditions is utilized when no potential is applied to both ends of the transport medium by assuming 0V at the one end (in this case the higher temperature end is chosen). The potential of the other end is computed by the simulation and should indeed correlate to the direction of the electron flow. The DN boundary conditions is mathematically defined as follows.

$$U_{bound,L} = 0 \tag{4-21}$$

$$\left(\frac{dU}{dz}\right)_{bound,R} = 0 \tag{4-22}$$

The DD boundary conditions is utilized when a potential difference is applied at both temperature ends. In this case, the boundary conditions can be represented as follows.

$$U_{bound,L} = U_L \tag{4-23}$$

$$U_{bound,R} = U_R \tag{4-24}$$

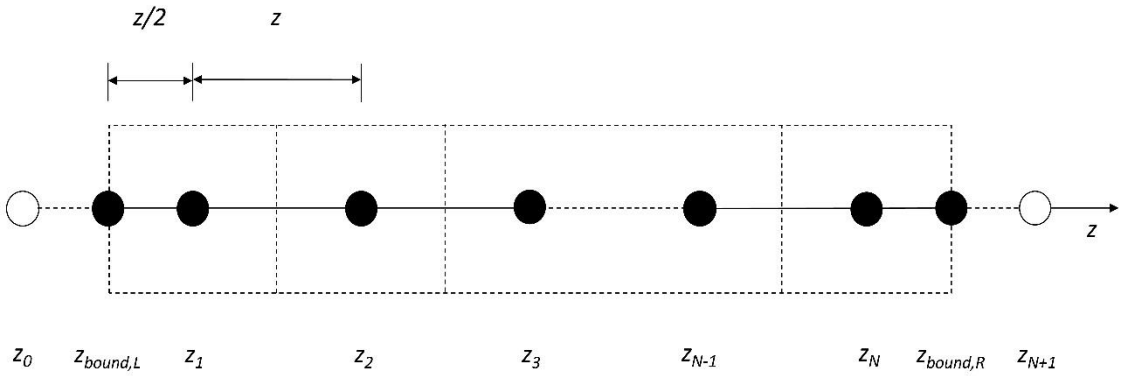

Figure 4.3 Discretization used to solve the Poisson‟s equation for Dirichlet-Neumann (DN) boundary conditions and Dirichlet-Dirichlet (DD) boundary conditions. Discretization is chosen based on the computational grid system (as defined by the dotted lines) defined for storage of electron energy.

Prior to forming the matrix, an appropriate discretization must be chosen in parallel to the grid system defined before. This can be done as shown in Figure 4.3. The mesh chosen has to match the grid system used to store the electron energy, since the electron density is obtained from the MC simulation at each time step and then fed into the Poisson‟s equation solver. To solve the Poisson‟s equation, the system of equations involving all the nodes defined in Figure 4.3 has to be obtained first. The second derivative of the centered finite difference approximation of the potential function $U(z_i)$ as shown in Eq. (4-25) can be applied to obtain a system of equations.

$$\left(\frac{d^2U}{dz^2}\right)_i = \frac{U_{i-1} - 2U_i + 2U_{i+1}}{z^2}, i = 1,2,...,N \tag{4-25}$$

For DN boundary problem, the equation for the first node involves a ghost node z_0. To obtain a solution to z_0, it is assumed that the first order derivative of $U(z_i)$ in between node z_0 and z_1 is constant, hence giving rise to the following relation.

$$\frac{U_{bound,L} - U_0}{z/2} = \frac{U_1 - U_{bound,L}}{z/2} \tag{4-26}$$

Based on Eq. (4-21), the above equation can be simplified to the following relation.

$$U_0 = -U_1 \tag{4-27}$$

On the right hand side where Neumann boundary condition is assumed, the first order derivative of $U(z_i)$ provides a straightforward way to solve for the ghost node z_{N+1}. From Eqs. (4-21) and (4-22), the following relation is obtained.

$$\left(\frac{dU}{dz}\right)_{bound,R} = \frac{U_{N+1} - U_{N-1}}{z} = 0 \tag{4-28}$$

Solving this equation yields the following relation.

$$U_{N+1} = U_{N-1} \tag{4-29}$$

As the boundary value $U_{bound,R}$ has not been defined, it can be extrapolated later from U_N, by assuming that the gradient from U_{N-1} to $U_{bound,R}$, is the same. The system for equations for the DN boundary problem can be written as follows.

$$\begin{bmatrix} -3 & 1 & 0 & 0 & 0 & \cdots & \cdots & 0 \\ 1 & -2 & 1 & 0 & 0 & \cdots & \cdots & 0 \\ 0 & 1 & -2 & 1 & 0 & \cdots & \cdots & 0 \\ 0 & 0 & 1 & -2 & 1 & \ddots & \cdots & 0 \\ 0 & 0 & 0 & 1 & -2 & \ddots & \ddots & \vdots \\ \vdots & \vdots & \vdots & \ddots & \ddots & \ddots & \ddots & 0 \\ 0 & 0 & 0 & 0 & \ddots & \ddots & \ddots & 1 \\ 0 & 0 & 0 & 0 & 0 & 0 & 1 & -1 \end{bmatrix} \times \begin{bmatrix} U_1 \\ U_2 \\ U_3 \\ U_4 \\ U_5 \\ \vdots \\ U_{N-1} \\ U_N \end{bmatrix} = \begin{bmatrix} -(\Delta z)^2 f_1 - 2U_L \\ -(\Delta z)^2 f_2 \\ -(\Delta z)^2 f_3 \\ -(\Delta z)^2 f_4 \\ -(\Delta z)^2 f_5 \\ \vdots \\ -(\Delta z)^2 f_{N-1} \\ -(\Delta z)^2 \frac{f_N}{2} \end{bmatrix} \tag{4-30}$$

For DD problem, the forming of the equation for the first node, where potential is applied, is the same as the procedures in the DN boundary problem. Eq. (4-26) also applies here, but a potential of U_L is applied instead of 0V. Thus, the equation becomes

$$U_0 = 2U_L - U_1 \tag{4-31}$$

On the right hand side, Eq. (4-26) is modified to obtain the following expression.

$$U_{N+1} = 2U_R - U_N \tag{4-32}$$

Thus, the system for equations for the DD boundary problem can be written as follows.

$$\begin{bmatrix} -3 & 1 & 0 & 0 & 0 & \cdots & \cdots & 0 \\ 1 & -2 & 1 & 0 & 0 & \cdots & \cdots & 0 \\ 0 & 1 & -2 & 1 & 0 & \cdots & \cdots & 0 \\ 0 & 0 & 1 & -2 & 1 & \ddots & \cdots & 0 \\ 0 & 0 & 0 & 1 & -2 & \ddots & \ddots & \vdots \\ \vdots & \vdots & \vdots & \ddots & \ddots & \ddots & \ddots & 0 \\ 0 & 0 & 0 & 0 & \ddots & \ddots & \ddots & 1 \\ 0 & 0 & 0 & 0 & 0 & 0 & 1 & -3 \end{bmatrix} \times \begin{bmatrix} U_1 \\ U_2 \\ U_3 \\ U_4 \\ U_5 \\ \vdots \\ U_{n-1} \\ U_n \end{bmatrix} = \begin{bmatrix} -(\Delta z)^2 f_1 - 2U_L \\ -(\Delta z)^2 f_2 \\ -(\Delta z)^2 f_3 \\ -(\Delta z)^2 f_4 \\ -(\Delta z)^2 f_5 \\ \vdots \\ -(\Delta z)^2 f_{n-1} \\ -(\Delta z)^2 f_1 - 2U_R \end{bmatrix} \tag{4-33}$$

The system of equations above forms a tridiagonal matrix. It can be solved via the Gaussian elimination method, or more specifically, the Thomas algorithm, which is a simplified form of the Gaussian elimination method for solving tridiagonal matrix systems (Lee 2011). Once the potentials at all the nodes are found, the energy of the electron ensemble crossing the electric field is updated as follows.

$$E = \left(E_{cond,\min} + \frac{\hbar^2 \vec{k}^2}{2m^*} \right) + e\left(U_{final} - U_{initial} \right) \tag{4-34}$$

Note that U_{final} and $U_{initial}$ are the potential at the current and last known location of the electron ensemble. To simplify the treatment of electron energy due to the electric field effect, in the event that the electron ensemble remains within the same computational grid, it will not experience any change in its energy. This saves up computational time for interpolation in between the mesh to obtain the exact potential difference between current position and last known position.

4.7 Account for Energy Absorbed by Lattice and Electron Generation by Phonons

The energy of each ensemble is altered in scattering events, and also due to the effect of the electric field. As there is no differentiation between electron-electron scattering and electron-phonon scattering at this point in time, energy cannot be transferred based on the identification of the events. In other words, without consideration of phonon absorption or emission processes in a more physical and discrete manner, the current model is unable to treat the interaction separately and have the exact amount of energy passed between scattered electron and absorbed or emitted phonon. In fact, within the scope of this model, such interactions have been both included within the relaxation time approximation model as per discussed in Chapter 4.4. This can be further improved in future but at this point, it is of interest to introduce a „hand-waving" method to treat the energy transported from electrons to phonons.

The proposed method is uncommon but represents a quick and easy way to treat the energy transfer between electrons and phonons. At the end of each time step, following the evaluation of the effect of electric field, the energy of each ensemble will be computed and checked. If the energy level of a particular ensemble is found to drop below the conduction band minimum, it will be „removed" from the medium. This is based on the assumption that no conduction electron can exist within the band gaps and thus it is assumed that this electron has recombined with the holes, thus its energy is transferred to phonons. Then again such interaction may involve emission of photons other than phonons, but for the sake of simplicity, it is assumed that the energy will go to lattice directly instead of going through several transitions. The energy of the removed ensemble will be recorded and stored by summing all energies from „removed" electrons and dividing them by the computational grid volume and the time elapsed to obtain the volumetric heat generation term for each computational grid. Mathematically, this can be shown as follows

$$\dot{E}'''_{gen}\left(x,y,z\right)=\frac{\sum E_{elec}\left(x,y,z\right)}{\Delta x\Delta y\Delta z\Delta t} \tag{4-35}$$

CHAPTER 5

Coupling of Phonon and Electron Transport

5.1 Overview of Coupled Electron-Phonon Transport

Electron-phonon interaction plays a huge part in the semiconductor transport. It has been studied for almost a century, but its complicatedness means the predictive non-empirical calculations have only become feasible in the past twenty years or so. Many studies have attempted to scrutinize this phenomenon mathematically by means of first principle calculation (Bernardi 2016; Giustino 2016; Gunst et al. 2016). It is to be noted that the detailed calculations will not be performed in this thesis as the focus is on the application side of it, hence to propose an alternative strategy to couple electron and phonon transport.

Electron-phonon interactions are an important mean for energy and momentum relaxation of energy carriers in semiconductors. It is an essential part for the understanding of charge transport, inelastic processes and heating effects in micro and nanoscale devices. The scenario in which hot electrons are injected into a semiconductor device would involve rigorous electron-phonon interactions that inevitably causes in heating of the device. As electrons are accelerated under the influence of an applied electric field, they will slowly gain energy and will eventually

have sufficient energy to emit a net amount of phonons (Pop 2014). This ultimately results in a phenomenon called Joule heating, which is a major concern in micro and nanoscale devices. It leads to a departure from the equilibrium especially in the phonon system, as evident in the rise in temperature within the medium. The thermodynamic laws detect that the system will have to find a way to return to equilibrium, thus dissipating this additional heat gained. Many literatures have dedicated effort in Joule heating and localized heating problems in semiconductor devices as they are one of the primary sources of device failures (Pop 2008; Pop et al. 2001; Pop, Dutton & Goodson 2005). It is worth noting again that in nanoscale devices, thermal profile is governed by which of the phonon polarization branches that receive the energy from the hot electrons, the rate at which they scatter the energy and also their group velocities. The heating within a device are normally a result of slow moving high frequency optical phonons carrying most of the energy, as the fast moving acoustic phonons are responsible to quickly carry energy away to the boundaries. An electro-thermal simulation in MOSFETs was carried out and found out that 79% of the heat generation by electron-phonon interaction is in the optical branches, with the longitudinal branch receiving the greatest percentage (Ni et al. 2012). Mid-to-high frequency bands of the acoustic phonon branches interact strongly with the longitudinal optical branch. While heat conduction is mainly dominated by acoustic modes, the heat generation is mainly due to the optical modes. Their work also incorporated full band description of electrons and phonons and considered 22 types of electron-phonon scattering events.

More MC simulation of coupled electron-phonon transport can be found in the literatures. Recent works (Kamakura et al. 2014; Kamakura et al. 2010) used this technique for transient electron-phonon transport in nanoscale devices and in small field effect transistors (FET). Their method involved a phonon simulator calibrated to yield the correct thermal conductivities and a standard MC model for electron transport as proposed by Jacoboni and Reggiani (1983) which includes both electron-phonon and electron-electron interactions. Heat generation rate can thus be calculated based on phonon emission from electrons, and the focus was placed solely on acoustic phonons as the main heat carrier. Optical phonons‟ contribution to the heat conduction was assumed negligible, but the relaxation time approximation was used to convert the optical modes to the acoustic modes via phonon-phonon scattering to account for the

thermal energy dissipation. Essentially, what really happens is the acoustic phonon transport will be used to generate a temperature distribution to be included in electron transport, while the electron transport will be used to compute the total phonon emission which will then be fed into the phonon simulation as volumetric heat generation. In their models, they were able to gain insights into hot spot generation and dissipation in nanoscale devices, which are especially useful information to understand heating issues. The similar strategy was also adopted by other studies (Raleva et al. 2008; Rowlette & Goodson 2008). One of the most common issues faced by all was the difference in time scale for electron and phonon simulations. In general, they were dealt with individually before being included in a self-consistent loop. In semi-classical BTE, the coupled system involving electron-optical phonon-acoustic phonon-heat bath can be described as (Raleva et al. 2008)

$$\left(\frac{\partial}{\partial t}+\upsilon_{elec}(k)\cdot\nabla_r+\frac{e}{\hbar}E(r)\cdot\nabla_k\right)f=\sum_q\left\{W_{emi,q}^{k+q\to k}+W_{abs,q}^{k+q\to k}-W_{emi,-q}^{k\to k+q}-W_{abs,q}^{k\to k+q}\right\} \tag{5-1}$$

$$\left(\frac{\partial}{\partial t}+\upsilon_{ph}(q)\cdot\nabla_r\right)g=\sum_k\left\{W_{emi,q}^{k+q\to k}-W_{abs,q}^{k\to k+q}\right\}+\left(\frac{\partial g}{\partial t}\right)_{ph-ph} \tag{5-2}$$

The distribution function f and g refers to electron distribution function and phonon distribution functions respectively, while the term $W_{emi,q}^{k+q\to k}$ refers to the probability for electron transition from $k+q$ to k due to phonon q emission. $W_{abs,q}^{k+q\to k}$ on the other hand, refers to phonon absorption process. The probabilities of all the W terms depend heavily on the product of $f\cdot g$, and governs the energy transfer between electron and phonons. The electron transport, as expected, has to account for electric field as shown in Eq. (5-1), while phonon transport involves the phonon-phonon interaction as included on the right hand side of the Eq. (5-2). The time evolution of the energy transfer process is depicted in Figure 5.1.

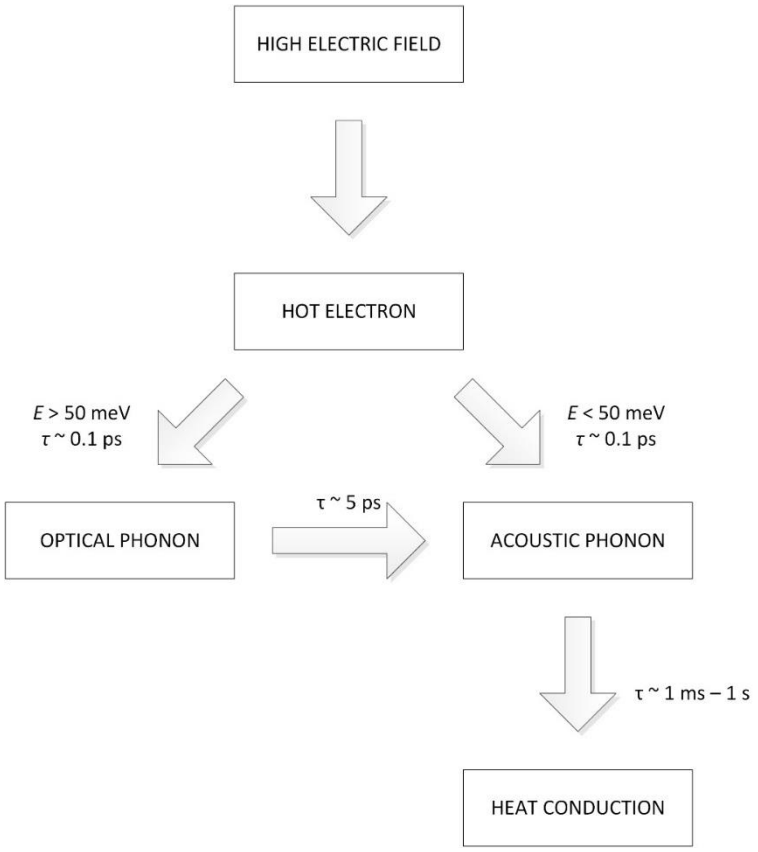

Figure 5.1 Energy interaction between phonons and electrons, and the characteristic time scales of energy transfer processes in Si (Pop, Sinha & Goodson 2006).

As seen throughout the years, the MC method has been widely used to model electron-phonon interactions and coupled electron-phonon transport models have been proposed to deal with mainly heat dissipation issues in electrical transport problems. Weaknesses still persist in that there are still simplifications and assumptions used in the modelling process. To date, one of the most sophisticated models that includes not only the full band structure developed from pseudopotentials but also the full phonon dispersion relation obtained from adiabatic bond-charge model, and treats the electron-phonon scattering rates as a function of energy and wave vector (Kunikiyo et al. 1994; Yoder & Hess 1994). Without doubt, these models can be burdensome for most computers to simulate, and will not be very practical for realistic applications. The fact is that as most of these models tend to look at electron transport foremost, the models are based on relatively complete MC electron transport simulations, but with simplifications on the phonon dispersion relations. However, results have shown that they are realistic and practical. Coming back to the treatment of electron-phonon interactions, the common

mathematical expression to account for this interaction is computed from Fermi‟s Golden Rule, which is derived from first-order time-dependent perturbation theory, (Ferry 2000; Pop, Sinha & Goodson 2002) as

$$\Gamma_{elec-ph}(k) = \frac{2\pi}{\hbar}\left|M(k)\right|^2 D\left(E_k \pm \hbar\omega_q\right) \tag{5-3}$$

The dependence on a few phonon information such as occupation states, wave function overlap integral and deformation potential characteristic is included in the matrix element *M(k)* in the above equation. The upper and lower signs in the equation correspond to the absorption and emission of a phonon. In most available models, the electron-phonon scattering is further scrutinized by differentiating intravalley and intervalley scattering. Intravalley scattering refers to scattering within the same conduction band valley and usually involves acoustic phonons, while intervalley scattering occurs between valleys. Pop et al. (2004) and Rowlette and Goodson (2008) incorporated both of these scattering rates in their coupled MC electron-phonon transport models. Within the context of electron transport, it will not be complete without the inclusion of a self-consistent Poisson‟s equation solver to account for the electric field, which was found to affect the electron-phonon scattering rate (Wang, Quan & Ruan 2011). Complete simulations such as these appears to have an advantage as they tend to predict the heat diffusion process more accurately than conventional ones such as the drift diffusion model (Pop 2008). Thus, such approaches are particularly effective to provide insight to non-equilibrium thermal dissipation occurring at the micro and nanoscale, something that classical physics often prove to be inaccurate (Nghiêm, Saint-Martin & Dollfus 2016).

Thus, this thesis proposes a methodology to couple phonon transport and electron transport to provide a more accurate picture of heat transport at the micro and nanoscale. The general idea of the strategy adopted in this work follows that found in several literatures (Kamakura et al. 2014; Mohamed, Aksamija & Ravaioli 2015; Pop, Dutton & Goodson 2003; Rowlette & Goodson 2008), such that energy generated from the MC electron transport simulation is passed on to the MC phonon transport simulation. Meanwhile, the MC phonon transport simulation will be generating the temperature profile accordingly and feedback to the MC electron transport simulation, which

essentially will be used to determine the energy and temperature dependent scattering rates. A simple graphical representation of the process is given in Fig. 5.2. It must be noted again that the current simulations do not include any injection of electrons from any external source, such as electron beam. It aims to simulate the heat transport within a semiconductor material independently, and thus examine the possibility of using this model for device simulations in the future. The temperature boundaries imposed merely maintain the number of electrons in the system statistically, assuming electrons recombine with holes at the lower temperature end when their energy falls below the conduction band minima, and electrons are generated at the higher temperature end when they gain sufficient energy to overcome the band gap and move into the conduction band. With that, the system considered is actually close to equilibrium, with the only perturbation coming from the temperature applied at both ends of the medium considered. Nonetheless, the same strategy can also be applied to other problems as per described in the aforementioned literatures.

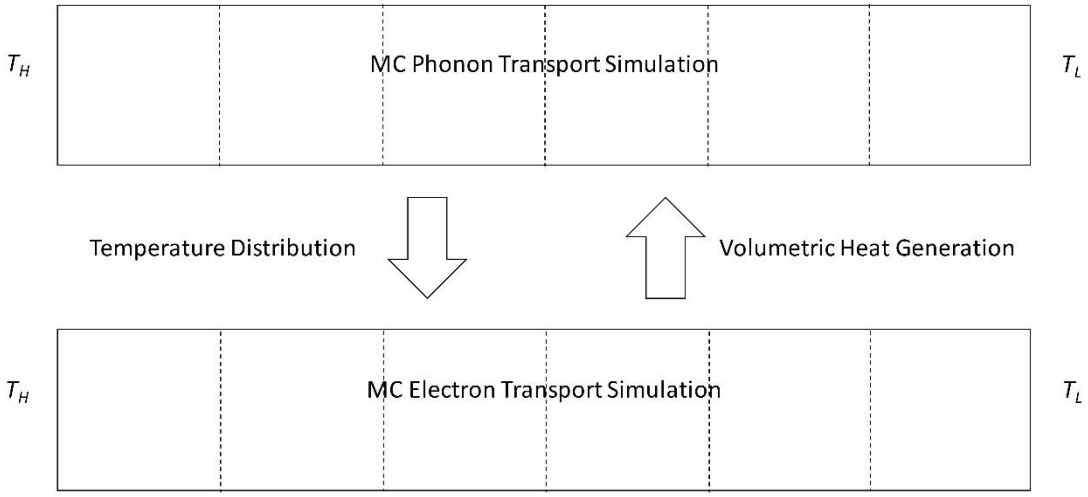

Figure 5.2 Proposed strategy to couple electron-phonon transport simulation. The MC electron transport simulation will generate the heat generation data to be fed into the MC phonon transport simulation. The MC phonon transport simulation on the other hand, will compute the temperature distribution to be fed into the MC electron transport for more realistic scattering rate computation.

5.2 Proposed Strategy to Couple MC Electron-Phonon Transport Simulations

Following the end of the MC electron transport simulation, the heat generation data is recorded and fed as part of the input data to the MC phonon transport simulation. For the sake of simplicity and to cater for the heat generation function in MC phonon Transport as per discussed in Chapter 3.7, the total energy of electrons passed on to phonons are recorded volumetrically as in Eq. (4-35), but by considering only a 1D profile in the *Z*-direction (see Figure 2.9 for the definition of the computational grid volume and direction).

The lattice temperature has been assumed to be constant throughout the medium in the independent electron transport. Without considering any phonon transport, it is impossible to come up with a realistic temperature distribution, especially if Joule heating occurs in the medium of interest. Under such circumstance, thermal equilibrium will be perturbed and the temperature distribution will change. Therefore, by accounting for the volumetric heat generation that leads to phonon generation following Eq. (3-35), any rise of temperature can be computed in the MC phonon transport simulation.

As aforementioned, one of the main concerns is the different time scales to be considered in the coupled MC electron and phonon transport simulations. Electrons and phonons have different relaxation times and it is thus difficult to begin with the same time step without compromising on the simulation efficiency. To overcome this, it is therefore proposed that the simulations be considered at steady state only. The MC electron and phonon transport simulations are allowed to run independently until a steady state is achieved, before the information is stored and passed on. In this case, several iterations may be required to achieve converged results.

CHAPTER 6

Simulation Results

6.1 MC Phonon Transport Simulation Results

6.1.1 Bulk Thermal Conductivity Simulation

The thermal conductivities obtained at the diffusive limit are compared with the known bulk values obtained from the literatures (Maycock 1967) for temperatures of 200K, 250K, 300K, 350K and 400K as a form of verification of the transport model. The results have previously been published in the Numerical Heat Transfer, Part B: Fundamentals (Bong & Wong 2014).

In order to confirm the diffusive regime and that the comparison is viable, simulations was carried out to inspect the thermal conductivity at 300K for different medium thickness (from 0.1μm to 8μm) but the same cross section (500nm × 500nm). The X- and Y-boundaries were all assumed adiabatic with specular reflection, such that they could be assumed to be of infinite lengths. Theoretically, the thermal conductivity will converge to a constant value in the diffusive regime, which can be further confirmed by the presence of a continuous temperature gradient when the steady state or equilibrium condition is achieved (Wong, Francoeur & Pinar Mengüç 2011). In other words, there should be no discontinuities at both ends of the medium in the temperature distribution because a discontinuity characterizes ballistic transport.

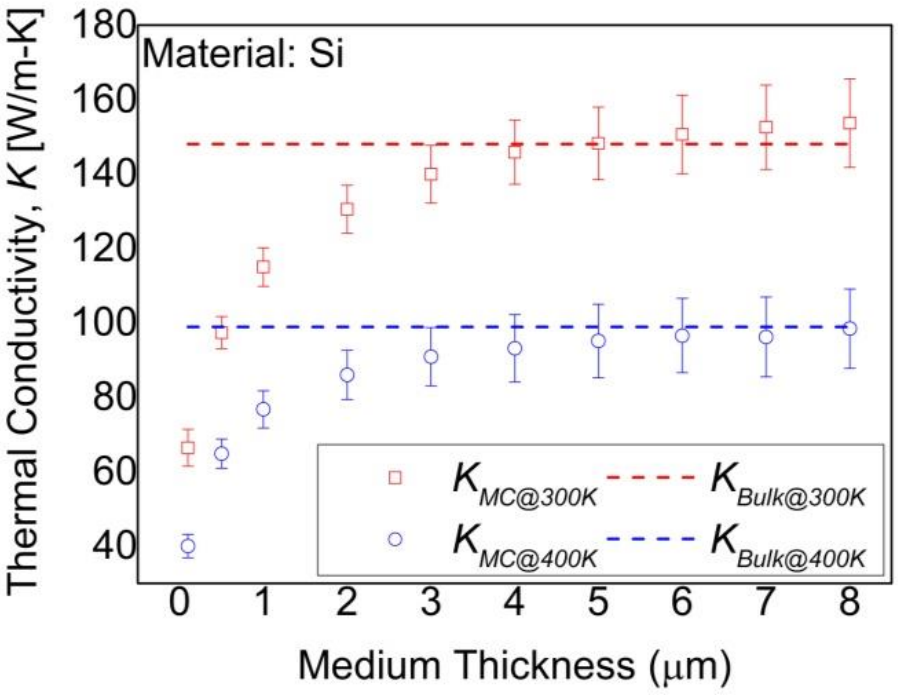

(a)

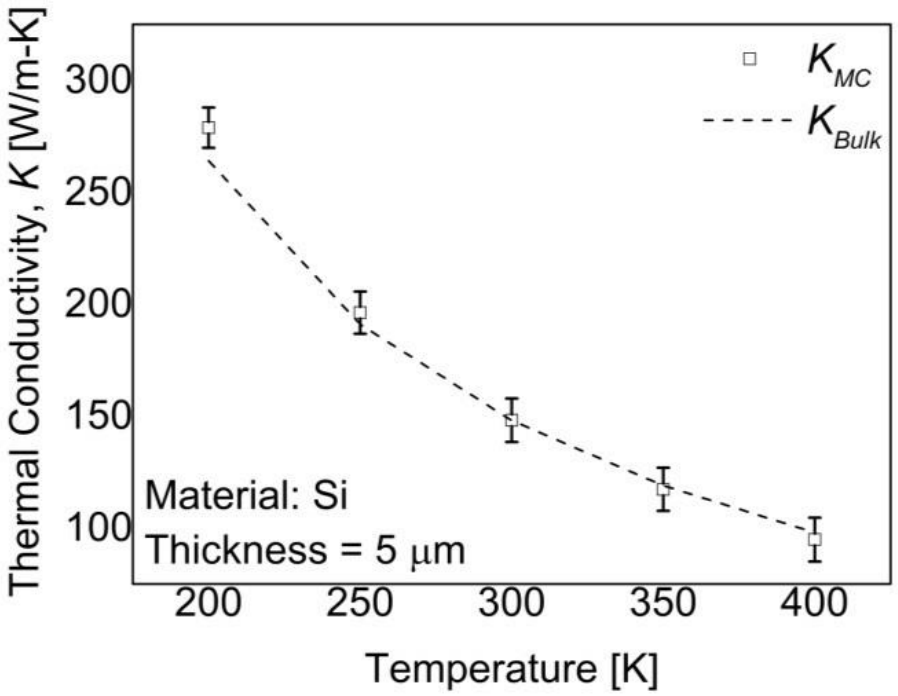

(b)

Figure 6.1 Verification of the thermal conductivity computed by the MC simulation against known bulk values obtained from the literature (Maycock 1967) for Si.

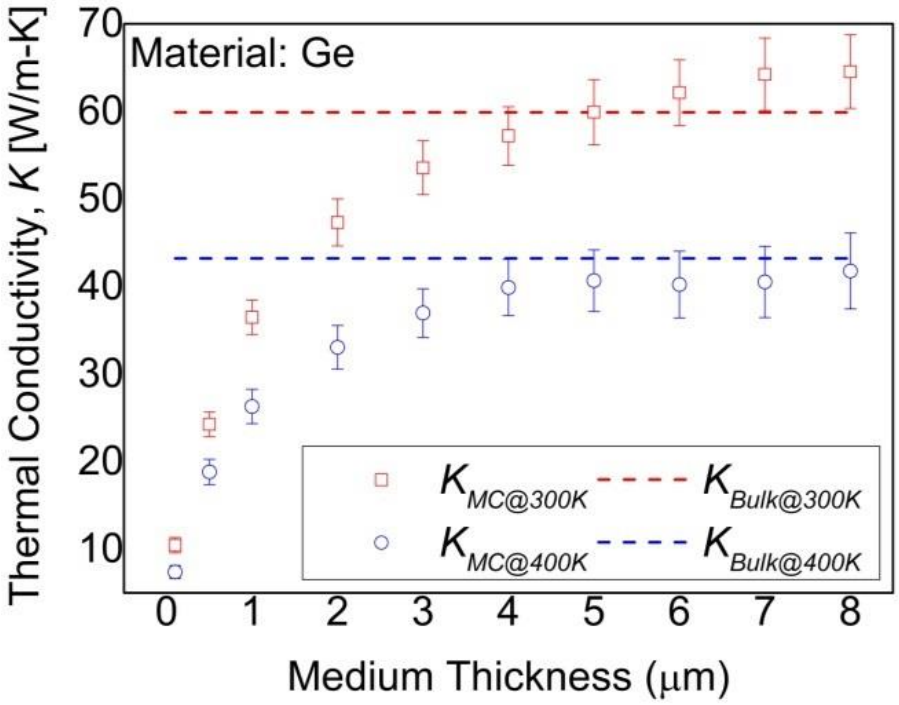

(a)

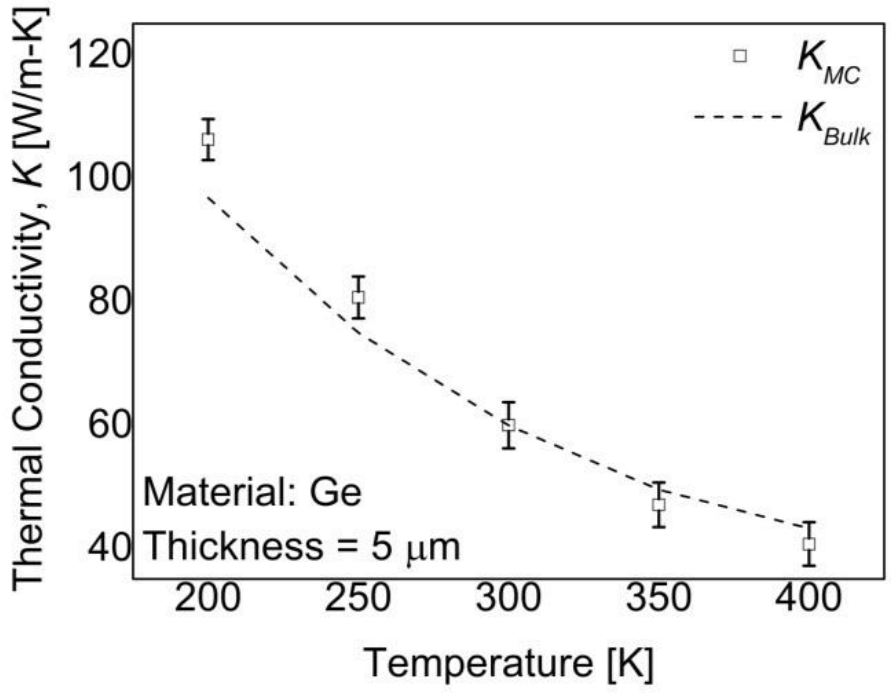

(b)

Figure 6.2 Verification of the thermal conductivity computed by the MC simulation against known bulk values obtained from the literature (Maycock 1967) for Ge.

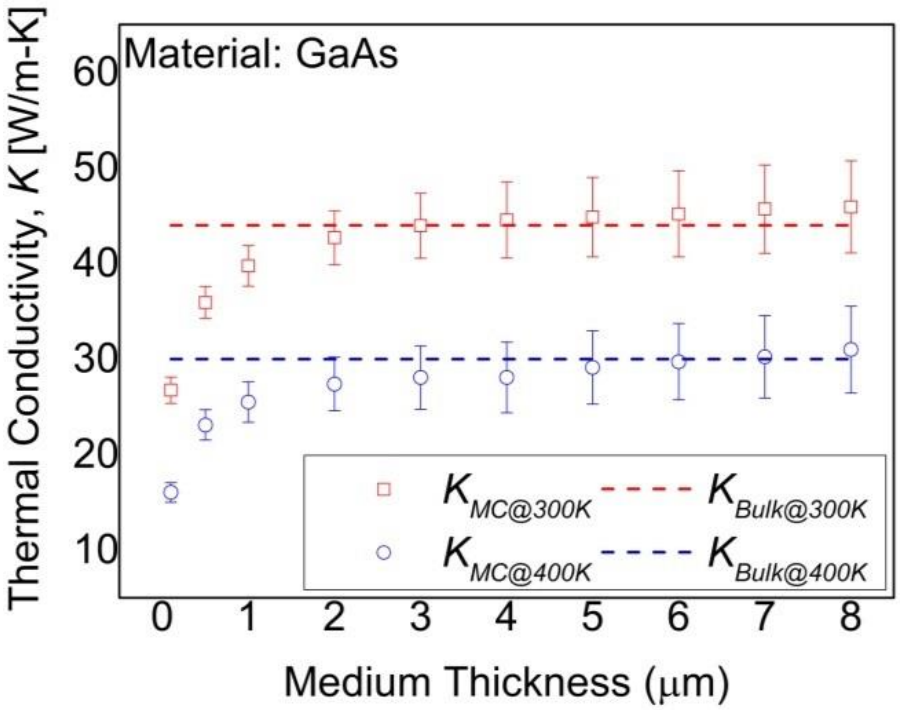

(a)

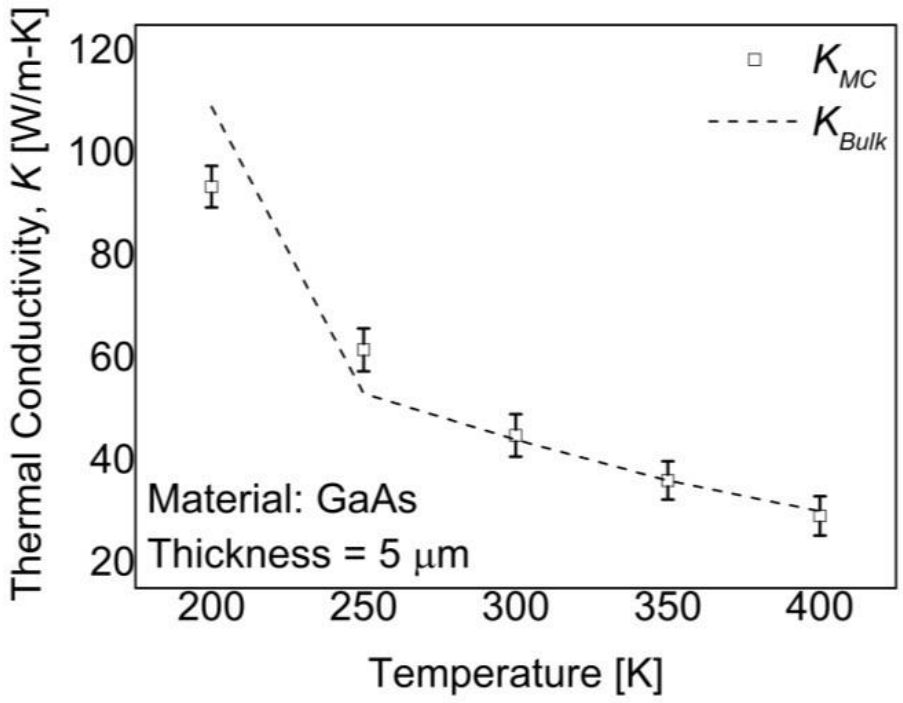

(b)

Figure 6.3 Verification of the thermal conductivity computed by the MC simulation against known bulk values obtained from the literature (Maycock 1967) for GaAs.

From Figure 6.1(a), Figure 6.2(a) and Figure 6.3(a), the heat transport is diffusive at a thickness of 5μm for Si and Ge, while the diffusive limit for GaAs lies at 4μm. The thermal conductivities for each of the Si, Ge and GaAs medium converge to their respective bulk values beyond the diffusive limit and stay fairly constant. At thickness lower than the diffusive limit, the thermal conductivities of all the three materials decreased significantly, consistent with known theories on semi-ballistic and ballistic transport. At smaller length scales, phonons are able to travel from one end to another in a shorter amount of time and the number of scattering events concurrently decreases. Note that the bulk thermal conductivities were calibrated to suit the current model by adjusting the parameters B_L, B_T and B_{TU} as per discussed in Chapter 3.4. Note that the differences to the values for Si used previously by Wong et al. (Wong, Francoeur & Pinar Mengüç 2011) is largely due to the implementation of anisotropic scattering in the current model. Any other different model would still call for yet different values of the respective parameters.

A second comparison was done on the bulk thermal conductivities at temperature range of 200K to 400K (as shown in Figure 6.1(b), Figure 6.2(b) and Figure 6.3(b)) , where the computed values agreed fairly well at 300K, but deviates slightly at 200K and 400K for all the three materials. It is important to note that not all the possible scatterings had been accounted for in the current model. Scatterings are often dominated by imperfections and boundary scatterings at lower temperatures where population of the long wavelength phonon increases, but phonon-phonon scatterings are dominant at higher temperatures (Asheghi et al. 1997; Asheghi et al. 1998). However, this work has assumed only the perfect intrinsic materials with specular reflection, hence discounting the effect of surface roughness. The consideration of each of these effects will be significant in improving the simulation results but is currently out of the scope of the current study. Furthermore, GaAs is different from Si and Ge in the sense that it contains two different elements (Ga and As) with different sizes and properties. In the current study, it was assumed as a single element without any consideration of the impact of each of the individual elements which are foreign to one another, hence likely to cause the deviation of the computed bulk thermal conductivity at temperatures lower than 300K. Nonetheless, at any temperatures of 300K or above, the current model is

able to provide a sufficiently good prediction of the thermal conductivity of GaAs and thus the heat distribution in the material.

6.1.2 Si Nanostructure Thermal Conductivity Simulation

The MC phonon transport simulation was used to predict the thermal conductivity of Si nanowires. In reality, simulations involving nanostructures will require knowledge of the material properties at the nanoscale, such as changes in dispersion relations, scattering rates etc. Such information nevertheless, are found to be scarce in the available literatures. As pointed out in most studies however, it is still safe to assume the bulk approximations for the length scales considered within the scope of this study (Chantrenne et al. 2005; Randrianalisoa & Baillis 2008). For Si nanowire simulations, the diameter considered were 115nm, 56nm, 37nm and 22nm. Due to the closeness of the results obtained using cuboid and cylinder geometry, the cuboid geometry was used for reasons of simplicity and consistency in all results. For better depiction of the geometry, the *X*- and *Y*- dimensions of a square cross section of a cuboid were computed based on the following mathematical expression

$$\frac{\pi d^2}{4} = XY, X = Y \tag{6-1}$$

Hence, the corresponding cross sectional areas of the „squared" nanowires were 101.9nm, 49.6nm, 32.8nm and 19.5nm respectively, while the simulated length was set at 2000nm. A temperature difference of 5K was applied between both ends of the Si nanowire, i.e. 2.5K above and 2.5K below the temperature of interest. The simulation results were compared to the experimental results obtained from the literature (Li et al. 2003), and were shown in Figure 6.4. The current model appeared to have produced identical results to the experimental data at 115nm, 56nm and 37nm, but struggled to reproduce the experimental data, as with some of the available MC phonon transport simulations available at present (Chantrenne et al. 2005; Randrianalisoa & Baillis 2008). This could be due to the phonon confinement effect and boundary scattering effect which ultimately lead to drastic decrease in the thermal conductivity in the nanowire

(Zou & Balandin 2001). These are some considerations that could be accounted for in future studies to improve the prediction by any MC phonon simulation models.

The MC phonon transport simulation was also used to predict the in-plane thermal conductivity in Si thin film. The data obtained from the current simulation model was found to closely resemble the experimental data obtain from the literatures for Si thin films with thicknesses of 3000nm, 1600nm, 830nm, 410nm, 100nm and 20nm (Asheghi et al. 1997; Liu & Asheghi 2006). Results are shown in Figure 6.5, Figure 6.6 and Figure 6.7. For the current simulations, the *X*- and *Y*- dimensions of the thin film were set at 20000nm, and are both assumed to be of diffusive nature. A temperature difference of 5K was applied between both ends of the thin film, i.e. 2.5K above and 2.5K below the temperature of interest.

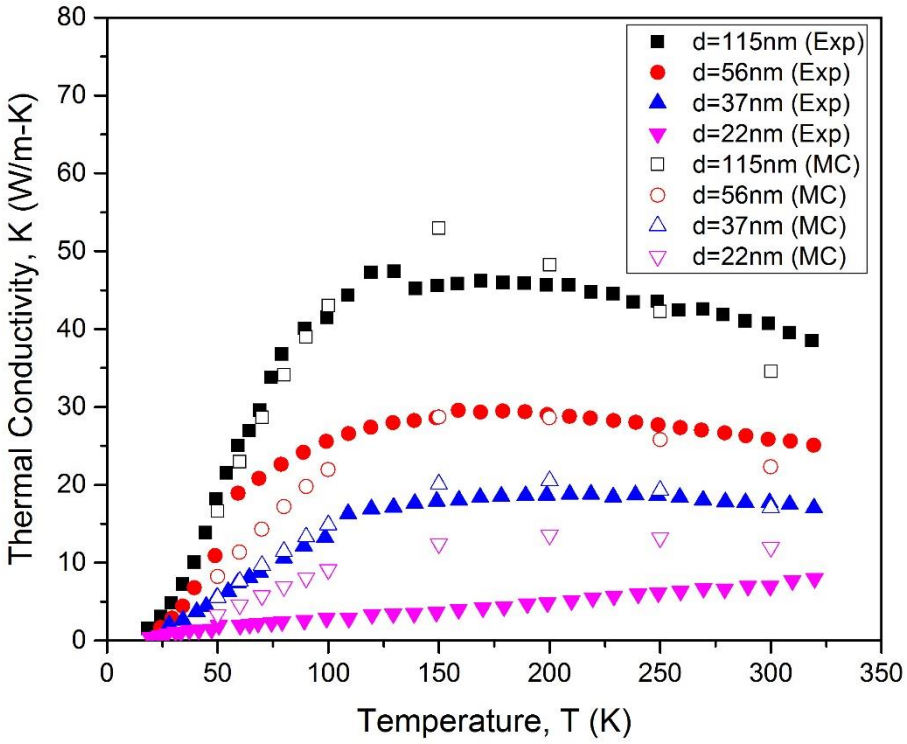

Figure 6.4 Comparison of MC phonon transport simulation results with experimental results from (Li et al. 2003) for Si nanowires. „Exp" denotes experimental data, while „MC" denotes simulated results.

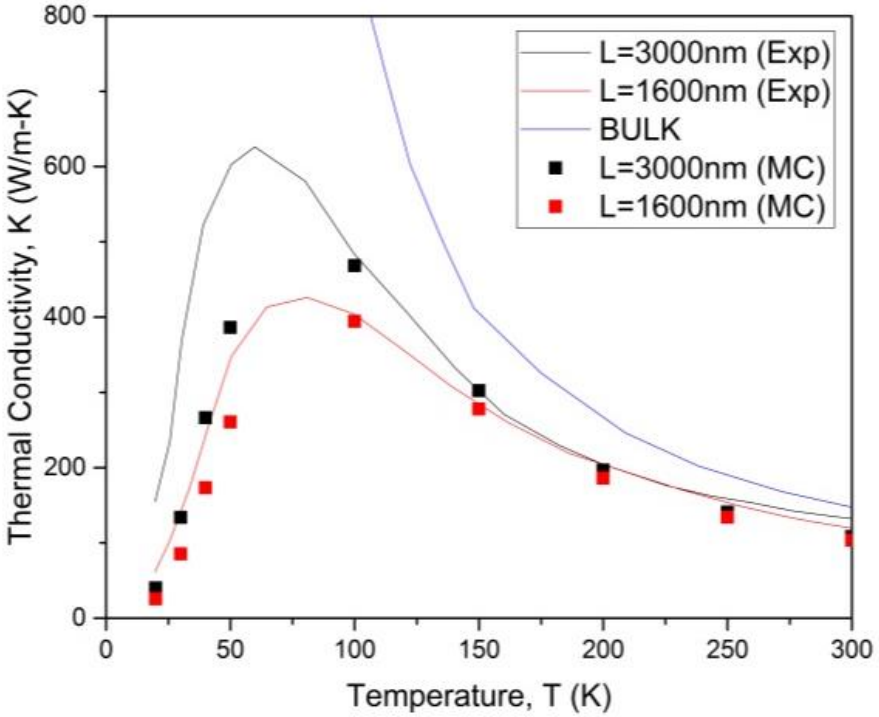

Figure 6.5 Comparison of MC Phonon simulation results with experimental results from the literatures for Si thin film of 3000nm and 1600nm. „Exp" denotes experimental data, while „MC" denotes simulated results.

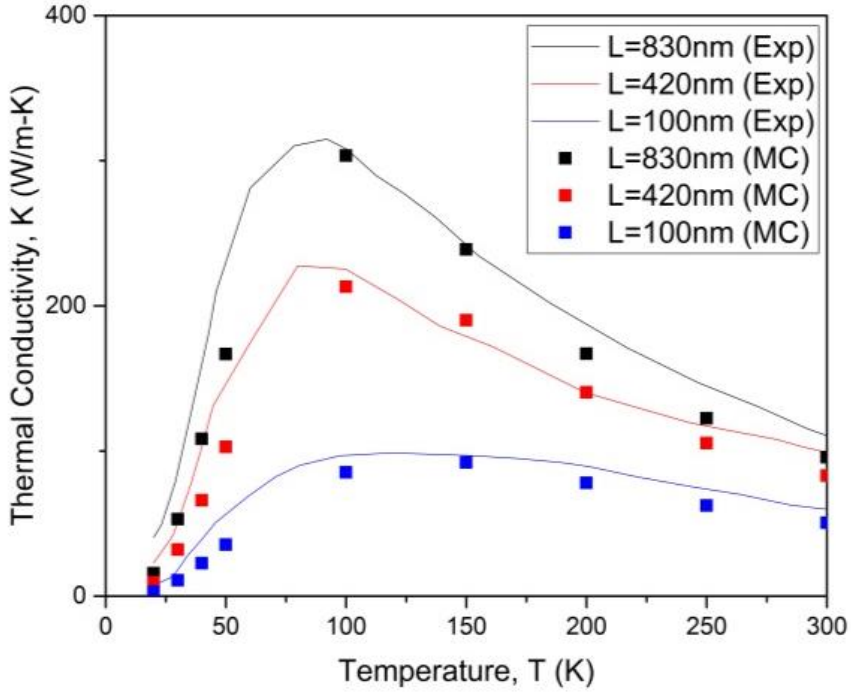

Figure 6.6 Comparison of MC Phonon simulation results with experimental results from the literatures for Si thin film of 100nm, 420nm and 830nm. „Exp" denotes experimental data, while „MC" denotes simulated results.

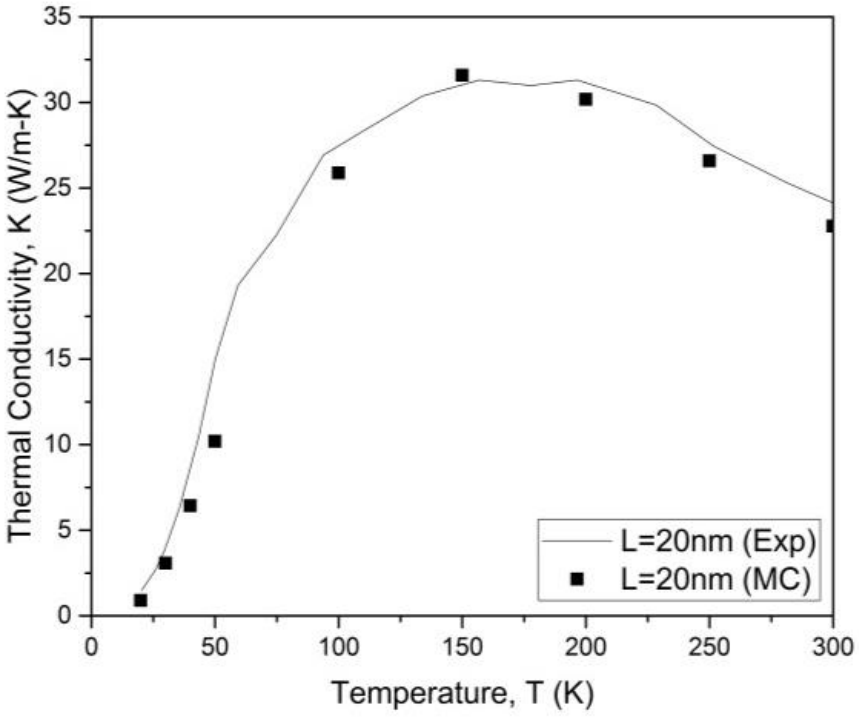

Figure 6.7 Comparison of MC Phonon simulation results with experimental results from the literatures for Si thin film of 20nm.

Such full fledge comparisons have also been conducted by using an analytical model constructed based on the harmonic theory of solids (Chantrenne et al. 2005; Chantrenne et al. 2007). The current simulation results showed a similar trend to the results obtained from the analytical model – the thermal conductivities are often found to be lower than that obtained in the experiments. As with the case of Si nanowire simulations, several effects at the nanoscale were not considered in the current study. They can however, be scrutinized in the future works aiming to produce considerably a more matching set of results to the experimental data.

6.1.3 Assessment of the Effect of Anisotropic Scattering in Si Thin Films

An assessment of the effect of anisotropic scattering in Si thin films at 300K and 400K was recently published in Journal of Physics and Chemistry of Solids (Bong & Wong 2016). These temperatures are selected due to future interest in applying the result of the current study to practical situations related computer chips and photovoltaic cells of which the operating temperatures lie within this range (Nam et al. 2014).

The results obtained by applying the HG probability density function were first verified by comparing the computed thermal conductivity to that obtained from the literature, assuming $g = 0$ for fully isotropic scattering, which was found to be consistent with the results shown in Chapter 6.1.1. In order to investigate the effect of forward and backward scattering, the value of g is set from -1.00 to +0.75, which corresponds to highly backward scattering scenarios and highly forward scattering scenarios. At this point, the transport behaviour for $g = +1.00$ was not simulated, as it would represent a fully ballistic transport in which phonons are allowed to travel in a straight line without any collisions, thus rendering thermal conductivity meaningless. Moreover, having ballistic transport at the length scale of a few micrometres is unrealistic from the physics standpoint. Considering all the above, the simulation for $g = +1.00$ has been omitted in this work. The results obtained for $T = 300$K and $T = 400$K are shown in Figure 6.8 and Figure 6.9 respectively.

From the results obtained, it is clear that a preference in the phonon scattering direction will affect the thermal conductivity. As g approaches unity which indicates a highly forward scattering mechanism, higher thermal conductivity is obtained as compared to that computed while assuming isotropic scattering ($g = 0.00$). In contrast, as g approaches -1.00 from 0.00, the thermal conductivity computed will be less than that computed using isotropic scattering. At both $T = 300$K and $T = 400$K, forward scattering has far more influence on the thermal conductivity as compared to backward scattering. At $T = 300$K, backward scattering is only able to reduce the thermal conductivity slightly (approximately in the range of 2% – 30%), while forward scattering can increase the thermal conductivity from 67% to 100%. Meanwhile at $T = 400$K, backward scattering only reduces the thermal conductivity in the range of 2% - 11%, while forward scattering only increases the thermal conductivity in the range of 2% to 45%. Clearly, as the frequency of scattering increases in the event of increasing temperature, the directional preference has less impact on the heat transport. Under such circumstance, phonons tend to be scattered more frequently, resulting in a more chaotic energy exchange phenomenon. Statistically, higher scattering frequency would lead to more energy exchanges in between phonons, thus creating more „obstacles“ for phonons that hinder their forward movement, thus reducing the net heat flux going through the medium at any point in time. Therefore, the directional preference will not be able to

increase or decrease the thermal conductivity dramatically as compared to that at T = 300K.

Furthermore, as the medium thickness decreases, the effect of anisotropic scattering becomes more pronounced. Largest difference as compared to isotropic scattering is achieved when the medium thickness is 100nm. However, it has to be noted that the extent is non-linear. An exponential increase in thermal conductivity is observed when g is increased from 0.00 to +0.75. An exponential decrease in thermal conductivity however, is not necessary true when g is decreased from 0.00 to -1.00. While an exponential decrease in thermal conductivity is apparent for low medium thickness, the same trend does not extend to higher medium thickness (more than 3μm at T = 300K and 2μm at T = 400K). For higher medium thickness approaching the bulk length scale, the thermal conductivity will increase slightly after a minimum is reached at around g = -0.75. Despite this, speculations on the possible causes of the aforementioned behaviour should be avoided at all cost at this point. Further investigations will have to be carried out in the future to answer those doubts. Such anisotropic effect can be of immense value not only for improving heat transfer, but also in the thermoelectric field. With a better understanding on anisotropic scattering, material science may be able to manipulate it in order to improve the material‟s thermal conductivity, or its dimensionless material figure of merit.

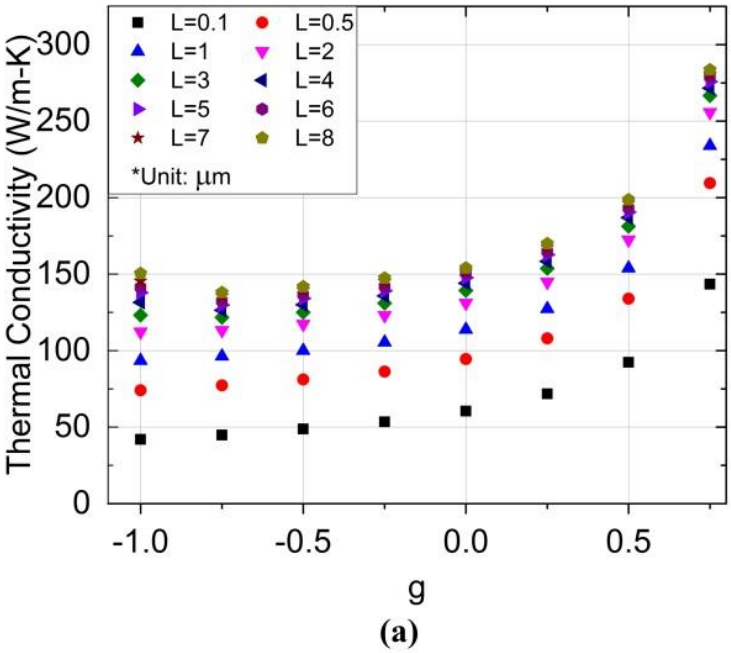

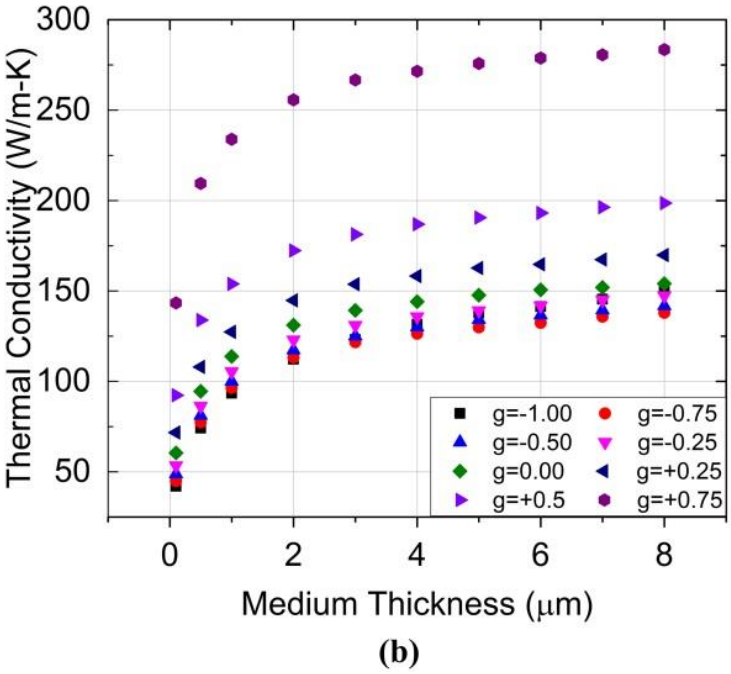

Figure 6.8 Effects of different g on the thermal conductivity at different medium thickness at 300K.

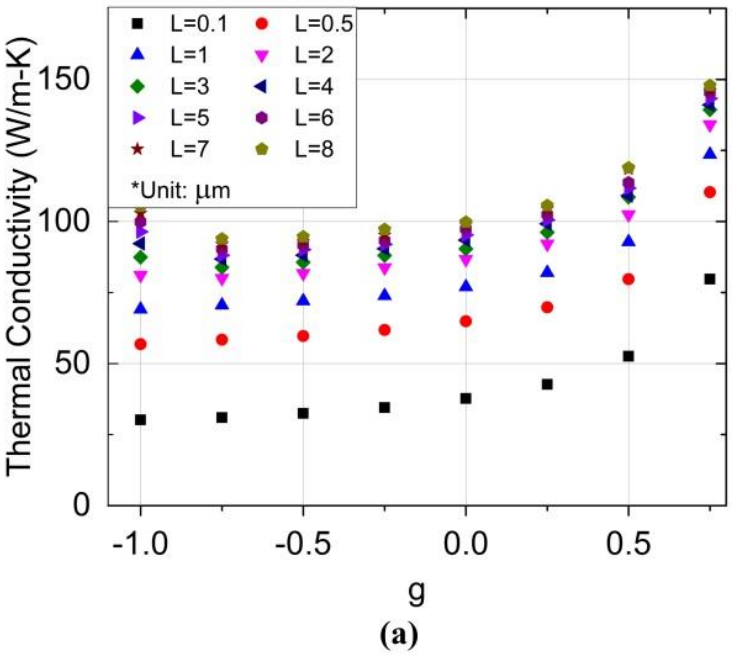

(a)

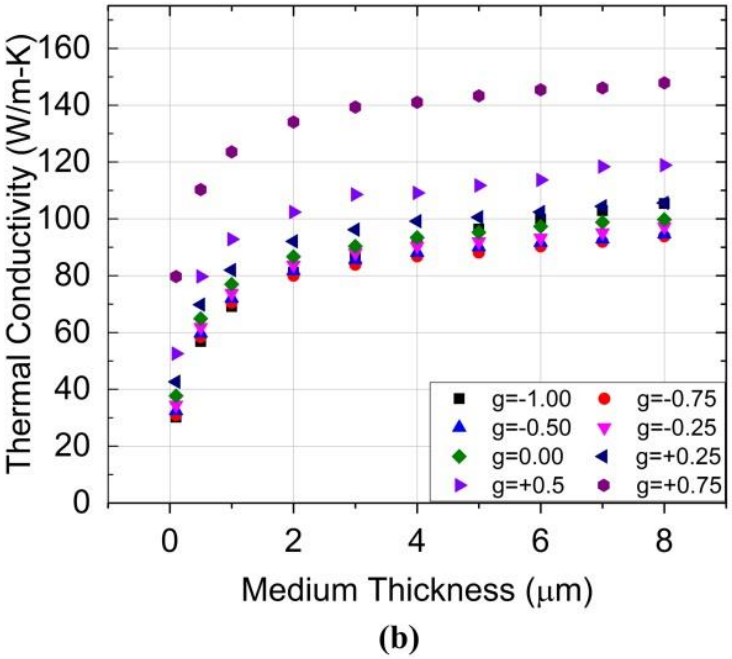

(b)

Figure 6.9 Effects of different *g* on the thermal conductivity at different medium thickness at 400K.

6.1.4 Assessment of Temperature Profile in GaAs Thin Films Considering Heat Generation from an External Source

The evolution of the temperature profile in GaAs thin film with the inclusion of volumetric heat generation due to absorption from photons was recently published in Journal of Quantitative Spectroscopy and Radiative Transfer (Lau, Bong & Wong 2016). Studies pertaining similar phenomena in silicon and amorphous silicon have also been done prior to this study (Lai et al. 2016; Wong et al. 2013). In essence, as heat (in this case, energy carried by photons) is absorbed by the thin film layer, phonons will be generated and the temperature is bound to rise. This „parcel" of energy was computed independently by a near-field radiative heating simulation which is not within the current scope of discussion, and then passed on to the MC phonon transport simulation. The thin film layer is assumed to be intrinsic GaAs of thicknesses 1μm, 3μm and 5μm exposed to near-field radiation from an emitter. The type of material assumed contradicts the initial assumption for the near-field radiative heating simulation which differentiates the *n*-type and *p*-type layers. The incorporation of the different doped layers requires information on the corresponding material properties in order to ensure an accurate MC simulation. This information however, is not readily available. Careful recalibration of the MC simulation will also be required based on the new set of input. However, as the main interest of the current work lies in verifying whether or not a temperature gradient exists in the thin film layer subjected to near-field radiative heating, the aforementioned assumption is therefore undertaken for the sake of simplicity.

Initially, the temperature of the GaAs thin film layer was assumed to be at 300 K. Once heat was absorbed from the near-field radiative heating process, additional phonons are "created" following the local heat absorption rate. Thus, the temperature profile at the start will resemble that of the heat absorption profile. It has to be noted that however, due to the relatively small amount of energy below band gap, it was insufficient to generate phonons at small time intervals of several picoseconds. As such, even though the simulation continued for a long period of time, no phonons were generated and the temperature remained constant at 300 K throughout. This does not represent the true picture as continuous local heating will increase local temperature over time.

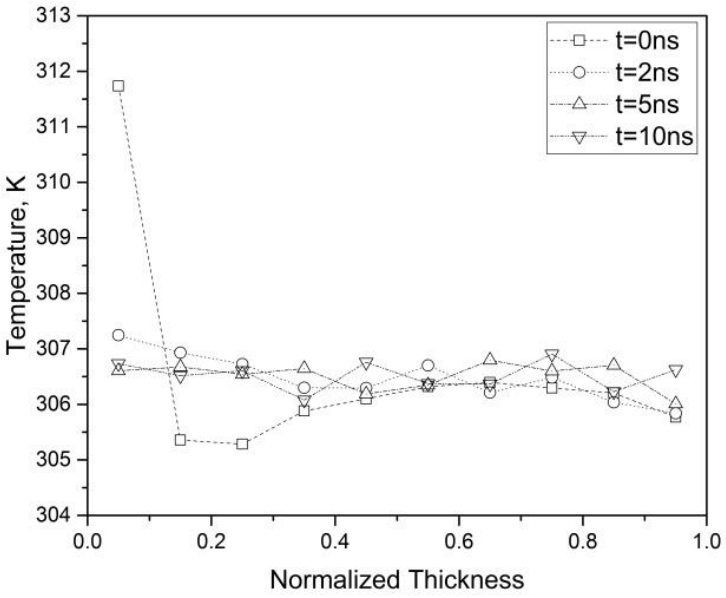

(a)

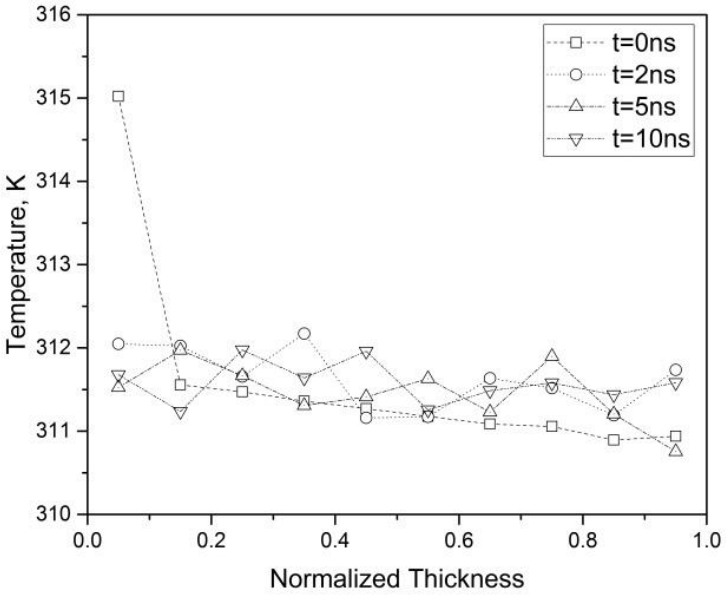

(b)

Figure 6.10 Temperature profile in GaAs 1μm thin film layer at emitter temperature of (a) 1000K and (b) 2000K

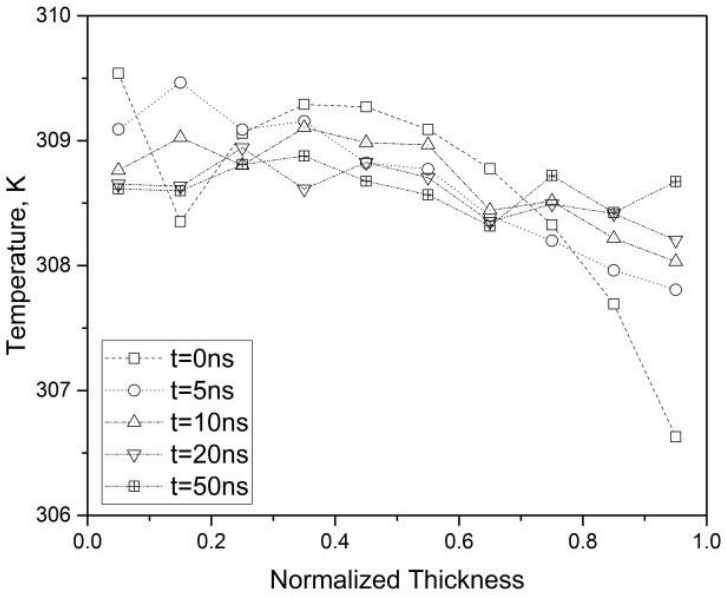

(a)

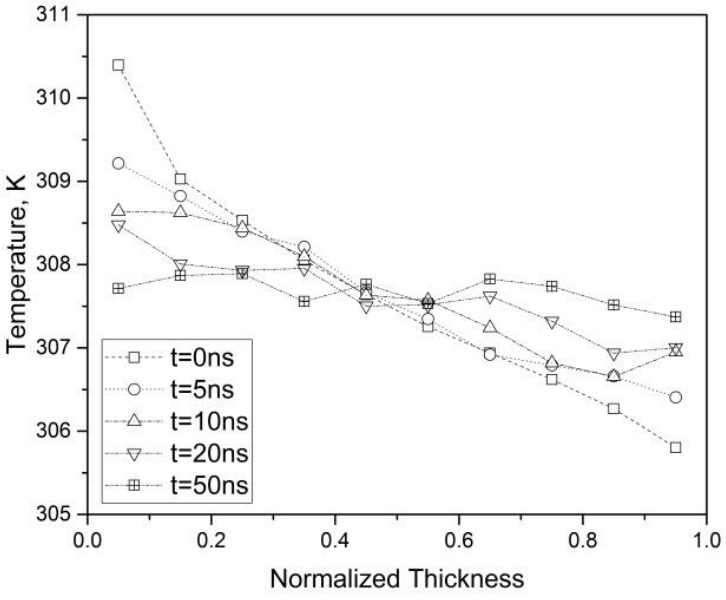

(b)

Figure 6.11 Temperature profile in GaAs 3μm thin film layer at emitter temperature of (a) 1000K and (b) 2000K

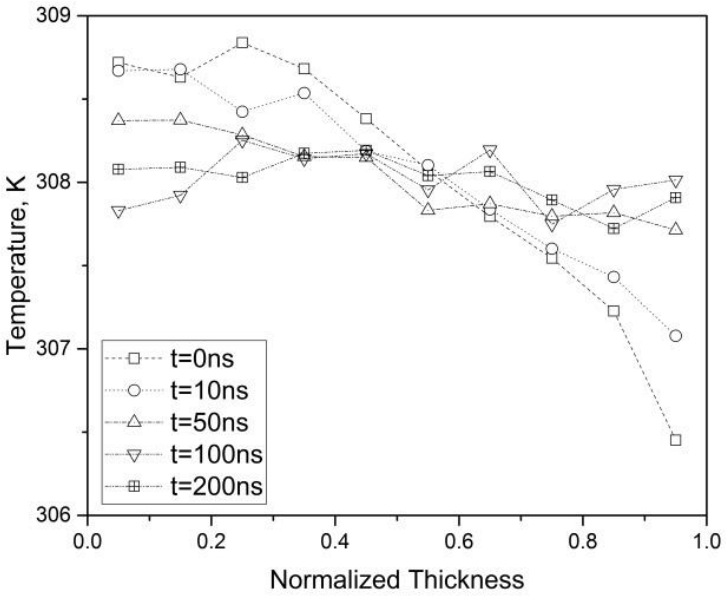

(a)

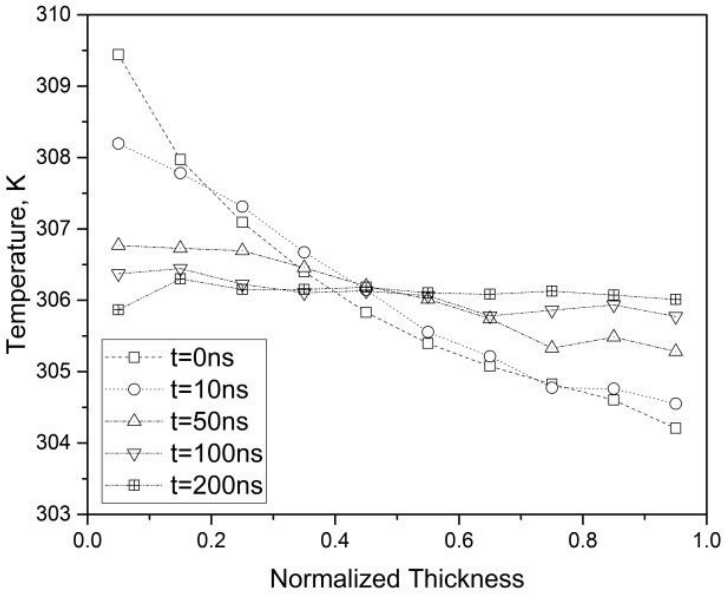

(b)

Figure 6.12 Temperature profile in GaAs 5μm thin film layer at emitter temperature of (a) 1000K and (b) 2000K

In view of this particular issue, the heat absorbed was accumulated up to 100ms and 10ms for emitter temperatures of 1000 K and 2000 K respectively before releasing the entire "parcel" of energy into the thin film layer. Therefore, the heat absorbed time was numerically forced in the simulation. The time 100ms and 10ms were used respectively in order to achieve a considerable rise in temperature, thus providing a clearer view of the evolution of the temperature profile. Any lower values would lead to a lower temperature rise and the change in temperature profile would not be as distinct enough, since the temperature range would be much smaller. The use of any higher values is doable, but at the expense of longer computational time. Here, the amount of energy accumulated was sufficient to increase the temperatures up to several Kelvins, and was able to provide us with the initial temperature profile at t = 0ns as shown in Figure 6.10, Figure 6.11 and Figure 6.12. This was done so to demonstrate that the transient near-field thermal radiation heating occurs at a much slower pace compared to the transient response of phonon conduction in GaAs. Even with the accumulated amount of near-field energy over a random selected timing hitting the material simultaneously, the temperature gradient would still fade over time before the next amount set in. As a result, there would be no temperature gradient within the film established over time. Rather, the entire film was at a uniform temperature which increased as time progressed.

Note that the term normalized thickness used in both figures is computed as the ratio of thickness of the medium up to a particular point to the total thickness of the medium. It shows the thickness as a fraction of the total medium thickness. In both cases considered in this work, the local temperature at the start as well as the temperature at steady state was the highest in 1μm thin film, and it gradually decreases as thickness increases to 3μm and 5μm. On the other hand, the transient process was longer in materials of higher thickness. While it took approximately 10ns to achieve steady state at a thickness of 1μm, it took up to 50ns at 3μm and 200ns at 5μm. The main implication here is that it will take a power density that is several orders of magnitude higher than that was obtained for GaAs to generate phonons at any particular instant in time. With a low heat absorption rate, a very small phonon population is created at any instant to transport the energy slowly through the material. This coupled with a low material thermal conductivity means that the generated phonons will generally remain within the thin film and will be taking a longer amount of time to reach the lower

temperature end. In view of the relatively short amount of time it takes to achieve steady state and the time for accumulating the energy prior to releasing it in the medium, the difference ranges from 5 to 7 orders of magnitude in all the cases considered. As such, it is possible that over time, a temperature gradient may not be expected within the thin film layer and the temperature rise over a long period of time due to near-field radiative heating may closely resemble a single constant value. Thus, any crude computations related to the thin film can be carried out by assuming a single temperature over time instead of assuming a temperature gradient. A similar conclusion was also obtained based on a previous work (Wong et al. 2013); however, the material used in that particular work was silicon, which has different phonon properties than those of gallium arsenide.

6.1.5 Resetting of Phonon Frequency after Scattering

In any instances when scattering occurs, the frequency or energy of the scattered phonon has to be reset while the additional energy has to be added or removed to prevent any artificial changes which would then upset energy conservation. The current MC phonon transport model treats the conservation of energy of the phonon ensembles statistically by modifying the CPDF of the scattered frequency spectrum with the probability of scattering and bypassing the requirement of a creation / destruction scheme (Lacroix, Joulain & Lemonnier 2005). In this approach, the rate of destruction of a phonon frequency is equal to the rate of creation of the same phonon frequency, and it should ensure that any increase or decrease should cancel each other out so that energy conservation is met. A violation of the energy conservation would be evident if any net energy increase or decrease is observed. The results obtained for Si, Ge and GaAs simulations are shown in Figure 6.13, Figure 6.14 and Figure 6.15 respectively, which clearly shows that for all the three materials considered, there was a clear net energy being added or removed at any time step considered in the simulation. However, over the course of the simulation, it was clearly observed that the energy revolved around 0J, i.e. there had been no artificial net addition or removal of energy from the medium considered. In other words, the principle of conservation of energy can be fulfilled statistically by modifying the CPDF of the scattered frequency spectrum with the probability of scattering.

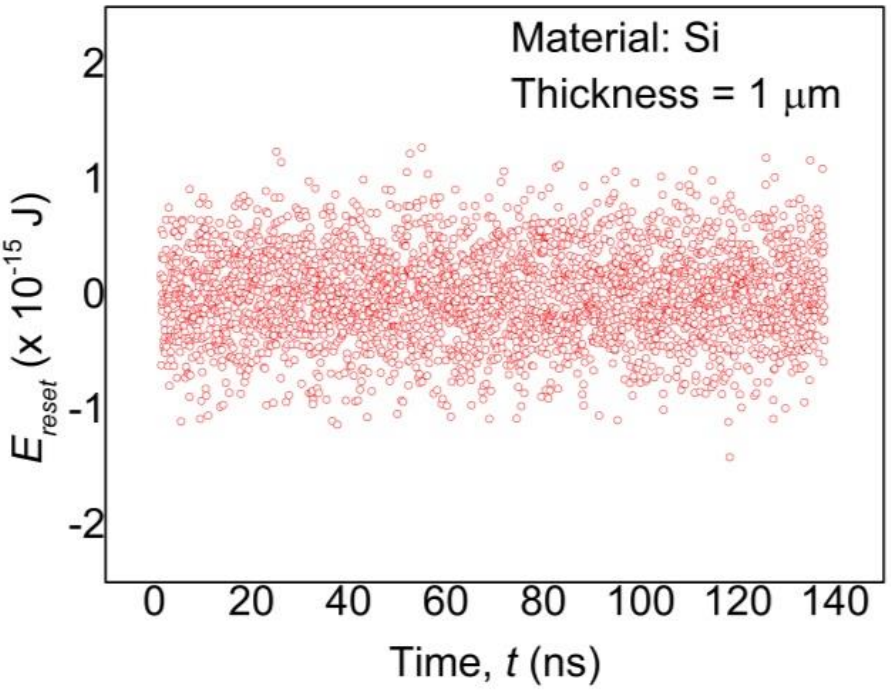

Figure 6.13 Resetting of phonon energy by tracking the energy added or removed at each time step following a scattering event in Si thin film.

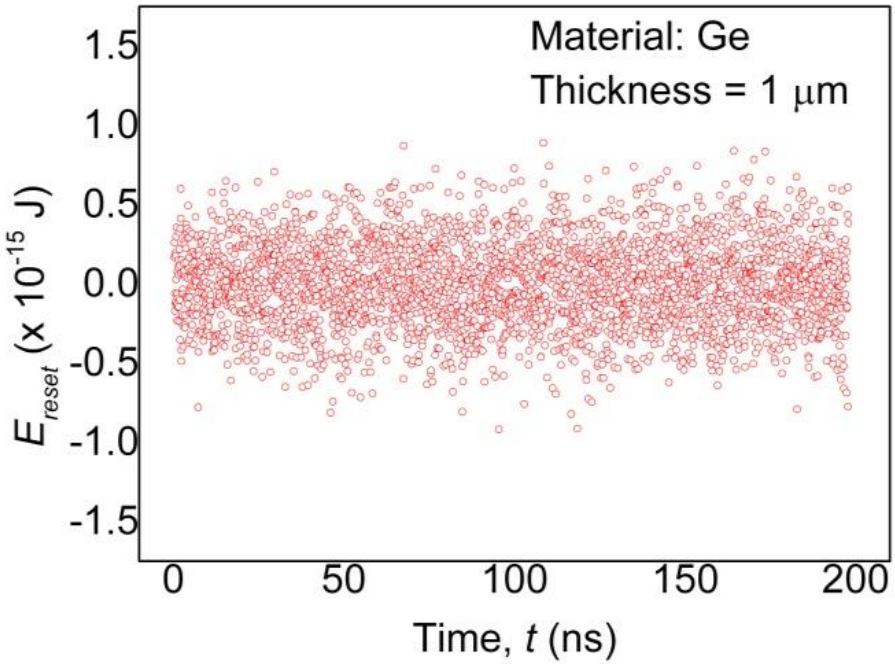

Figure 6.14 Resetting of phonon energy by tracking the energy added or removed at each time step following a scattering event in Ge thin film.

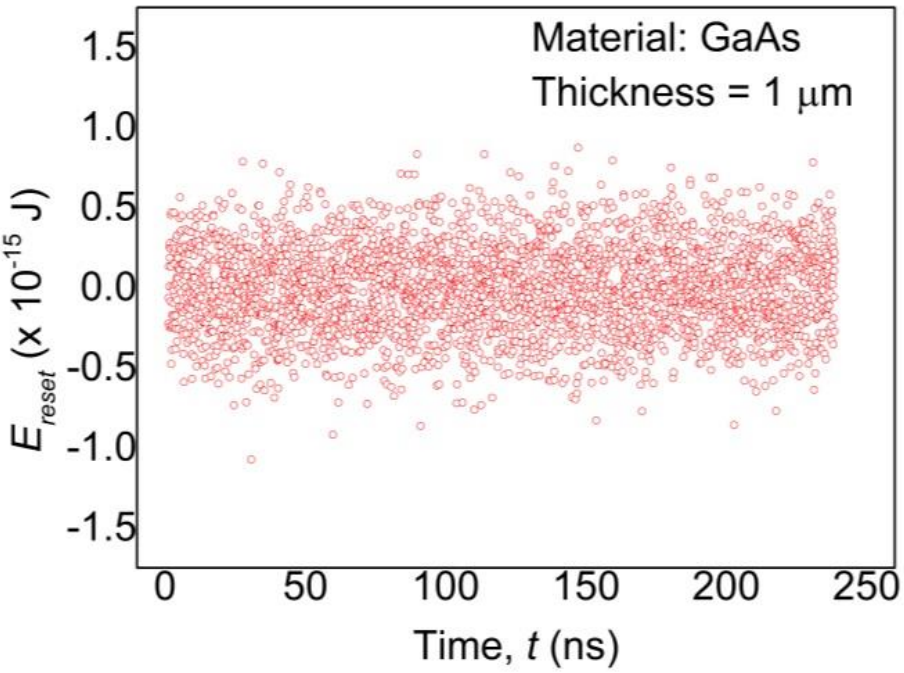

Figure 6.15 Resetting of phonon energy by tracking the energy added or removed at each time step following a scattering event in GaAs thin film.

6.2 MC Electron Transport Simulation Results

6.2.1 Assessment of Constant Electron Temperature (at 300K) Profile

The proposed model for the MC electron transport simulation was utilized to simulate electron transport in Si, Ge and GaAs – three very common semiconductor materials used in the industry. In order to check the validity of the current proposed model, several simulations were completed to assess the constant temperature profile within the simulated medium of Si, Ge and GaAs. This is however, not the best way to verify the MC electron transport model when external forces are included. However, as equilibrium temperature is used in initial CPDF computations and the simulations run at temperature close to room temperatures without the introduction of external energy sources, a looks at the temperature profile will profile a quick and easy way to check on the transport model.

As previously mentioned, the current study aims at simulation close to the room temperature, therefore the constant temperature opted was 300K. It is also noted that the temperature profile computed will be close to the equilibrium temperature with the lattice, as no external heat source is considered. In the first case, the constant temperature profile in Si, Ge and GaAs thin films of 5μm in the *Z*-direction was assessed. The *X*- and *Y*-dimensions were set to be in the micro and miliscale as the number of conducting electrons are too inadequate to be statistically viable for the MC simulation. Nonetheless, with the assumption of specular reflection at these boundaries, they were still assumed to be of infinite length. Thus, the defined dimensions will not affect the transport process. On the other hand, all boundaries are set to be adiabatic. This implies that no electrons will be entering or leaving the medium, thus the total number of ensembles remained constant throughout the simulation. The results are shown in Figure 6.16, which clearly shows that the temperature profile remained close to 300K throughout the simulations. Under such consideration, the number of electron ensemble in the medium remained constant throughout the simulation.

In the second case, the constant temperature profile in Si, Ge and GaAs thin films of varying thickness in the *Z*-direction (100nm, 500nm, 1000nm, 2000nm and 5000nm) was assessed. Both ends in the *Z*-direction of the thin films were set as isothermal boundaries. This is proposed to cater for the number of electrons which may have recombined with holes at the lower temperature end, and electron-hole pairs which may be generated at the higher temperature end. Based on the results shown in Figure 6.17 – Figure 6.19, the proposed model worked well for Si and Ge thin films, but showed irregularities in GaAs thin films below 1μm. For GaAs thin films below 1μm, the temperature distinctly rose above 300K. There is also notable amount of statistical noise present in all the results obtained. An increase in the number of ensembles was unable to resolve the issue, thus eliminating the possibility of it being a numerical error. While a check on the number of ensembles over time for Si thin film as shown in Figure 6.20 showed no distinct net increase in the number of ensembles, the plot for 0.1μm GaAs thin film in Figure 6.21 suggested otherwise. The likeliest source of this artificial net increase could have resulted from the scattering rate used. Without detailed study on this matter, no speculative conclusions can be drawn here. It would provide an interesting case for further studies in the future.

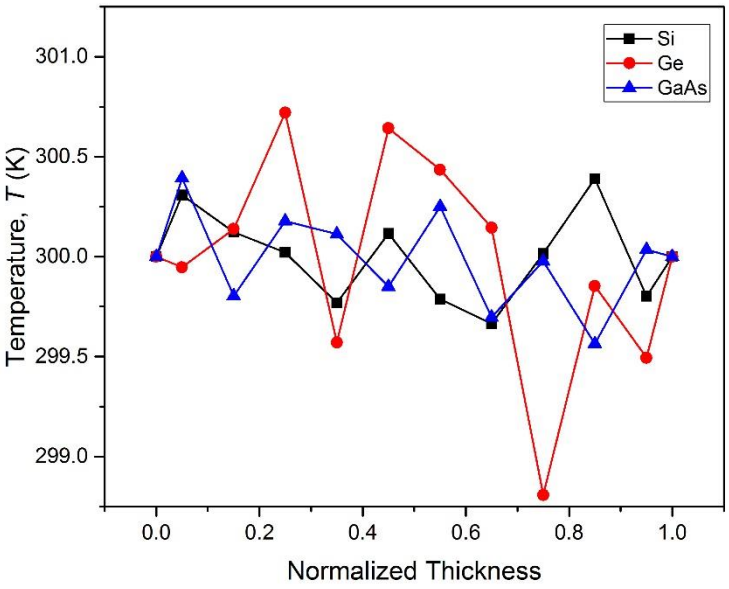

Figure 6.16 Plot of constant temperature (at 300K) profile in Si, Ge and GaAs thin films of 5μm in the *Z*-direction with all adiabatic boundaries.

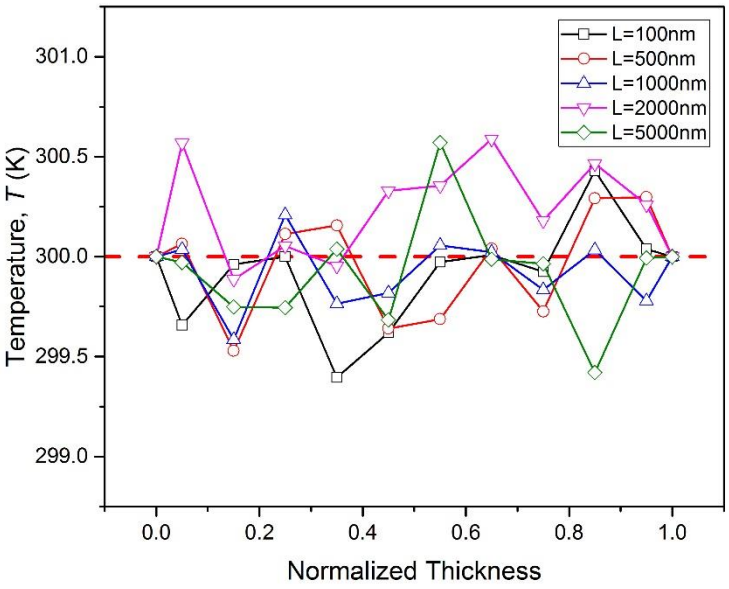

Figure 6.17 Plot of constant temperature (at 300K) profile in Si thin films of varying thickness with isothermal boundaries in the *Z*-direction.

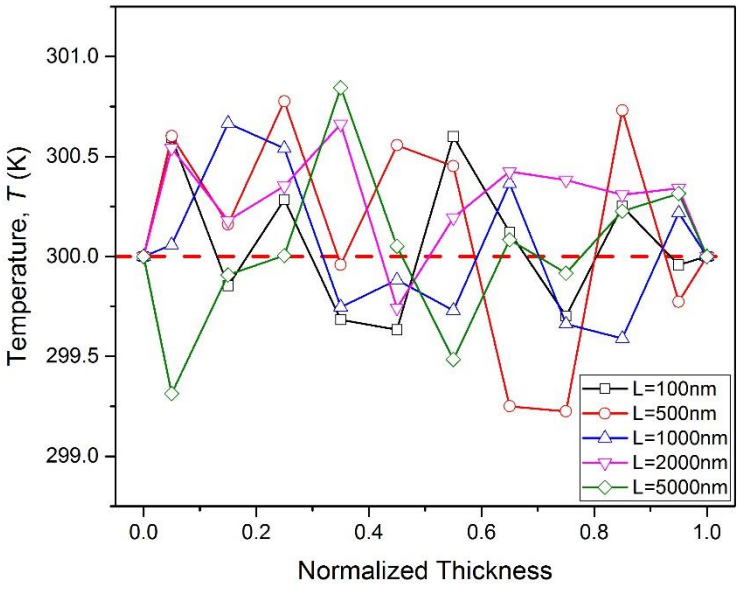

Figure 6.18 Plot of constant temperature (at 300K) profile in Ge thin films of varying thickness with isothermal boundaries in the *Z*-direction.

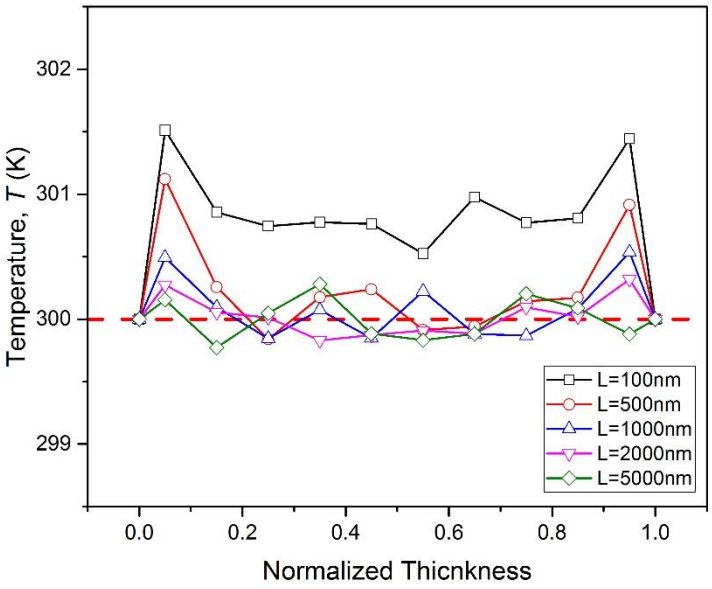

Figure 6.19 Plot of constant temperature (at 300K) profile in GaAs thin films of varying thickness with isothermal boundaries in the *Z*-direction.

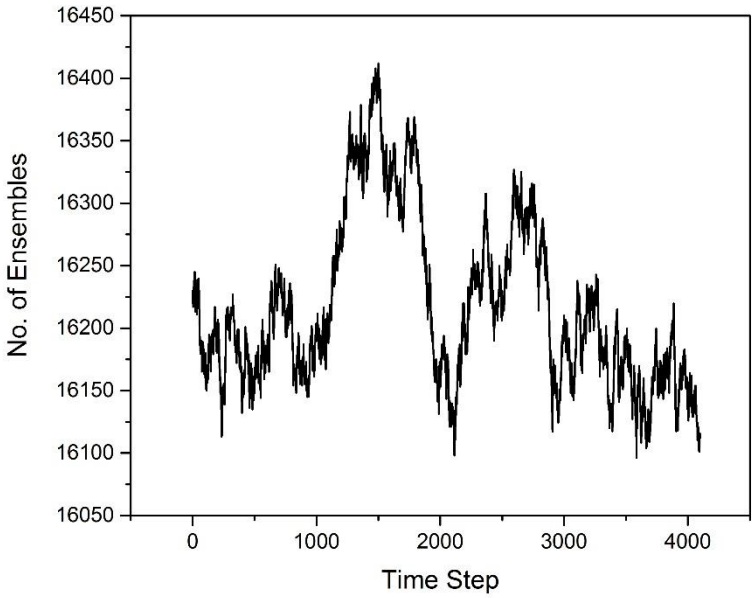

Figure 6.20 Plot of changes in number of ensembles in 5μm Si thin film at 300K assuming isothermal boundaries.

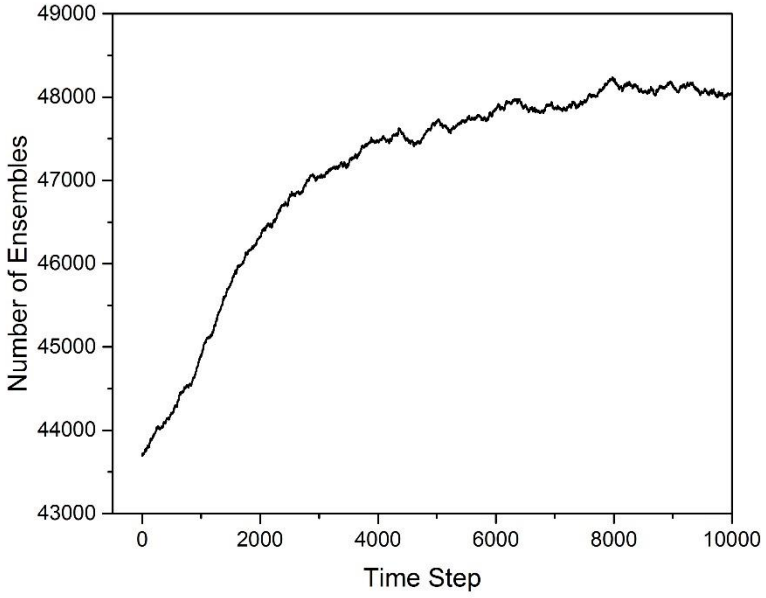

Figure 6.21 Plot of changes in number of ensembles in 0.1μm GaAs thin film at 300K assuming isothermal boundaries.

6.2.2 Assessment on the Evolution of the Electron Temperature Profile due to Varying Medium Thickness

The evolution of temperature profile in the Si, Ge, and GaAs thin films were plotted as in Figure 6.22 – Figure 6.24. In this case, a temperature gradient of 302K-298K was applied in the *Z*-direction. Both boundaries in the *Z*-direction were assumed to be isothermal. The other boundaries were all assumed to be adiabatic with specular reflection for thin film simulations. The results lightly illustrate the ballistic-to-diffusive transition in the thin films, which is consistent with the predictions in MC phonon transport simulations. The simulation results for Si and Ge remain acceptable, although a sudden spike in the temperature of the computational volume right next to the temperature boundary in 500nm thin film may be just due to some numerical errors in the computation. The simulation results for GaAs again remain a curious case, as the temperature right next to the temperature boundary is consistently higher than the applied temperature. Again the scattering rates used in this case may need to be further studied to verify its validity in the current model.

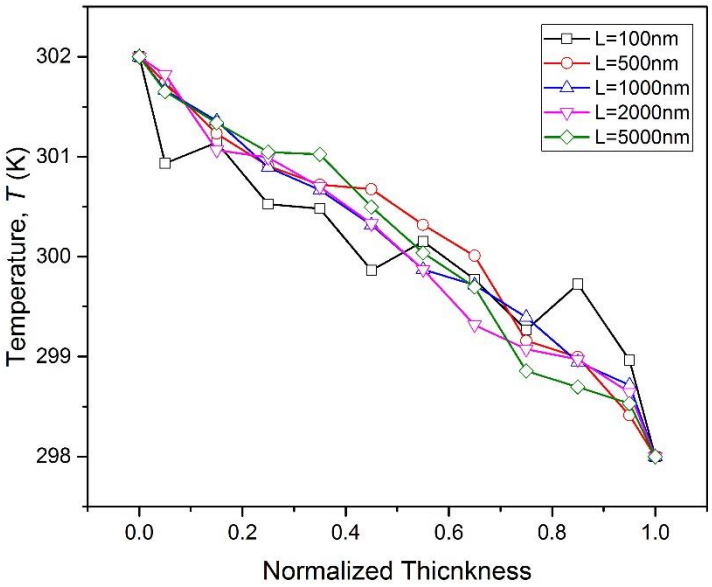

Figure 6.22 Plot of temperature profile in Si thin films of varying thickness with isothermal boundaries in the *Z*-direction, with an applied thermal gradient of 302K-298K.

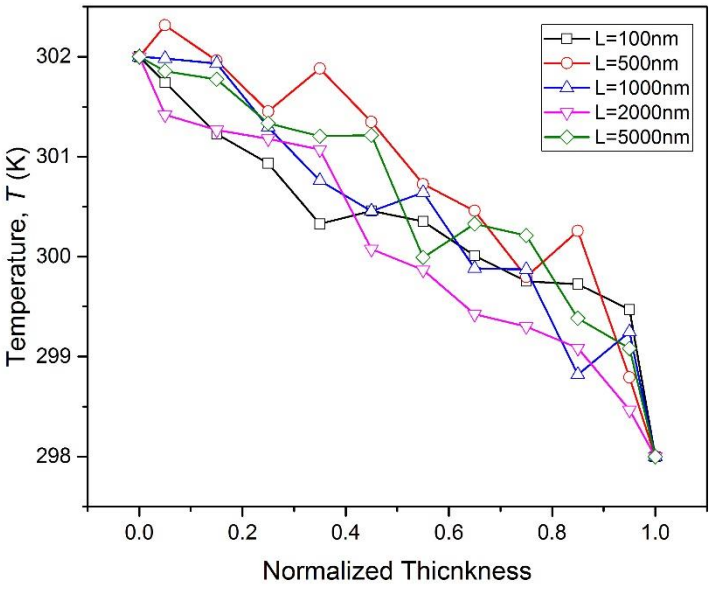

Figure 6.23 Plot of temperature profile in Ge thin films of varying thickness with isothermal boundaries in the *Z*-direction, with an applied thermal gradient of 302K-298K.

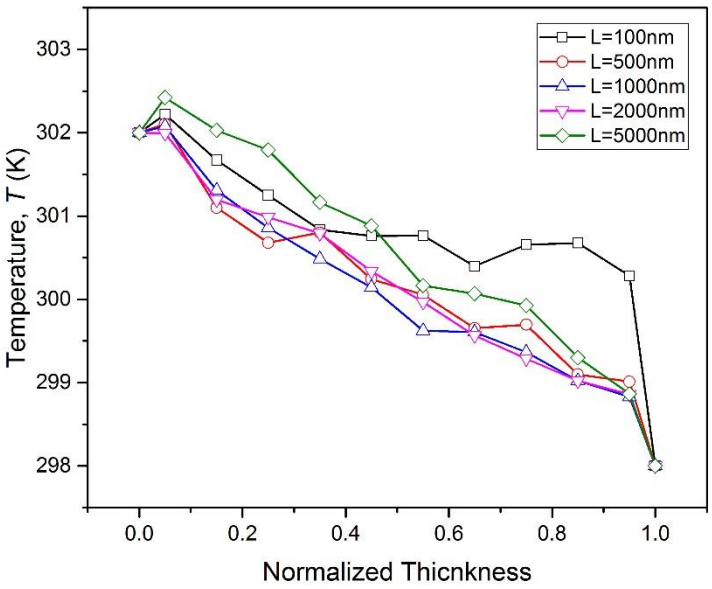

Figure 6.24 Plot of temperature profile in GaAs thin films of varying thickness with isothermal boundaries in the *Z*-direction, with an applied thermal gradient of 302K-298K.

6.2.3 Computation of the Electric Field

The computation of the electric field is verified by applying voltages on both ends of the medium of interest, in this case in the Z-direction. The electric field computed by the Poisson"s equation solver proposed in Chapter 4.6 is shown in the following figure, assuming 1V is applied on one side and 0V on the other, and vice versa. Based on the results shown in Figure 6.25, self-consistent Poisson"s equation solver is able to compute the constant potential gradient applied at both ends of the medium.

Next, the self-generated potential gradient in the medium was assessed. Under this circumstance, the potential at one end of the medium was assumed to be 0V, while the „built-in" electric field was allowed to build up based on the changes in the carrier distribution and density over the course of the simulation. Sample plots of the „built-in" electric field in Si thin film due to local and applied temperature gradient is shown in Figure 6.26

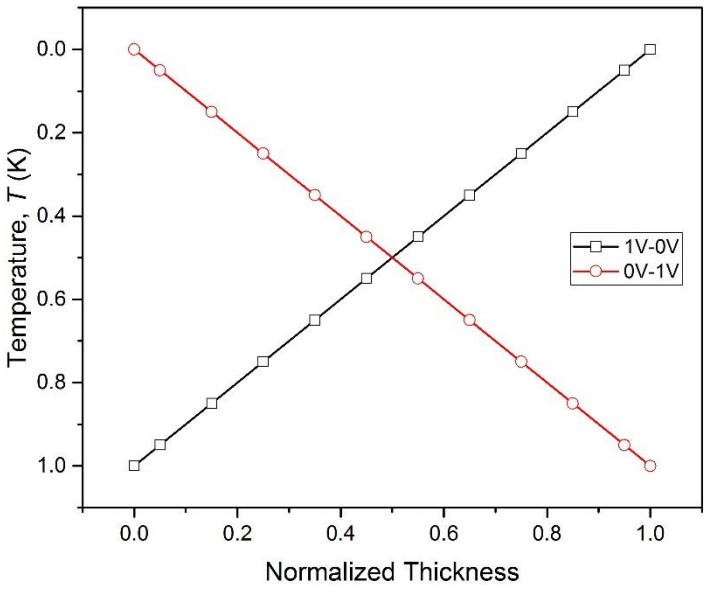

Figure 6.25 The electrical potential profile for an applied voltage of 1V-0V and 0V-1V.

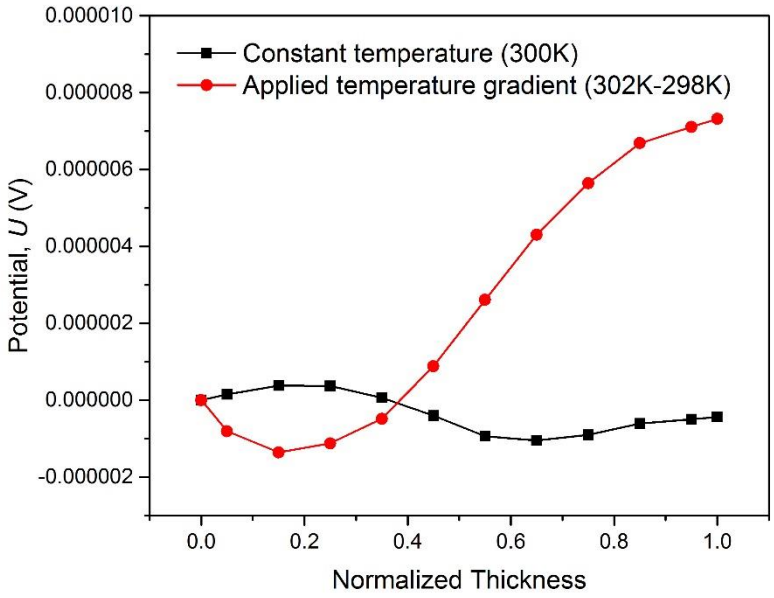

Figure 6.26 The self-generated electrical potential profile due to local and applied temperature gradient without any applied voltage.

6.3 Coupling of Electron-Phonon Transport Results

6.3.1 Assessment of the Temperature Profile

The temperature profile of Si thin film of varying thickness with applied temperature gradient of 310K-290K was obtained from MC electron transport simulation assuming a constant lattice temperature at 300K, as shown in Figure 6.27. Later, the simulation was performed in MC phonon transport simulation to obtain the exact temperature distribution, as shown in Figure 6.29. This temperature profile was then added into the MC electron transport simulation to produce to results as shown in Figure 6.28. There is no distinct difference in the temperature profiles based on the results obtained with constant lattice temperature and exact lattice temperature obtained from the MC phonon transport simulation.

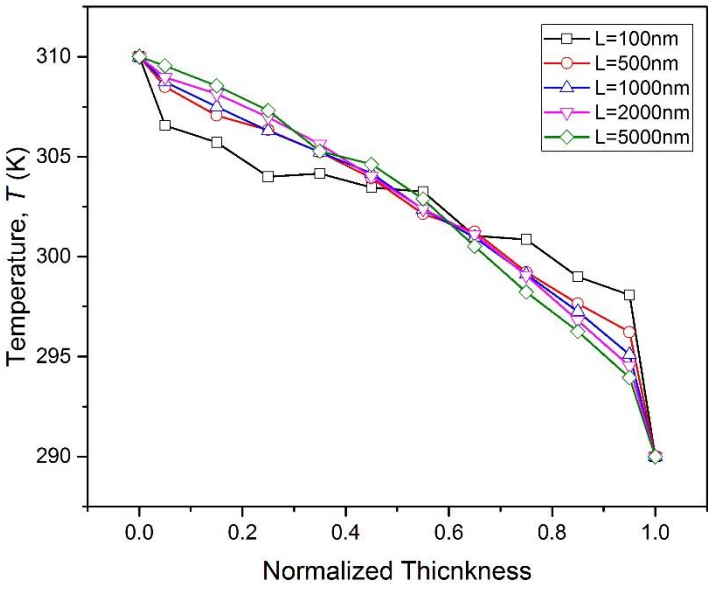

Figure 6.27 Plot of temperature profile in Si thin films of varying thickness with an applied thermal gradient of 310K-290K, obtained from electron transport simulation assuming constant lattice temperature at 300K.

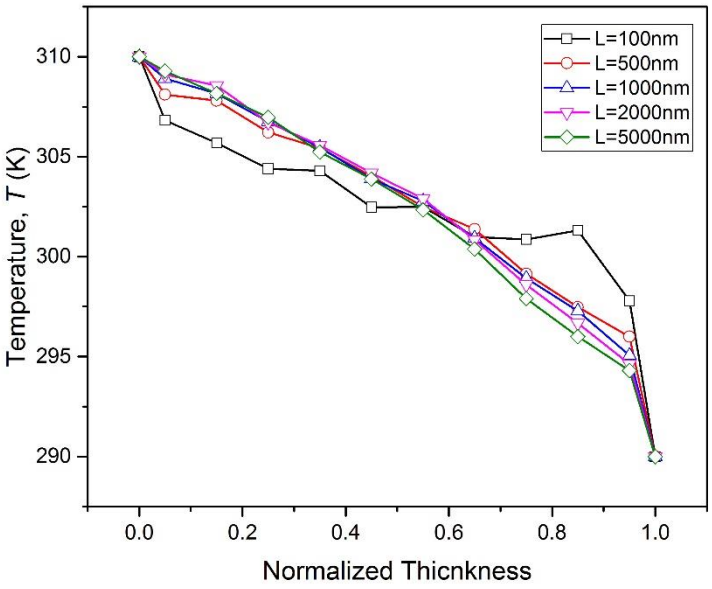

Figure 6.28 Plot of temperature profile in Si thin films of varying thickness with an applied thermal gradient of 310K-290K, obtained with the inclusion of lattice temperature from MC phonon transport simulation.

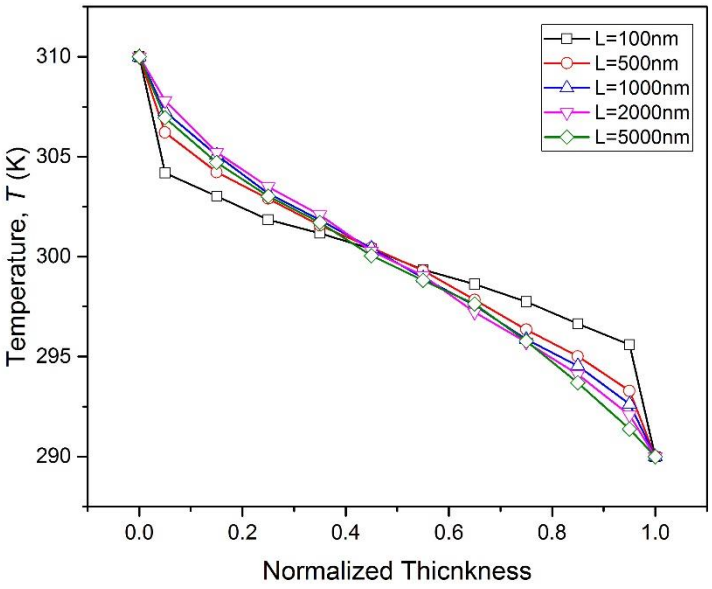

Figure 6.29 Plot of temperature profile in Si thin films of varying thickness with an applied thermal gradient of 310K-290K, obtained from MC phonon transport simulation.

6.3.2 Limitation of the Current Simulations

The proposed electron transport model does not differentiate the types of scattering event that has occurred at any particular time within the medium. In the event of scattering, energy of the electron ensemble is reset and isotropy is assumed when sampling the new directions. This may be a cause of concern as the energy related to the generation or absorption of phonon is not properly treated. The current model treats the transfer of energy from electrons to phonons by tracking the electron ensembles of which the energy level drops below the conduction band minima. However, as the simulations done were conducted with all close to thermal equilibrium assumptions, there is no dramatic change in that respect to effect any changes in MC phonon transport simulation. As such, the current study represents an alternative approach at the preliminary stage to treating electron transport. Further improvement to the current model may be required to allow more in depth studies on electron transport and the coupling process in the future. In essence, the net energy transferred to phonons needs to be addressed in earnest.

6.4 A Parametric Study using the MC Phonon Transport Simulation

A parametric study was carried out using the MC phonon transport simulation, in which the results was published in Numerical Heat Transfer, Part B: Fundamental (Bong & Wong 2014). As in every MC carrier transport simulation in general, there are a few parameters of concern, which if not chosen correctly, might compromise the simulations by creating undesirable statistical noise, unnecessarily slowing down the simulations or worse, and producing erratic results. The few concerns to be addressed in parametric study include the scaling factor, $W_{scaling}$, reference temperature, T_{ref}, and the discretization of the frequency table and CDPF tables, N_b.

6.4.1 The Scaling Factor

In ensemble MC simulations, phonons are not tracked independently, but are grouped together in ensembles. The number of phonons represented by each ensemble is determined by $W_{scaling}$. While the initial total number of phonons in the medium remains unchanged, the number of ensembles tracked will be determined by the $W_{scaling.}$ Thus, the choice of $W_{scaling}$ will have a direct effect on the accuracy of the results obtained from the simulations, as well as the computational time required. Figure 6.30, Figure 6.31 and Figure 6.32 show the thermal conductivity and temperature profile obtained with different $W_{scaling}$ for Si, Ge and GaAs respectively, each with a thickness of 1μm and a cross section of 500nm × 500nm. Starting with a low $W_{scaling}$ of 100, the thermal conductivity computed for Si, Ge and GaAs had an average standard deviation of 1.39%, 1.77% and 1.74% respectively, which is generally considered accurate and acceptable. By increasing the $W_{scaling}$ to 1000, the average standard deviation lied around 5% for each of the three materials simulated, thus proven to be still reliable and within an acceptable range. However, another ten-fold increase resulted in an average standard deviation of around 15-20%, which now compromises the accuracy of the simulation. With a lower number of ensembles being simulated, the statistical noise increases dramatically. At this point, there are not enough ensembles to reflect the true transport event occurring in the medium, which is evident from the temperature profiles obtained especially for Ge. The temperature profiles for all the materials are reasonably consistent at $W_{scaling}$ of 1000 and below, but started to deviate from the norm with

further increment of $W_{scaling.}$ Without sufficient number of phonon ensembles, too many phonons are lumped into one single ensemble, and their behaviour, though in reality different, are now averaged to be the same. With sufficient number of ensembles, such statistical noise would be evened out statistically, resulting in a more realistic depiction of the true transport phenomenon. Thus, fewer irregularities would be observed. It should also be noted that the larger the transport medium, the higher the number of phonons to be considered. Simulations with the same $W_{scaling}$ would result in more accurate results due to the increased number of ensembles tracked independently. This however, comes at the expense of computational time, which would be significantly increased once the number of ensembles tracked is increased. In the event of limited computational resources, a higher $W_{scaling}$ would be useful to provide an approximate picture of the carrier behaviour, but a lower $W_{scaling}$ is still required to provide accurate results. In our current model, $W_{scaling}$ of 1000 is sufficient to ensure accurate results while maintaining a reasonable amount of computational time.

6.4.2 Discretization of the Frequency Spectrum and CPDF Tables

In the discretization of the frequency spectrum and CPDF tables, the results obtained with different discretization, N_b for three different materials, each with the same dimension as given in the previous section, is shown in Figure 6.33, Figure 6.34 and Figure 6.35. It is clearly notable that the higher discretization used, the more accurate were the results obtained. By looking at the thermal conductivity computed, it is notable that lower N_b resulted in higher thermal conductivity for Si (10.7% higher) and GaAs (8.5% higher) but lower thermal conductivity for Ge (3.7% lower). The deviation from the mean value suggested inaccuracy in the simulation outcome and such low N_b should be avoided even though it decreases the computation time. At N_b of 1000 and above, the computed thermal conductivity converged to a single value and remained fairly constant thereafter, thus justifying that a choice of 1000 would be sufficient to give a consistent and accurate set of simulation results. Any further increase in the discretization would significantly increase computational time without improving the outcome. Furthermore, with lower N_b, the thermal conductivity lied too far away from the average computed value, which was particularly evident for Si and GaAs.

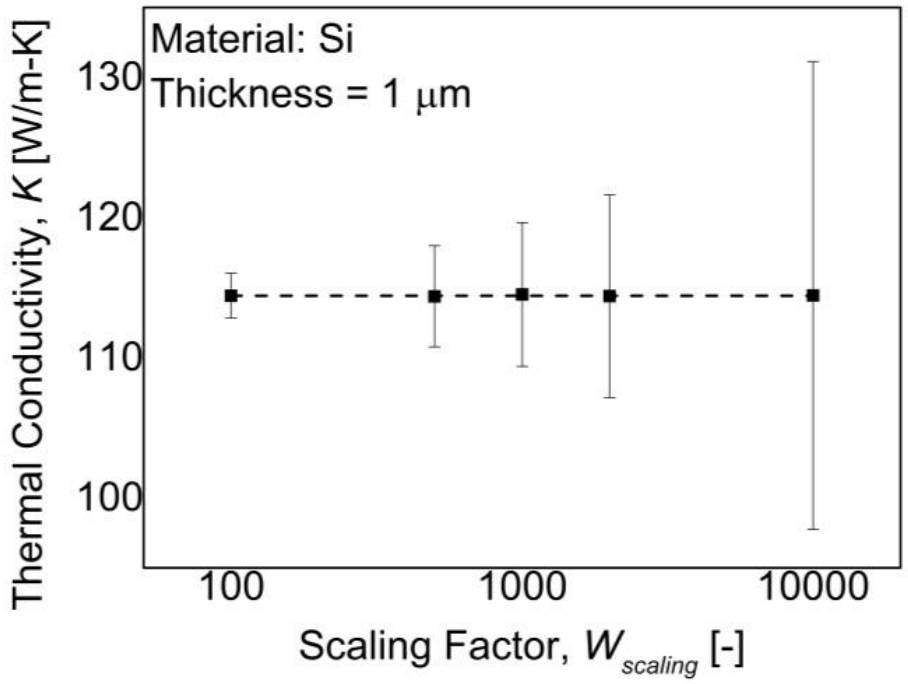

(a)

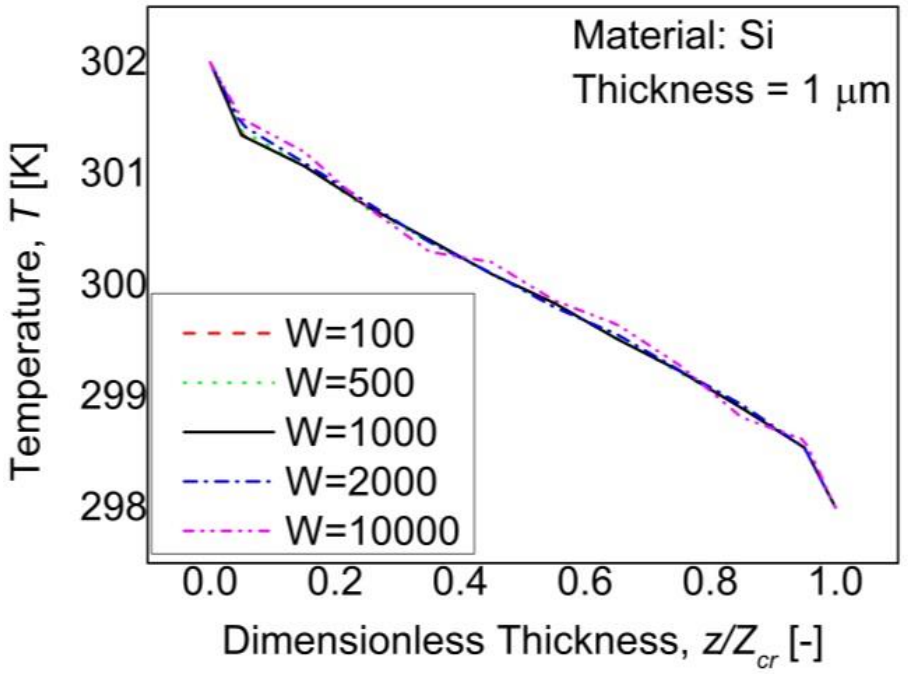

(b)

Figure 6.30 Effects of different $W_{scaling}$ on the Si thermal conductivity and the temperature distribution within the medium.

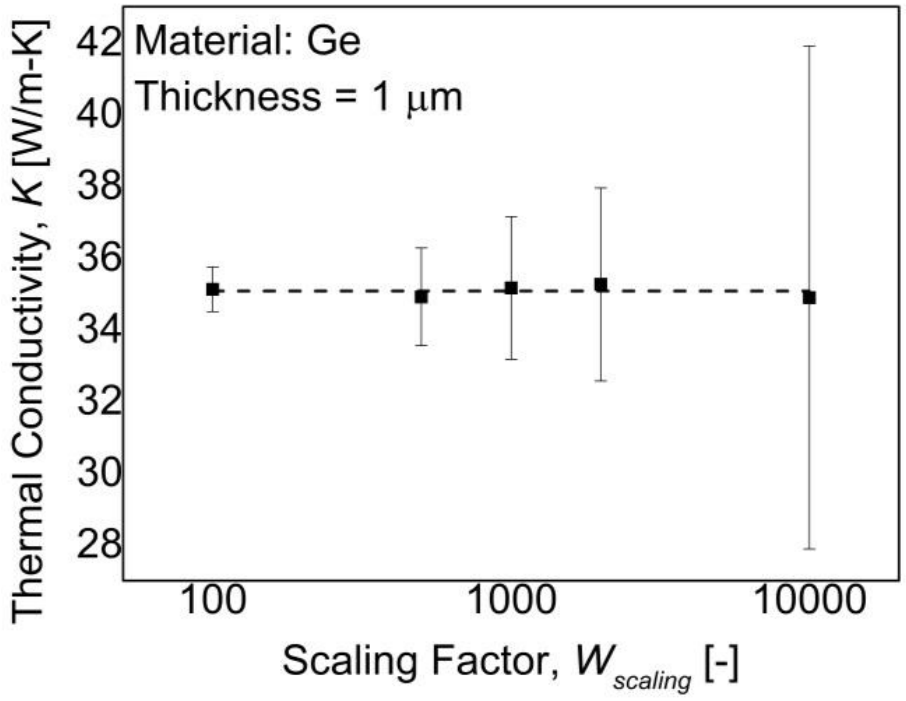

(a)

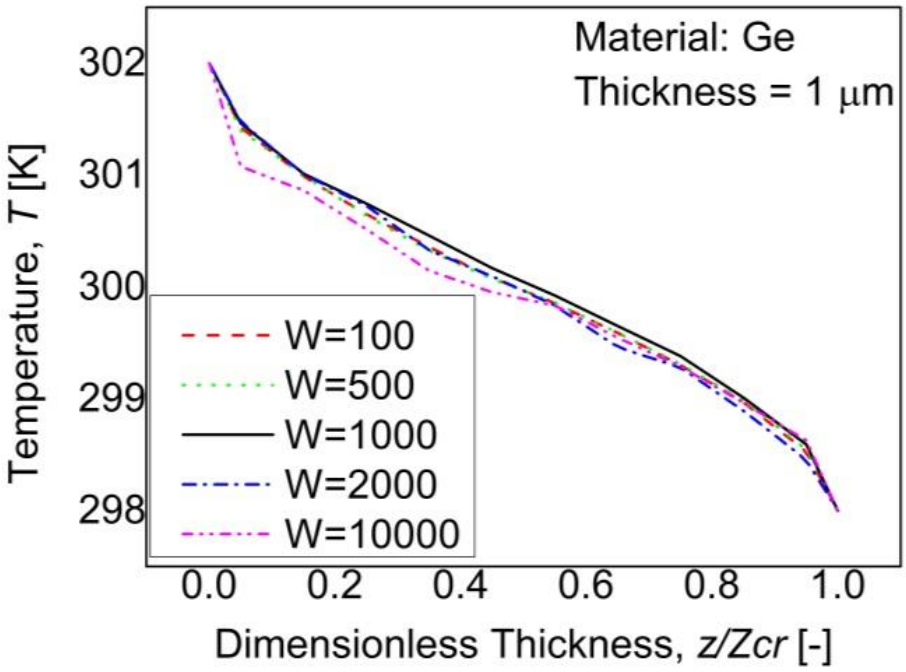

(b)

Figure 6.31 Effects of different $W_{scaling}$ on the Ge thermal conductivity and the temperature distribution within the medium.

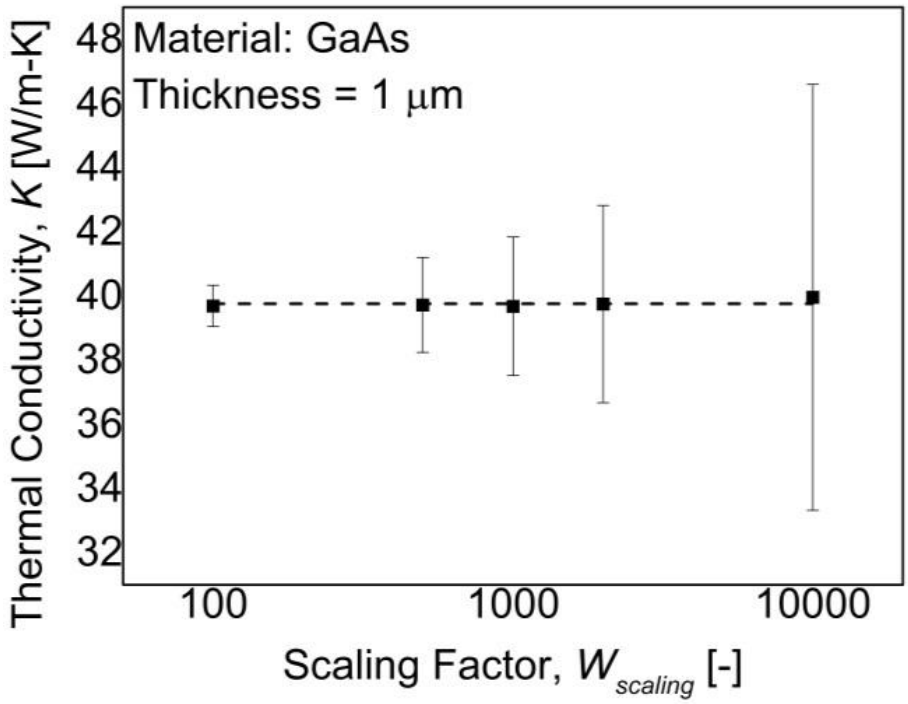

(a)

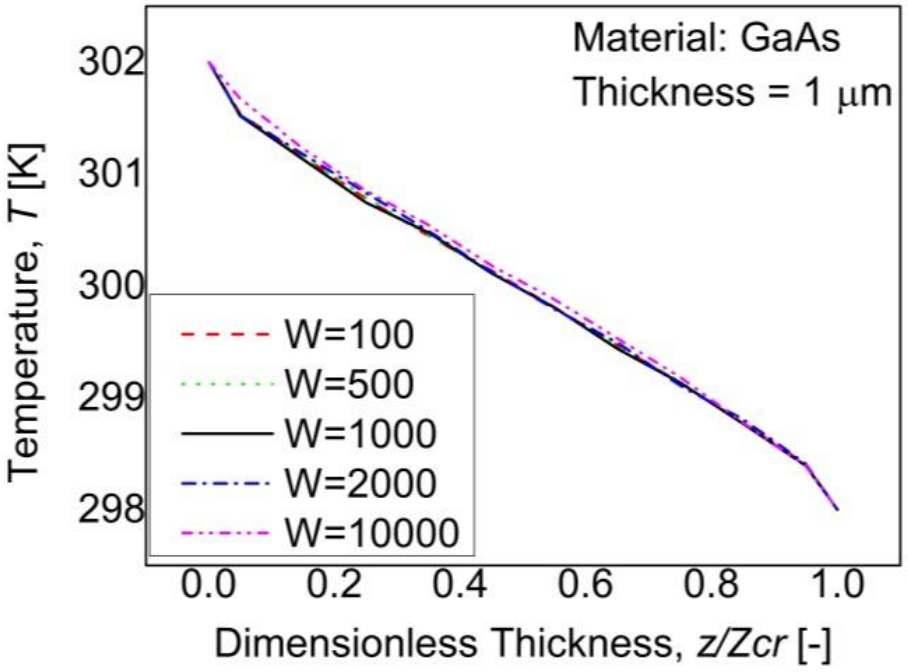

(b)

Figure 6.32 Effects of different $W_{scaling}$ on the GaAs thermal conductivity and the temperature distribution within the medium.

As compared to $W_{scaling}$ however, the choice of N_b will not affect the errors computed from the simulation. Although the value of thermal conductivity computed varied at lower N_b, the statistical error remained fairly constant at approximately 5% in all cases due to a consistent choice of $W_{scaling}$ used. The temperature profile meanwhile, showed good consistency for N_b of 1000 and above, but deviated from the norm at lower N_b. As a higher N_b will significantly increase the computational time without significant improvement on the accuracy of the outcome, a discretization of 1000 is favourable for this model to achieve accurate results in a reasonable amount of computation time.

6.4.3 Selecting the Reference Temperature

As previously noted, an additional variable known as the reference temperature T_{ref} is introduced in the current phonon transport model. The main reason behind this approach is to reduce the computational time. In essence, all activities below T_{ref} will not be considered. In other words, any phonons of temperatures below T_{ref} at any frequency will not be included in the simulation. Therefore, the total number of phonons considered is significantly less than having to consider the full phonon capacity (starting from 0K to the simulation temperature). In order to highlight the advantage of this concept, we have looked at the effect of different T_{ref} used on the required CPU time. Note that all runs were conducted on the same desktop computer (Dell Precision T7500) running on an Intel Xeon X5675 processor with a clock speed of 3.07GHz and 12GB of RAM. The simulation temperature range was set at 302K on the hot end and 298K on the cold end, and the initial temperature is set to be equivalent to the temperature at the cold end. T_{ref} was set initially at 1K below the initial temperature, and then slowly decreased further from the initial temperature. The decrement of T_{ref} means that more phonons are considered in the simulation, thus increasing the number of phonons simulated. The time of interest on the other hand, was set to 50ns.

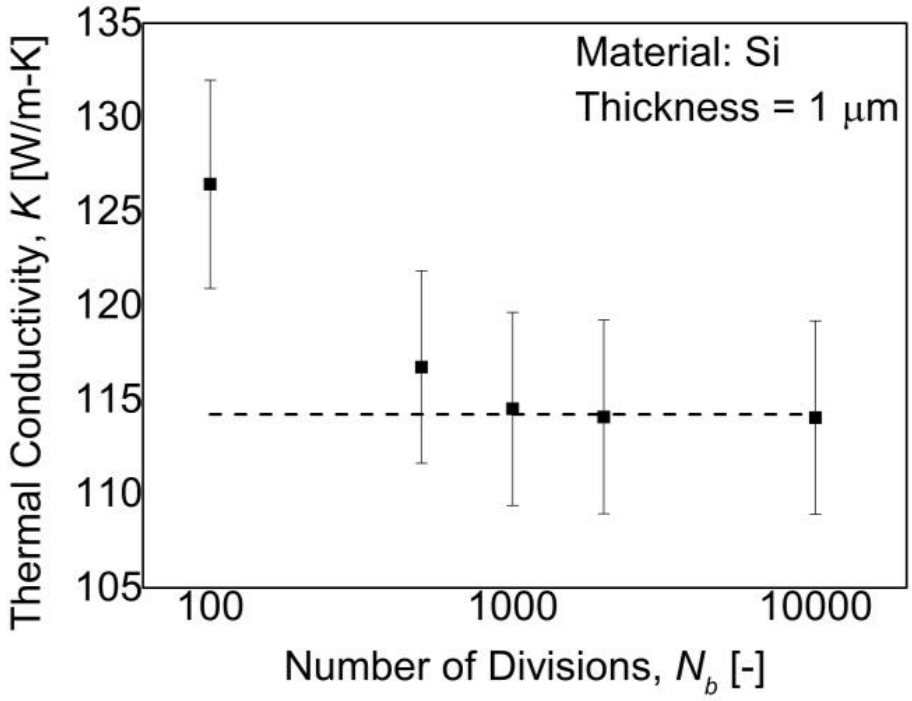

(a)

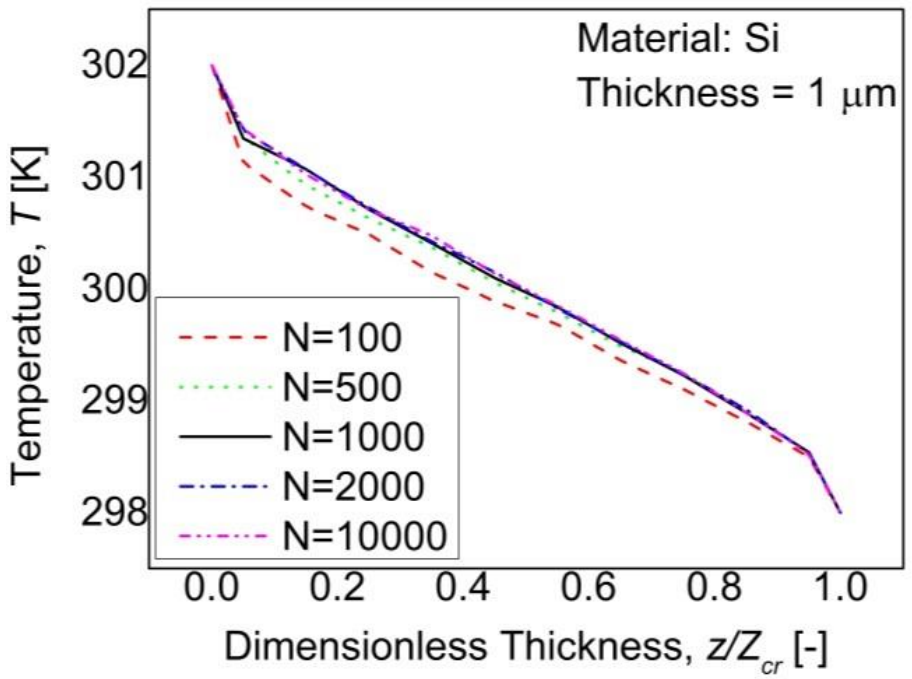

(b)

Figure 6.33 Effects of different N_b on the Si thermal conductivity and the temperature distribution within the medium.

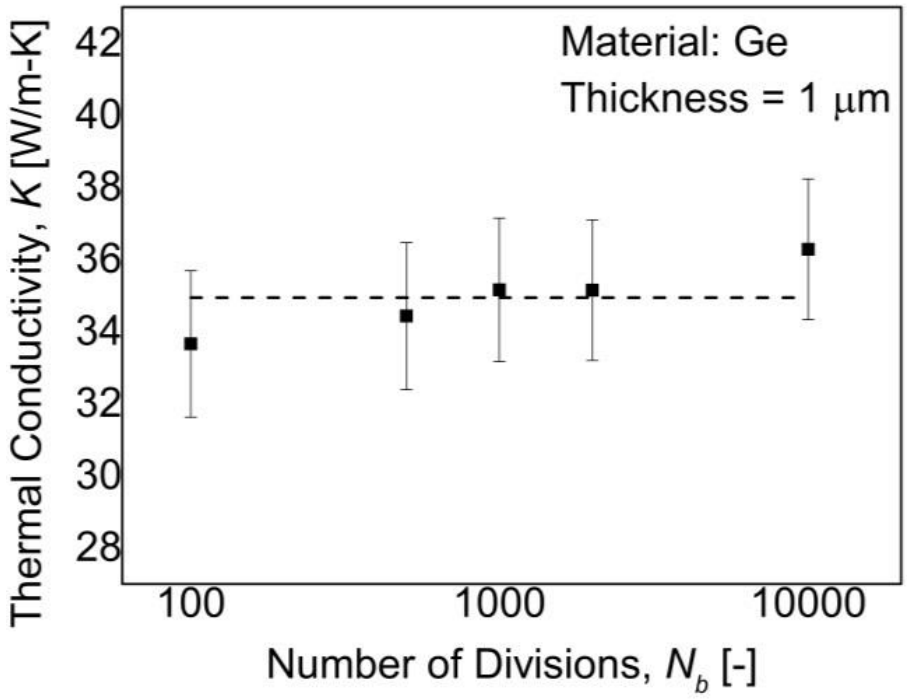

(a)

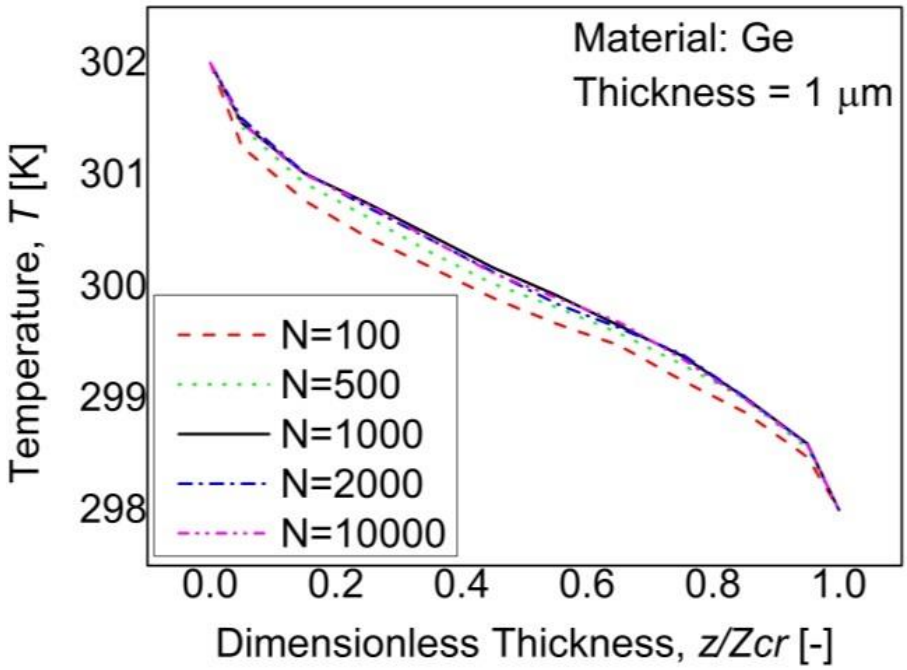

(b)

Figure 6.34 Effects of different N_b on the Ge thermal conductivity and the temperature distribution within the medium.

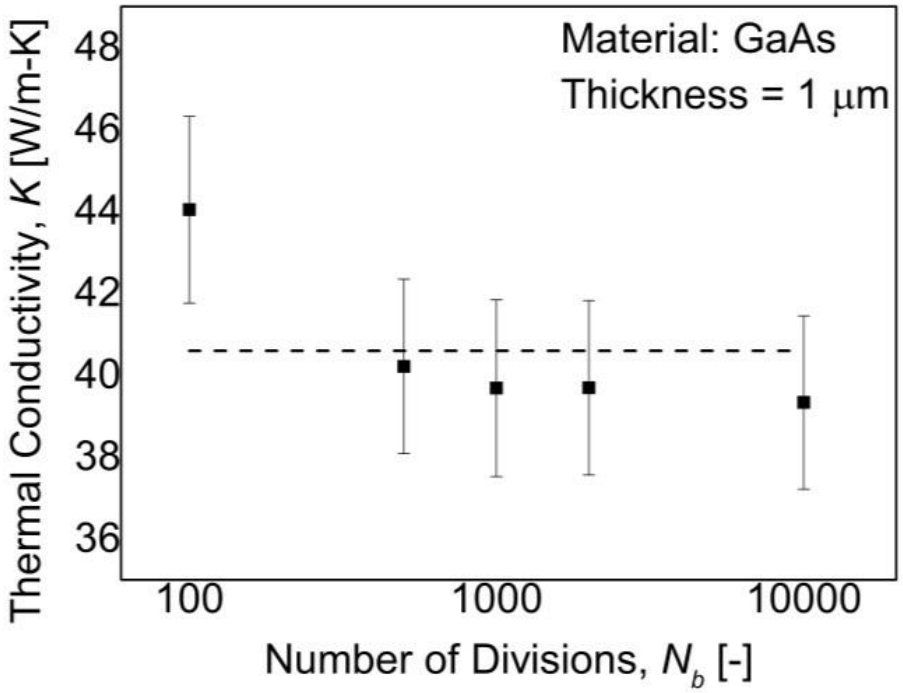

(a)

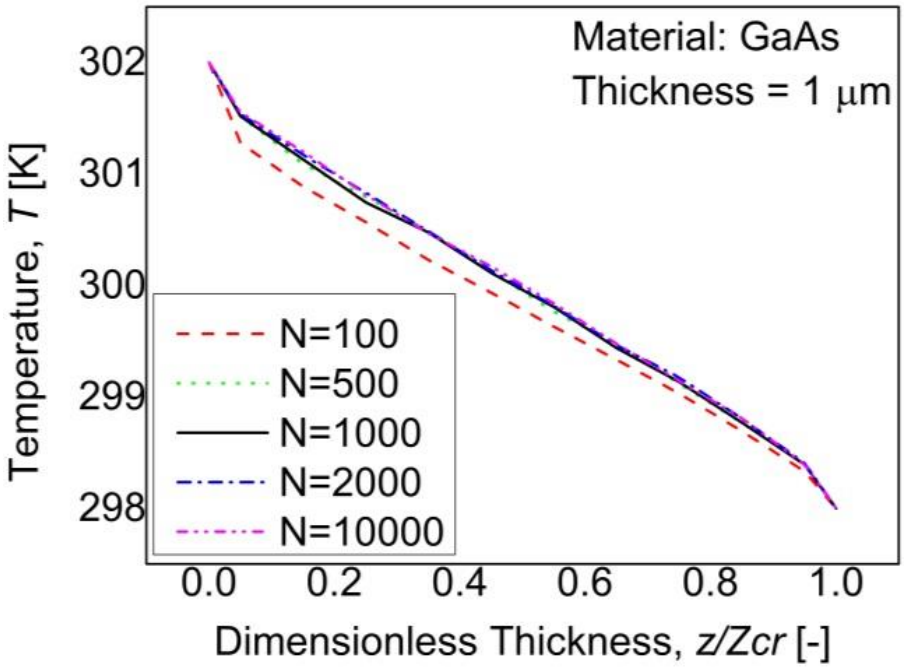

(b)

Figure 6.35 Effects of different N_b on the GaAs thermal conductivity and the temperature distribution within the medium.

It is obvious from the results in Figure 6.36, Figure 6.37 and Figure 6.38 that the closer T_{ref} is to the initial temperature, the lesser the required amount of CPU time would be. The CPU time for the simulation was found to be inversely proportional to T_{ref} when the $W_{scaling}$ is held constant. A quick look at the computational time for each of the three materials revealed that the simulation for Ge took the longest to complete. This is mainly due to the fact that Ge has a small phonon mean free path. Thus, the phonons undergo more scattering in Ge than in Si at the same temperature and along the same characteristic length. In addition, T_{ref} will also have an effect on the accuracy of the results. At lower T_{ref} where the number of ensembles is huge, the standard deviation of the computed thermal conductivity was generally larger than at higher T_{ref}, which can be attributed mainly to the statistical noises. This was particularly a severe issue in Si, where the standard deviation went up to over 35% when T_{ref} chosen was at 50K below the initial temperature, which if considered from statistical point of view is unacceptable. The thermal conductivity computed at this point was also too far out from the averaged value, thus compromising the accuracy of the simulation. With T_{ref} set close to the initial temperature however, the standard deviation was reduced significantly, while the thermal conductivity computed tended to converge to a value and remained fairly constant thereafter. Therefore, for the best results from the model proposed in this study, it is highly recommended that T_{ref} be set close to the initial temperature to reduce computational time and to statistical noise, hence ensuring the accuracy of the results.

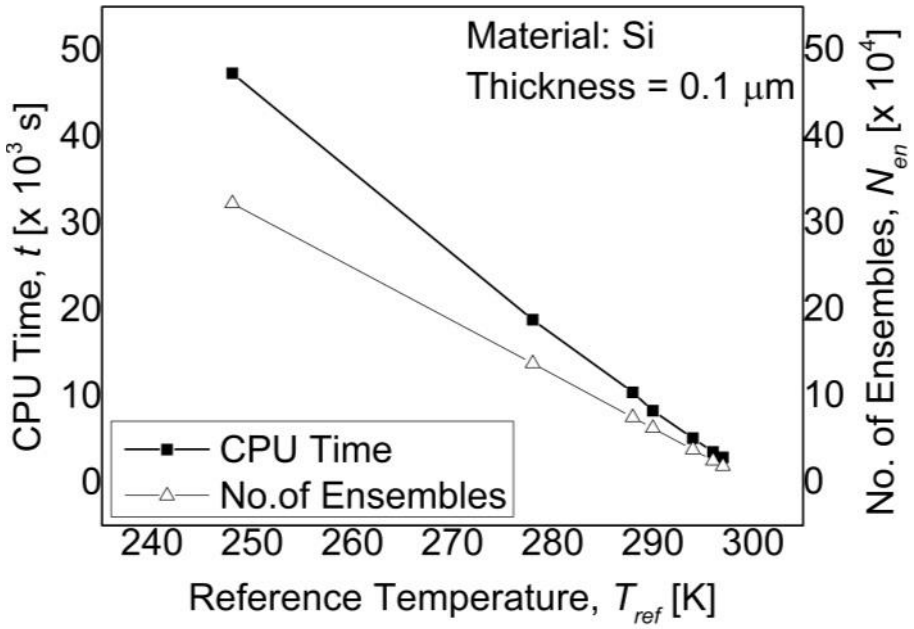

(a)

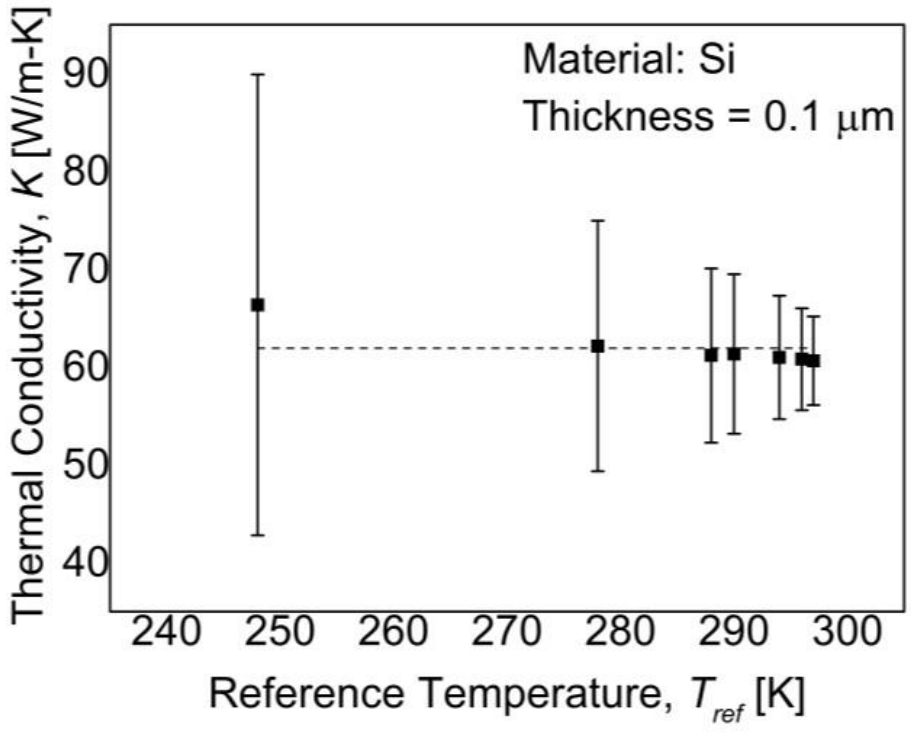

(b)

Figure 6.36 Effects of different T_{ref} on the computational time and the standard deviation of the computed Si thermal conductivity K for a constant $W_{scaling}$ of 1000.

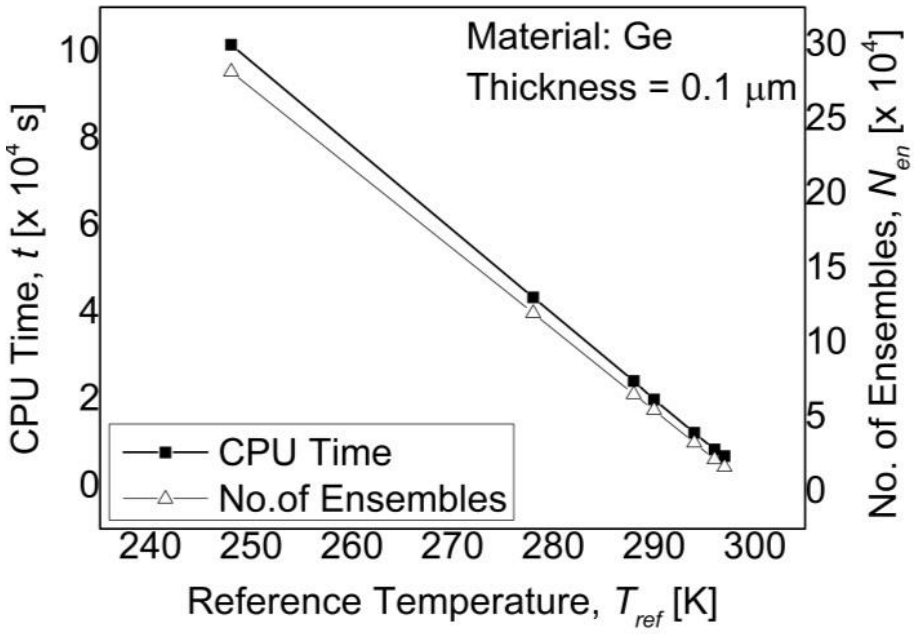

(a)

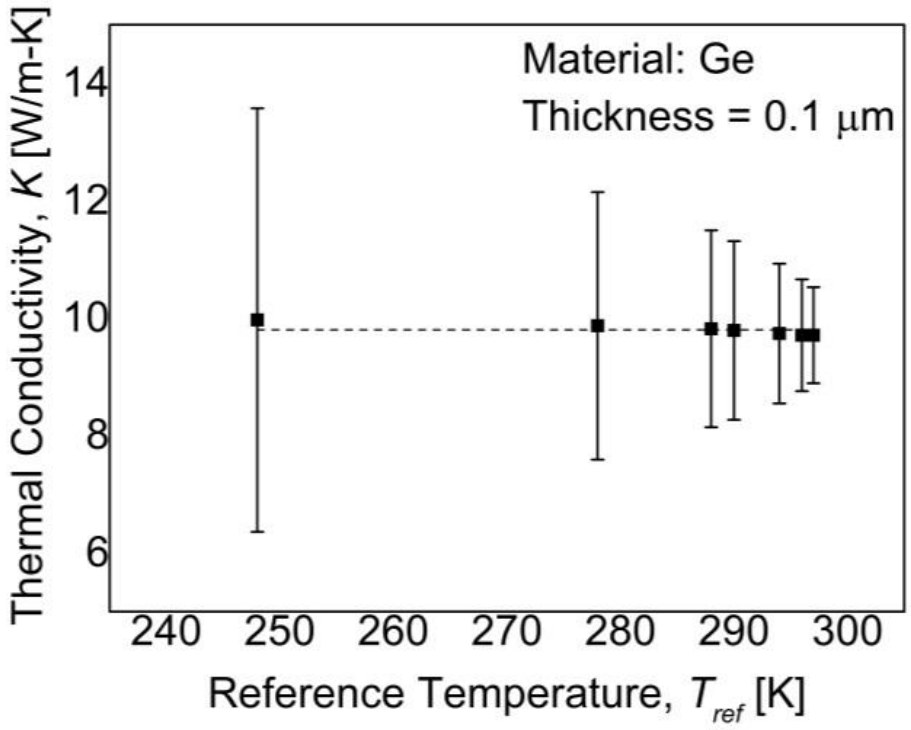

(b)

Figure 6.37 Effects of different T_{ref} on the computational time and the standard deviation of the computed Ge thermal conductivity K for a constant $W_{scaling}$ of 1000.

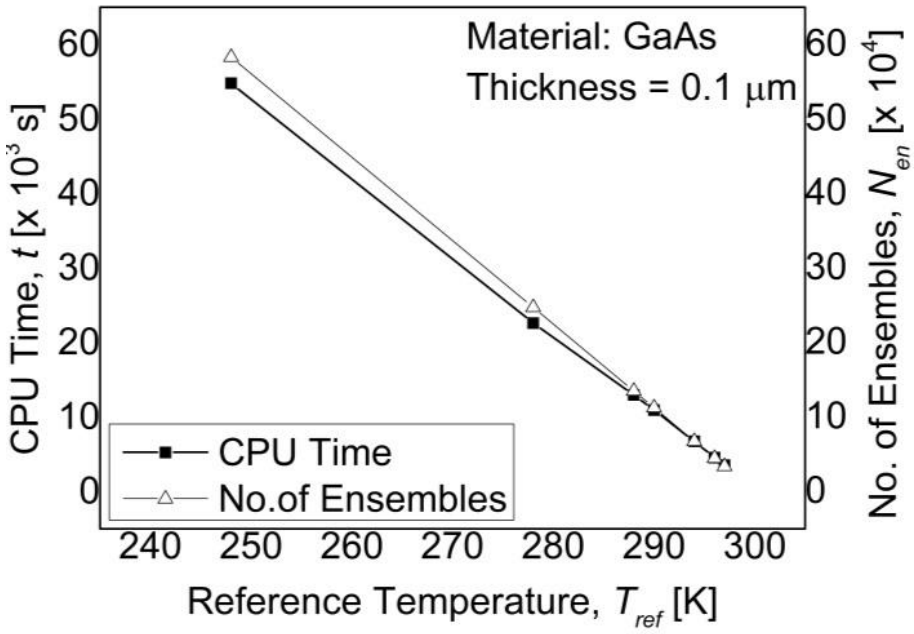

(a)

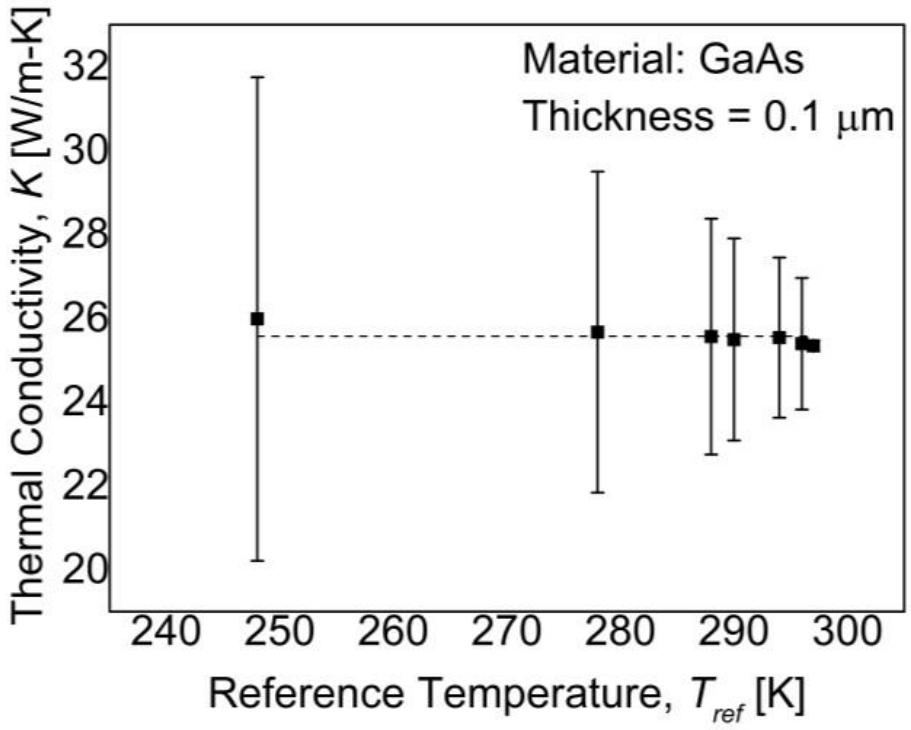

(b)

Figure 6.38 Effects of different T_{ref} on the computational time and the standard deviation of the computed GaAs thermal conductivity K for a constant $W_{scaling}$ of 1000.

CHAPTER 7

Conclusions and Future Works

7.1 Conclusions

The solution to the BTE for phonon transport and electron transport in Si, Ge and GaAs, and a methodology to couple electron and phonon transport have been discussed in detail in this thesis.

The proposed MC phonon transport simulation includes an additional term T_{ref} for more efficient simulation, as the only the phonon spectrum above the T_{ref} will be simulated. The drawback of such approach is that any interactions between the phonons of higher and lower energy level would be neglected. This thesis also proposes anisotropy in phonon scattering by adopting the HG probability density, which introduces a preference in the backward or forward scattering. In general, forward scattering increases thermal conductivity while backward scattering reduces it, but the extent of the effect was found to be non-linear, and that the forward scattering has a more significant effect than the backward scattering. The incorporation of heat generation ensures that the MC phonon transport simulation can be coupled with other energy carrier transport including radiation and electron transport. The simulation results have been verified with a comparison of the bulk thermal conductivities obtained experimentally from the available literatures (Maycock 1967). The proposed MC model

can also be used for simulation of heat transport in common nanostructures such as thin films and nanowires.

The proposed MC electron transport simulation still represents a preliminary work in progress. It includes a parabolic band structure with the scattering rates obtained from relaxation time approximation proposed by Gonzalez et al. (1999), which accounts for both the electron energy and the lattice temperature. A self-consistent Poisson‟s equation solver is also included in the model, which computes the potential at each computational volume at the end of every time step. The net amount of energy transferred to phonons is computed at the end of each time step by assuming that the energy of any electrons with less than the energy of the conduction band minima will be causing phonon generation. To date, only the temperature profile generated by the MC electron simulation has been assessed.

The coupled electron-phonon transport simulation was performed with the exclusion of any external heat source in the current simulations. At conditions close to the thermal equilibrium between both electrons and phonons, no net energy transport is accounted for in the current simulations, and the electron distribution and number over time resemble those at equilibrium condition.

In short, the current proposed model provides a foundation work for future investigation of heat transport phenomena at the micro and nanoscale. Several improvements are required to enhance the model and more verifications are required especially for electron transport simulations. The potential of applying an improved and fully developed model in this research to various applications in the field of nanotechnology will be endless such as predictions of thermal conductivities or temperature profiles of nanostructures, computations of temperature distribution due to electron-beam heating at the nanoscale, temperature calculations in the nano-gap thermo-photovoltaic cells, etc.

7.2 Recommendations for Future Works

It is hereby noted again that the current work in this thesis is still at a preliminary stage, especially where coupled electron-phonon transport is concerned. There are several improvements that can be done in the future to improve the current transport model, followed by verifications with experimental results in the literatures.

The phonon transport model may be improved by including the optical phonons especially for simulation of the transient process. This would allow for a more complete picture of the exchange of energy between electrons and phonons as well (see Figure 5.1 for the electron-phonon interaction). The phonon-impurity scattering rates can also be incorporated for simulation of doped semiconductors, which are commonly used in the industry these days.

The electron transport model can yet be improved by the inclusion of the Pauli exclusion principle, which states that no two electrons can occupy the same quantum state within a quantum system at the same time. This can be a form of validation for the current electron transport model to confirm that the model is physically accurate.

Another possible improvement would be the inclusion of holes and doping in the electron transport model. As aforementioned, modern day semiconductor industry commonly introduces impurities in intrinsic semiconductor materials in order to alter its electrical properties. Most devices involve *n*-doped and *p*-doped materials and thus lead to the necessity to include doping effect in carrier transport simulations. Therefore, in order to accurately account for the electric field effect, holes density will need to be incorporated as well, in addition to the acceptors‟ and donors‟ density.

The electron-phonon interaction can be further improved by including the rate of phonon absorption and phonon generation, both of which have not been accounted for in this model. The intervalley and intravalley electron-phonon scattering rates may also be incorporated to provide a better view of the energy transport process, as have been highlighted in the works of Pop, Dutton and Goodson (2004). Such information may be vital to account for simulations involving Joule heating in the future.

Joule heating remains largely untouched in the current study. The current proposed model will need to be improved with the above suggestions and be verified again to ensure that it is able to capture the essence of Joule heating in semiconductor devices. This is important for both the electro-thermal and thermoelectric simulations to be considered in the future.

Last but not least, the simulation process can be parallelized to ensure better simulation efficiency. Parallel computing is a very effective and attractive approach to gain computation speed and to reduce computational time. It calls for more extensive programming skills to create and implement the parallelization algorithm to break down the various tasks. The software and hardware components must also be selected carefully to cater for such tasks. Done correctly, this will greatly improve the efficiency of such simulations.

In short, the above recommendations, if incorporated, will be able to provide a more complete fundamental coupled electron-phonon transport modelling, which can be applied to simulate heat transport under a variety of different conditions.

References

Akkerman, A & Murat, M 2015, 'Electron–phonon interactions in silicon: Mean free paths, related distributions and transport characteristics', *Nuclear Instruments and Methods in Physics Research Section B: Beam Interactions with Materials and Atoms*, vol. 350, pp. 49-54.

Asen-Palmer, M, Bartkowski, K, Gmelin, E, Cardona, M, Zhernov, A, Inyushkin, A, Taldenkov, A, Ozhogin, V, Itoh, K & Haller, E 1997, 'Thermal conductivity of germanium crystals with different isotopic compositions', *Physical Review B*, vol. 56, no. 15, p. 9431.

Ashcroft, NW & Mermin, ND 1976, *Solid State Physics,* Saunders Company, Philadelphia.

Asheghi, M, Leung, Y, Wong, S & Goodson, K 1997, 'Phonon-boundary scattering in thin silicon layers', *Applied Physics Letters*, vol. 71, no. 13, pp. 1798-1800.

Asheghi, M, Leung, YK, Wong, SS, Touzelbaev, MN & Goodson, KE 1998, 'Temperature-Dependent Thermal Conductivity of Single-Crystal Silicon Layers in SOI Substrates', *Journal of Heat Transfer*, vol. 120, no. 1, pp. 30-36.

Ashraf, S & Sharma, A 2006, 'Temperature and energy dependent electron–electron scattering rate in a disordered quantum wire', *Physica E: Low-dimensional Systems and Nanostructures*, vol. 33, no. 1, pp. 35-40.

Baillis, D & Randrianalisoa, J 2009, 'Prediction of thermal conductivity of nanostructures: Influence of phonon dispersion approximation', *International Journal of Heat and Mass Transfer*, vol. 52, no. 11, pp. 2516-2527.

Bernardi, M 2016, 'First-principles dynamics of electrons and phonons', *The European Physical Journal B*, vol. 89, no. 11, p. 239.

Bhandari, C & Verma, G 1965, 'Role of Longitudinal and Transverse Phonons in Lattice Thermal Conductivity of GaAs and InSb', *Physical Review*, vol. 140, no. 6A, p. A2101.

Boltzmann, L 1964, *Lectures on gas theory,* Univ of California Press.

Bong, VNS & Wong, BT 2014, 'Solution of the Boltzmann Transport Equation for Phonon Transport via the Speed-Up Transient Monte Carlo Method Using Reference Temperature', *Numerical Heat Transfer, Part B: Fundamentals*, vol. 66, no. 3, pp. 281-306.

Bong, VNS & Wong, BT 2015a, 'Prediction of thermal conductivity of silicon nanowires via phonon Monte Carlo simulation: Exact treatment of cylindrical boundary,' *Physics & Materials Symposium: International Conference on Applied Sciences and Industrial Technology (ICASIT2015)*, AIP Publishing, 020017.

Bong, VNS & Wong, BT 2015b, 'A study of phonon anisotropic scattering effect on silicon thermal conductivity at nanoscale,' *Physics & Materials Symposium: International Conference on Applied Sciences and Industrial Technology (ICASIT2015)*, AIP Publishing, 020016.

Bong, VNS & Wong, BT 2016, 'The effect of phonon anisotropic scattering on the thermal conductivity of silicon thin films at 300K and 400K', *Journal of Physics and Chemistry of Solids*, vol. 88, pp. 41-46.

Borzdov, V & Petrovich, T 1997, 'Monte Carlo simulation of the low-temperature mobility of two-dimensional electrons in a silicon inversion layer', *Semiconductors*, vol. 31, no. 1, pp. 72-75.

Brockhouse, BN 1959, 'Lattice Vibrations in Silicon and Germanium', *Physical Review Letters*, vol. 2, no. 6, pp. 256-258.

Brunetti, R, Jacoboni, C, Nava, F, Reggiani, L, Bosman, G & Zijlstra, R 1981, 'Diffusion coefficient of electrons in silicon', *Journal of Applied Physics*, vol. 52, no. 11, pp. 6713-6722.

Burkardt, J 2011, 'Jacobi Iterative Solution of Poisson‟s Equation in 1D',

Cahill, DG, Ford, WK, Goodson, KE, Mahan, GD, Majumdar, A, Maris, HJ, Merlin, R & Phillpot, SR 2003, 'Nanoscale thermal transport', *Journal of Applied Physics*, vol. 93, no. 2, pp. 793-818.

Cahill, DG, Goodson, K & Majumdar, A 2002, 'Thermometry and thermal transport in micro/nanoscale solid-state devices and structures', *Transactions-American Society of Mechanical Engineers Journal of Heat Transfer*, vol. 124, no. 2, pp. 223-241.

Callaway, J 1959, 'Model for lattice thermal conductivity at low temperatures', *Physical Review*, vol. 113, no. 4, p. 1046.

Canali, C, Jacoboni, C, Nava, F, Ottaviani, G & Alberigi-Quaranta, A 1975, 'Electron drift velocity in silicon', *Physical Review B*, vol. 12, no. 6, p. 2265.

Chantrenne, P, Barrat, J, Blase, X & Gale, J 2005, 'An analytical model for the thermal conductivity of silicon nanostructures', *Journal of applied physics*, vol. 97, no. 10, p. 104318.

Chantrenne, P, Joulain, K, Terris, D & Lacroix, D 2007, 'Prediction of the thermal conductivity of nanofilms,' *Journal of Physics: Conference Series*, IOP Publishing, 012080.

Chen, G 2000, 'Phonon heat conduction in nanostructures', *International Journal of Thermal Sciences*, vol. 39, no. 4, pp. 471-480.

Chen, G 2005, *Nanoscale Energy Transport and Conversion,* Oxford Press, New York.

Chen, G 2006, 'Nanoscale heat transfer and nanostructured thermoelectrics', *Components and Packaging Technologies, IEEE Transactions on*, vol. 29, no. 2, pp. 238-246.

Chen, G, Narayanaswamy, A & Dames, C 2004, 'Engineering nanoscale phonon and photon transport for direct energy conversion', *Superlattices and Microstructures*, vol. 35, no. 3, pp. 161-172.

Chen, G, Zeng, T, Borca-Tasciuc, T & Song, D 2000, 'Phonon engineering in nanostructures for solid-state energy conversion', *Materials Science and Engineering: A*, vol. 292, no. 2, pp. 155-161.

Chen, Y, Li, D, Lukes, JR & Majumdar, A 2005, 'Monte Carlo simulation of silicon nanowire thermal conductivity', *Journal of Heat Transfer*, vol. 127, p. 1129.

Chung, JD, McGaughey, AJH & Kaviany, M 2004, 'Role of Phonon Dispersion in Lattice Thermal Conductivity Modelling', *Journal of Heat Transfer*, vol. 126, pp. 376-380.

Cohen, ML & Bergstresser, T 1966, 'Band structures and pseudopotential form factors for fourteen semiconductors of the diamond and zinc-blende structures', *Physical Review*, vol. 141, no. 2, p. 789.

Cumber, P & Beeri, Z 1998, 'A parallelization strategy for the discrete transfer radiation model', *Numerical Heat Transfer, Part B*, vol. 34, no. 3, pp. 287-302.

Ding, ZJ & Shimizu, R 1996, 'A Monte Carlo modeling of electron interaction with solids including cascade secondary electron production', *Scanning*, vol. 18, no. 2, pp. 92-113.

Ferry, D 2000, *Semiconductor transport,* CRC Press.

Feynman, RP 1960, 'There's plenty of room at the bottom', *Engineering and Science*, vol. 23, no. 5, pp. 22-36.

Fischetti, M & Laux, S 1996a, 'Monte Carlo simulation of electron transport in Si: The first 20 years,' *Solid State Device Research Conference, 1996. ESSDERC'96. Proceedings of the 26th European*, IEEE, 813-820.

Fischetti, MV & Laux, SE 1988, 'Monte Carlo analysis of electron transport in small semiconductor devices including band-structure and space-charge effects', *Physical Review B*, vol. 38, no. 14, p. 9721.

Fischetti, MV & Laux, SE 1996b, 'Band structure, deformation potentials, and carrier mobility in strained Si, Ge, and SiGe alloys', *Journal of Applied Physics*, vol. 80, no. 4, pp. 2234-2252.

Fischetti, MV, O'Regan, TP, Narayanan, S, Sachs, C, Jin, S, Kim, J & Zhang, Y 2007, 'Theoretical study of some physical aspects of electronic transport in nMOSFETs at the 10-nm gate-length', *Electron Devices, IEEE Transactions on*, vol. 54, no. 9, pp. 2116-2136.

Fobelets, K, Ding, P, Mohseni Kiasari, N & Durrani, Z 2012, 'Electrical Transport in Polymer-Covered Silicon Nanowires', *Nanotechnology, IEEE Transactions on*, vol. 11, no. 4, pp. 661-665.

Gamiz, F & Fischetti, M 2001, 'Monte Carlo simulation of double-gate silicon-on-insulator inversion layers: The role of volume inversion', *Journal of Applied Physics*, vol. 89, no. 10, pp. 5478-5487.

Gamiz, F, Godoy, A, Donetti, L, Sampedro, C, Roldan, J, Ruiz, F, Tienda, I, Rodriguez, N & Jimenez-Molinos, F 2009, 'Monte Carlo simulation of nanoelectronic devices', *Journal of computational electronics*, vol. 8, no. 3-4, pp. 174-191.

Gámiz, F, Godoy, A, Sampedro, C, Rodriguez, N & Ruiz, F 2008, 'Monte Carlo simulation of low-field mobility in strained double gate SOI transistors', *Journal of computational electronics*, vol. 7, no. 3, pp. 205-208.

Giustino, F 2016, 'Electron-phonon interactions from first principles', *arXiv preprint arXiv:1603.06965*,

Gonzalez, B, Palankovski, V, Kosina, H, Hernandez, A & Selberherr, S 1999, 'An energy relaxation time model for device simulation', *Solid-state electronics*, vol. 43, no. 9, pp. 1791-1795.

Gressman, PT & Strain, RM 2010, 'Global classical solutions of the Boltzmann equation with long-range interactions', *Proceedings of the National Academy of Sciences*, vol. 107, no. 13, pp. 5744-5749.

Gueye, SB, Talla, K & Mbow, C 2014, 'Solution of 1D Poisson Equation with Neumann-Dirichlet and Dirichlet-Neumann Boundary Conditions, Using the Finite Difference Method', *Journal of Electromagnetic Analysis and Applications*, vol. 6, no. 10, p. 309.

Gunst, T, Markussen, T, Stokbro, K & Brandbyge, M 2016, 'First-principles method for electron-phonon coupling and electron mobility: Applications to two-dimensional materials', *Physical Review B*, vol. 93, no. 3, p. 035414.

Hao, Q, Chen, G & Jeng, M-S 2009, 'Frequency-dependent Monte Carlo simulations of phonon transport in two-dimensional porous silicon with aligned pores', *Journal of Applied Physics*, vol. 106, no. 11, pp. 114321-114321-10.

Henyey, LG & Greenstein, JL 1941, 'Diffuse radiation in the galaxy', *The Astrophysical Journal*, vol. 93, pp. 70-83.

Hernández-Vélez, M 2006, 'Nanowires and 1D arrays fabrication: An overview', *Thin solid films*, vol. 495, no. 1, pp. 51-63.

Holland, M 1963, 'Analysis of lattice thermal conductivity', *Physical Review*, vol. 132, no. 6, p. 2461.

Iijima, S 1991, 'Helical microtubules of graphitic carbon', *nature*, vol. 354, no. 6348, pp. 56-58.

Jacoboni, C & Reggiani, L 1983, 'The Monte Carlo method for the solution of charge transport in semiconductors with applications to covalent materials', *Reviews of Modern Physics*, vol. 55, no. 3, p. 645.

Jeng, M-S, Yang, R-G, Song, D & Chen, G 2008, 'Modeling the thermal conductivity and phonon transport in nanoparticle composites using Monte Carlo simulation', *Journal of Heat Transfer*, vol. 130, no. 4, pp. 040301.1-044503.4.

Joy, DC 1995, *Monte Carlo modeling for electron microscopy and microanalysis,* Oxford University Press.

Ju, Y & Goodson, K 1999, 'Phonon scattering in silicon films with thickness of order 100 nm', *Applied Physics Letters*, vol. 74, no. 20, pp. 3005-3007.

Kamakura, Y, Adisusilo, I, Kukita, K, Wakimura, G, Koba, S, Tsuchiya, H & Mori, N 2014, 'Coupled Monte Carlo simulation of transient electron-phonon transport in small FETs,' *Electron Devices Meeting (IEDM), 2014 IEEE International*, IEEE, 7.3. 1-7.3. 4.

Kamakura, Y, Mori, N, Taniguchi, K, Zushi, T & Watanabe, T 2010, 'Coupled Monte Carlo simulation of transient electron-phonon transport in nanoscale devices,' *Simulation of Semiconductor Processes and Devices (SISPAD), 2010 International Conference on*, IEEE, 89-92.

Klemens, P 1951, 'The thermal conductivity of dielectric solids at low temperatures (theoretical)', *Proceedings of the Royal Society of London. Series A. Mathematical and Physical Sciences*, vol. 208, no. 1092, pp. 108-133.

Kroese, DP, Brereton, T, Taimre, T & Botev, ZI 2014, 'Why the Monte Carlo method is so important today', *Wiley Interdisciplinary Reviews: Computational Statistics*, vol. 6, no. 6, pp. 386-392.

Kukita, K, Adisusilo, IN & Kamakura, Y 2013, 'Monte Carlo simulation of diffusive-to-ballistic transition in phonon transport', *Journal of computational electronics*, pp. 1-7.

Kukita, K, Adisusilo, IN & Kamakura, Y 2014, 'Monte Carlo simulation of thermal conduction in silicon nanowires including realistic phonon dispersion relation', *Japanese Journal of Applied Physics*, vol. 53, no. 1, p. 015001.

Kukita, K & Kamakura, Y 2013, 'Monte Carlo simulation of phonon transport in silicon including a realistic dispersion relation', *Journal of Applied Physics*, vol. 114, no. 15, p. 154312.

Kunikiyo, T, Takenaka, M, Kamakura, Y, Yamaji, M, Mizuno, H, Morifuji, M, Taniguchi, K & Hamaguchi, C 1994, 'A Monte Carlo simulation of anisotropic electron transport in silicon including full band structure and anisotropic impact-ionization model', *Journal of Applied Physics*, vol. 75, no. 1, pp. 297-312.

Lacroix, D, Joulain, K & Lemonnier, D 2005, 'Monte Carlo transient phonon transport in silicon and germanium at nanoscales', *Physical Review B*, vol. 72, no. 6, p. 064305.

Lacroix, D, Joulain, K, Terris, D & Lemonnier, D 2006, 'Monte Carlo simulation of phonon confinement in silicon nanostructures: Application to the determination of the thermal conductivity of silicon nanowires', *Applied Physics Letters*, vol. 89, no. 10, pp. 103104-103104-3.

Lai, JJ, Bong, VNS, Wong, BT & Mustapha, KB 2016, 'Modeling of Light Propagation and Phonon Conduction inside Metallic Nanoparticles Enhanced Thin-Film Solar Cells,' *Journal of Nano Research*, Trans Tech Publ, 26-35.

Lau, JZ-J, Bong, VNS & Wong, BT 2016, 'Parametric investigation of nano-gap thermophotovoltaic energy conversion', *Journal of Quantitative Spectroscopy and Radiative Transfer*, vol. 171, pp. 39-49.

Lee, W 2011, 'Tridiagonal matrices: Thomas algorithm', *MS6021, Scientific Computation, University of Limerick*,

Leyland, W, Harley, R, Henini, M, Shields, A, Farrer, I & Ritchie, D 2008, 'Energy-dependent electron-electron scattering and spin dynamics in a two-dimensional electron gas', *Physical Review B*, vol. 77, no. 20, p. 205321.

Li, D, Wu, Y, Kim, P, Shi, L, Yang, P & Majumdar, A 2003, 'Thermal conductivity of individual silicon nanowires', *Applied Physics Letters*, vol. 83, no. 14, pp. 2934-2936.

Li, J, Au Yeung, TC & Chan, HK 2012, 'Influence of electron scatterings on thermoelectric effect', *Journal of Applied Physics*, vol. 112, no. 3, pp. 034306-034306-5.

Liu, W & Asheghi, M 2006, 'Thermal conductivity measurements of ultra-thin single crystal silicon layers', *Journal of heat transfer*, vol. 128, no. 1, pp. 75-83.

Liu, Y, Song, C-l, Weng, W-j, Du, P-y & Han, G-r 2005, 'Simulation of scattering in dense medium by Monte Carlo method', *Journal of Zhejiang University Science*, vol. 6, no. 1, pp. 155-157.

Lugli, P & Ferry, D 1983, 'Effect of electron-electron scattering on Monte Carlo studies of transport in submicron semiconductors devices', *Physica B+ C*, vol. 117, pp. 251-253.

Maltby, J & Kornblum, B 1990, 'MONT3E: A Monte Carlo electron heat transfer code,' *Proceedings of the 1990 ACM/IEEE conference on Supercomputing*, IEEE Computer Society Press, 700-707.

Matulionis, A, Požela, J & Reklaitis, A 1975, 'Monte Carlo treatment of electron-electron collisions', *Solid State Communications*, vol. 16, no. 10, pp. 1133-1137.

Maycock, P 1967, 'Thermal conductivity of silicon, germanium, III–V compounds and III–V alloys', *Solid-state electronics*, vol. 10, no. 3, pp. 161-168.

Mazumder, S & Kersch, A 2000, 'A fast Monte Carlo scheme for thermal radiation in semiconductor processing applications', *Numerical Heat Transfer: Part B: Fundamentals*, vol. 37, no. 2, pp. 185-199.

Mazumder, S & Majumdar, A 2001, 'Monte Carlo study of phonon transport in solid thin films including dispersion and polarization', *Transactions-American Society of Mechanical Engineers Journal of Heat Transfer*, vol. 123, no. 4, pp. 749-759.

Mengüç, M & Viskanta, R 1983, 'Comparison of radiative transfer approximations for a highly forward scattering planar medium', *Journal of Quantitative Spectroscopy and Radiative Transfer*, vol. 29, no. 5, pp. 381-394.

Mingo, N 2003, 'Calculation of Si nanowire thermal conductivity using complete phonon dispersion relations', *Physical Review B*, vol. 68, no. 11, p. 113308.

Mingo, N, Yang, L, Li, D & Majumdar, A 2003, 'Predicting the thermal conductivity of Si and Ge nanowires', *Nano Letters*, vol. 3, no. 12, pp. 1713-1716.

Mittal, A & Mazumder, S 2010, 'Monte Carlo study of phonon heat conduction in silicon thin films including contributions of optical phonons', *Journal of Heat Transfer*, vol. 132, no. 5, p. 052402.

Modest, MF 1993, *Radiative Heat Transfer,* McGraw-Hill, Inc.

Mohamed, M, Aksamija, Z & Ravaioli, U 2015, 'Coupled electron and thermal transport simulation of self-heating effects in junctionless MOSFET,' *Journal of Physics: Conference Series*, IOP Publishing, 012026.

Montefusco, LB & Jacoboni, C 1972, 'Electron-electron in Monte Carlo transport calculations', *Solid State Communications*, vol. 10, no. 1, pp. 71-74.

Moore, GE 1998, 'Cramming more components onto integrated circuits', *Proceedings of the IEEE*, vol. 86, no. 1, pp. 82-85.

Nam, Y, Yeng, YX, Lenert, A, Bermel, P, Celanovic, I, Soljačić, M & Wang, EN 2014, 'Solar thermophotovoltaic energy conversion systems with two-dimensional tantalum photonic crystal absorbers and emitters', *Solar Energy Materials and Solar Cells*, vol. 122, pp. 287-296.

Nghiêm, TT, Saint-Martin, J & Dollfus, P 2016, 'Electro-thermal simulation based on coupled Boltzmann transport equations for electrons and phonons', *Journal of Computational Electronics*, vol. 15, no. 1, pp. 3-15.

Ni, C, Aksamija, Z, Murthy, JY & Ravaioli, U 2012, 'Coupled electro-thermal simulation of MOSFETs', *Journal of computational electronics*, vol. 11, no. 1, pp. 93-105.

Ni, C & Murthy, JY 2009, 'Parallel computation of the phonon Boltzmann transport equation', *Numerical Heat Transfer, Part B: Fundamentals*, vol. 55, no. 6, pp. 435-456.

Nilsson, G & Nelin, G 1971, 'Phonon Dispersion Relations in Ge at 80 Â°K', *Physical Review B*, vol. 3, no. 2, pp. 364-369.

Péraud, J-PM 2011, *Low variance methods for Monte Carlo simulation of phonon transport*, thesis, Massachusetts Institute of Technology.

Péraud, J-PM, Landon, CD & Hadjiconstantinou, NG 2014, 'Monte carlo methods for solving the boltzmann transport equation', *Annual Review of Heat Transfer*, vol. 17,

Phillpot, SR & McGaughey, AJ 2005, 'Introduction to thermal transport', *Materials Today*, vol. 8, no. 6, pp. 18-20.

Pop, E 2008, 'Electron-phonon interaction and Joule heating in nanostructures,' ASME,

Pop, E 2010, 'Energy dissipation and transport in nanoscale devices', *Nano Research*, vol. 3, no. 3, pp. 147-169.

Pop, E 2014, 'Monte Carlo transport and heat generation in semiconductors', *Annual Review of Heat Transfer*, vol. 17,

Pop, E, Banerjee, K, Sverdrup, P, Dutton, R & Goodson, K 2001, 'Localized heating effects and scaling of sub-0.18 micron CMOS devices,' *Electron Devices Meeting, 2001. IEDM'01. Technical Digest. International*, IEEE, 31.1. 1-31.1. 4.

Pop, E, Dutton, R & Goodson, K 2003, 'Detailed heat generation simulations via the Monte Carlo method,' *Simulation of Semiconductor Processes and Devices, 2003. SISPAD 2003. International Conference on*, IEEE, 121-124.

Pop, E, Dutton, RW & Goodson, KE 2004, 'Analytic band Monte Carlo model for electron transport in Si including acoustic and optical phonon dispersion', *Journal of Applied Physics*, vol. 96, p. 4998.

Pop, E, Dutton, RW & Goodson, KE 2005, 'Monte Carlo simulation of Joule heating in bulk and strained silicon', *Applied Physics Letters*, vol. 86, no. 8, pp. 082101-082101-3.

Pop, E & Goodson, KE 2006, 'Thermal phenomena in nanoscale transistors', *Journal of Electronic Packaging*, vol. 128, no. 2, pp. 102-108.

Pop, E, Sinha, S & Goodson, KE 2002, 'Monte Carlo modeling of heat generation in electronic nanostructures,' *ASME 2002 International Mechanical Engineering Congress and Exposition*, American Society of Mechanical Engineers, 85-90.

Pop, E, Sinha, S & Goodson, KE 2006, 'Heat generation and transport in nanometer-scale transistors', *Proceedings of the IEEE*, vol. 94, no. 8, pp. 1587-1601.

Raleva, K, Vasileska, D, Goodnick, SM & Nedjalkov, M 2008, 'Modeling thermal effects in nanodevices', *Electron Devices, IEEE Transactions on*, vol. 55, no. 6, pp. 1306-1316.

Ramayya, E & Knezevic, I 2010, 'Self-consistent Poisson-Schrödinger-Monte Carlo solver: electron mobility in silicon nanowires', *Journal of computational electronics*, vol. 9, no. 3-4, pp. 206-210.

Ramayya, E, Maurer, L, Davoody, A & Knezevic, I 2012, 'Thermoelectric properties of ultrathin silicon nanowires', *Physical Review B*, vol. 86, no. 11, p. 115328.

Ramayya, EB, Vasileska, D, Goodnick, SM & Knezevic, I 2007, 'Electron mobility in silicon nanowires', *Nanotechnology, IEEE Transactions on*, vol. 6, no. 1, pp. 113-117.

Randrianalisoa, J & Baillis, D 2008, 'Monte Carlo simulation of steady-state microscale phonon heat transport', *Journal of Heat Transfer*, vol. 130, no. 7

Rideau, D, Zhang, W, Niquet, Y, Delerue, C, Tavernier, C & Jaouen, H 2011, 'Electron-phonon scattering in Si and Ge: From bulk to nanodevices,' *Simulation of Semiconductor Processes and Devices (SISPAD), 2011 International Conference on*, IEEE, 47-50.

Rosini, M, Jacoboni, C & Ossicini, S 2002, 'Monte Carlo simulation of electron transport in Si/SiO_ {2} superlattices: Vertical transport enhanced by a parallel field', *Physical Review B*, vol. 66, no. 15, p. 155332.

Rowlette, J, Pop, E, Sinha, S, Panzer, M & Goodson, K 2005, 'Thermal simulation techniques for nanoscale transistors,' *Proceedings of the 2005 IEEE/ACM International conference on Computer-aided design*, IEEE Computer Society, 225-228.

Rowlette, JA & Goodson, KE 2008, 'Fully coupled nonequilibrium electron–phonon transport in nanometer-scale silicon FETs', *IEEE Transactions on Electron Devices*, vol. 55, no. 1, pp. 220-232.

Sampedro, C, Gámiz, F, Godoy, A & Jiménez-Molinos, F 2007, 'Quantum Ensemble Monte Carlo simulation of silicon-based nanodevices', *Journal of computational electronics*, vol. 6, no. 1-3, pp. 41-44.

Sangiorgi, E, Ricco, B & Venturi, F 1988, 'MOS< sup> 2</sup>: an efficient MOnte Carlo Simulator for MOS devices', *Computer-Aided Design of Integrated Circuits and Systems, IEEE Transactions on*, vol. 7, no. 2, pp. 259-271.

Sano, N 2011, 'Monte Carlo study of the Coulomb interaction in nanoscale silicon devices', *Japanese Journal of Applied Physics*, vol. 50, no. 1, p. 0108.

Sano, N, Tomizawa, M & Yoshii, A 1991, 'Monte Carlo analysis of hot electron transport and impact ionization in silicon', *Jpn. J. Appl. Phys*, vol. 30, p. 3662.

Shi, W, Peng, H, Wang, N, Li, CP, Xu, L, Lee, CS, Kalish, R & Lee, S-T 2001, 'Free-standing single crystal silicon nanoribbons', *Journal of the American Chemical Society*, vol. 123, no. 44, pp. 11095-11096.

Sidorov, A, V'yurkov, V & Orlikovsky, A 2004, 'Monte Carlo Simulation of Nanoscale SOI MOSFETs', *Russian Microelectronics*, vol. 33, no. 4, pp. 195-205.

Snowden, C 1998, *Introduction to semiconductor device modelling,* World Scientific.

Snowden, CM 1988, *Semiconductor Device Modelling,* Peter Peregrinus Ltd, London.

Srinivasan, S, Miller, R & Marotta, E 2004, 'Parallel computation of the Boltzmann transport equation for microscale heat transfer in multilayered thin films', *Numerical Heat Transfer, Part B: Fundamentals*, vol. 46, no. 1, pp. 31-58.

Tang, J & Hess, K 1983, 'Impact ionization of electrons in silicon (steady state)', *Journal of Applied Physics*, vol. 54, no. 9, pp. 5139-5144.

Terris, D, Joulain, K, Lemonnier, D, Lacroix, D & Chantrenne, P 2009, 'Prediction of the thermal conductivity anisotropy of Si nanofilms. Results of several numerical methods', *International Journal of Thermal Sciences*, vol. 48, no. 8, pp. 1467-1476.

Tiwari, M, Talwar, D & K Agrawal, B 1971, 'Phonon conductivity of GaAs', *Solid State Communications*, vol. 9, no. 13, pp. 995-997.

Van Zeghbroeck, B 2011, 'Principles of electronic devices', *University of Colorado*,

Vasileska, D, Mamaluy, D, Khan, H, Raleva, K & Goodnick, S 2008, 'Semiconductor device modeling', *Journal of Computational and Theoretical Nanoscience*, vol. 5, no. 6, p. 999.

Vasileska, D, Raleva, K & Goodnick, S 2008, 'Modeling heating effects in nanoscale devices: the present and the future', *Journal of computational electronics*, vol. 7, no. 2, pp. 66-93.

Vasileska, D, Raleva, K & Goodnick, SM 2010, 'Heating effects in nanoscale devices', *Cutting Edge Nanotechnology*,

Wang, L & Jacques, SL 1992, 'Monte Carlo modeling of light transport in multi-layered tissues in standard C', *The University of Texas, MD Anderson Cancer Center, Houston*, pp. 4-11.

Wang, N, Cai, Y & Zhang, R 2008, 'Growth of nanowires', *Materials Science and Engineering: R: Reports*, vol. 60, no. 1, pp. 1-51.

Wang, Z, Quan, L & Ruan, YW 2011, 'Simulation of Electron Transport in Silicon using Monte Carlo Method', *Advanced Materials Research*, vol. 284, pp. 871-874.

Waugh, JLT & Dolling, G 1963, 'Crystal Dynamics of Gallium Arsenide', *Physical Review*, vol. 132, no. 6, pp. 2410-2412.

Wolf, EL 2008, *Nanophysics and nanotechnology: an introduction to modern concepts in nanoscience,* John Wiley & Sons.

Wong, BT 2001, *Monte Carlo Techniques for the Solution of the Transient and Steady Radiative Transfer Equation*, thesis, University of Kentucky, Lexington, Kentucky.

Wong, BT 2012, 'Analysis of charge, momentum and energy transfer by an impinging sub-keV electron beam on a conductor via Monte Carlo simulation including secondary-electron generation', *International Journal of Heat and Mass Transfer*,

Wong, BT, Francoeur, M, Bong, VNS & Mengüç, MP 2013, 'Coupling of near-field thermal radiative heating and phonon Monte Carlo simulation: Assessment of temperature gradient in *n*-doped silicon thin film', *Journal of Quantitative Spectroscopy and Radiative Transfer*,

Wong, BT, Francoeur, M & Pinar Mengüç, M 2011, 'A Monte Carlo simulation for phonon transport within silicon structures at nanoscales with heat generation', *International Journal of Heat and Mass Transfer*, vol. 54, no. 9, pp. 1825-1838.

Wong, BT & Mengüç, MP 2002, 'Comparison of Monte Carlo techniques to predict the propagation of a collimated beam in participating media', *Numerical Heat Transfer: Part B: Fundamentals*, vol. 42, no. 2, pp. 119-140.

Wong, BT & Mengüç, MP 2003, 'Electronic thermal conduction in thin gold films,' ASME,

Wong, BT & Mengüç, MP 2004, 'Monte Carlo methods in radiative transfer and electron-beam processing', *Journal of Quantitative Spectroscopy and Radiative Transfer*, vol. 84, no. 4, pp. 437-450.

Wong, BT & Mengüç, MP 2008, *Thermal Transport for Applications in Micro/Nanomachining,* Springer, New York.

Wong, BT & Mengüç, MP 2010, 'A unified Monte Carlo treatment of the transport of electromagnetic energy, electrons, and phonons in absorbing and scattering media', *Journal of Quantitative Spectroscopy and Radiative Transfer*, vol. 111, no. 3, pp. 399-419.

Wong, BT, Mengüç, MP & Vallance, RR 2007, 'Thermal conduction induced by electron-beam', *International Journal of Heat and Mass Transfer*, vol. 50, no. 25, pp. 5099-5107.

Wu, R, Hu, R & Luo, X 2016, 'First-principle-based full-dispersion Monte Carlo simulation of the anisotropic phonon transport in the wurtzite GaN thin film', *Journal of Applied Physics*, vol. 119, no. 14, p. 145706.

Yoder, P & Hess, K 1994, 'First-principles Monte Carlo simulation of transport in Si', *Semiconductor Science and Technology*, vol. 9, no. 5S, p. 852.

Zhang, ZM 2007, *Nano/Microscale Heat Transfer,* McGraw-Hill, New York.

Ziman, JM 1960, *Electrons and Phonons,* Oxford University Press, New York.

Ziman, JM 1964, *Principles of the Theory of Solids,* Cambridge University Press, Cambridge.

Zou, J & Balandin, A 2001, 'Phonon heat conduction in a semiconductor nanowire', *Journal of Applied Physics*, vol. 89, no. 5, pp. 2932-2938.

Appendix A:
Computational Resources Specifications

A. System Information

Manufacturer	: Dell
Model	: Precision T7500
Processor	: Intel® Xeon® CPU (X5675)
Installed Memory (RAM)	: 12.0 GB
System type	: 64-bit Operating System, x64-based processor
Operating System	: Microsoft Windows 7 Enterprise
	: Microsoft Windows 10 Pro

B. Programming Language and Software

Programming Software	: Compaq Visual Fortran, PGI Visual Fortran 2013
Programming Language	: Fortran 90

C. Other Software

Plotting Software	: OriginPro 2015

Publications Arising from this Thesis

Bong, V.N.S. and Wong, B.T., 2014. Solution of the Boltzmann transport equation for phonon transport via the speed-up transient Monte Carlo method using reference temperature. *Numerical Heat Transfer, Part B: Fundamentals*, *66*(3), pp.281-306.

Wong, B.T., Francoeur, M., Bong, V.N.S. and Mengüç, M.P., 2014. Coupling of near-field thermal radiative heating and phonon Monte Carlo simulation: Assessment of temperature gradient in n-doped silicon thin film. *Journal of Quantitative Spectroscopy and Radiative Transfer*, *143*, pp.46-55.

Bong, V.N.S. and Wong, B.T., 2015, August. A study of phonon anisotropic scattering effect on silicon thermal conductivity at nanoscale. In T. Winie, R.H.Y. Subban and F.H. Muhammad eds., *AIP Conference Proceedings* (Vol. 1674, No. 1, p. 020016). AIP Publishing.

Bong, V.N.S. and Wong, B.T., 2015, August. Prediction of thermal conductivity of silicon nanowires via phonon Monte Carlo simulation: Exact treatment of cylindrical boundary. In T. Winie, R.H.Y. Subban and F.H. Muhammad eds., *AIP Conference Proceedings* (Vol. 1674, No. 1, p. 020017). AIP Publishing.

Bong, V.N.S. and Wong, B.T., 2016. The effect of phonon anisotropic scattering on the thermal conductivity of silicon thin films at 300K and 400K. *Journal of Physics and Chemistry of Solids*, *88*, pp.41-46.

Lau, J.Z.J., Bong, V.N.S. and Wong, B.T., 2016. Parametric investigation of nano-gap thermophotovoltaic energy conversion. *Journal of Quantitative Spectroscopy and Radiative Transfer*, *171*, pp.39-49.

Lai, J.J., Bong, V.N.S., Wong, B.T. and Mustapha, K.B., 2016. Modeling of Light Propagation and Phonon Conduction inside Metallic Nanoparticles Enhanced Thin-Film Solar Cells. In *Journal of Nano Research* (Vol. 38, pp. 26-35). Trans Tech Publications.